THE RELATIVE SIGNS OF COUPLING CONSTANTS IN FLUORINATED CYCLOPROPANES AND THE AGGREGATION OF AMYLOID-BETA (25-35) PEPTIDE

By

DAVID W. RICHARDSON

A DISSERTATION PRESENTED TO THE GRADUATE SCHOOL
OF THE UNIVERSITY OF FLORIDA IN PARTIAL FULFILLMENT
OF THE REQUIREMENTS FOR THE DEGREE OF
DOCTOR OF PHILOSOPHY

UNIVERSITY OF FLORIDA

2010

To my loving wife and beautiful daughter

ACKNOWLEDGMENTS

I would like to express my utmost gratitude to my mentor, Dr. Wallace Brey, for his guidance and endless patience. Through my academic career he taught me NMR from the ground up. The innumerable conversations about both the history and principles of NMR, and science and life in general, were invaluable to my growth as a scientist and person.

I would like to thank my friends and colleagues in the NMR facility, Dr. Ion Ghiviriga and Robert Harker. They furthered my knowledge of advanced NMR techniques and the function and maintenance of NMR spectrometers and groomed me for my future as a spectroscopist. I would also like to thank my lab mate Dr. Bethany Bechtel for often serving as a sounding board for my research thoughts and for providing ideas when I was at a loss.

I would like to acknowledge the members of my committee, Dr. Richard Yost, Dr. David Powell, and Dr. Joanna Long, for their patience and encouragement and for answering my many questions. I especially want to thank Dr. C. R. Bowers for his assistance in the final stages of editing this document.

I am thankful for my fellow graduate students. For their encouragement, assistance, and friendship. I especially want to thank Dr. Frank Kero, Dr. John Bowden, Dr. Jennifer Bryant, Dr. Joshua Caldwell, Daniel Magparangalan, and Mike Napolitano.

I would like to thank all the members of my family, both in blood and through marriage, for their support. I especially want to thank my parents. Throughout my life they have blessed me with endless love and support and have sacrificed more for me than I could ever hope to express in words.

I thank my daughter, Audrey, for always greeting me with a smile after a long day of work.

I owe an eternal debt to my wife and best friend Samantha. Her companionship, understanding, and encouragement are immeasurable. Without her support this would not have been possible.

Lastly, I would like to thank God for the many blessings.

TABLE OF CONTENTS

page

LIST OF TABLES

LIST OF FIGURES

Abstract of Dissertation Presented to the Graduate School
of the University of Florida in Partial Fulfillment of the
Requirements for the Degree of Doctor of Philosophy

THE RELATIVE SIGNS OF COUPLING CONSTANTS IN FLUORINATED CYCLOPROPANES AND THE AGGREGATION OF AMYLOID-BETA (25-35) PEPTIDE

By

David W. Richardson

May 2010

Chair: Clifford R. Bowers
Major: Chemistry

Cyclopropanes present interesting molecules to study due to their unique bond angles and strain in the three-membered ring. Protonated cyclopropanes have been extensively studied using nuclear magnetic resonance (NMR), but little work has been done with their fluorinated analogues. Double-resonance, or spin-tickling, NMR was used to determine the signs of three-bond vicinal fluorine-fluorine coupling constants and their relationship with temperature. Certain molecules were shown to conflict with the previously published relationship between the sign of the coupling constants in cyclopropanes and their temperature dependence.

Amyloid-β peptide (Aβ) is the main component of plaques found in the brains of patients with Alzheimer's disease. Aβ is a soluble 39 to 42 residue peptide resulting from the proteolytic cleavage of the amyloid precursor protein. As a result of conformational changes, Aβ transforms from independent soluble monomers to insoluble, plaque-forming oligomers. This transformation is assumed to lead to the deleterious effects of Alzheimer's disease (AD). Some debate remains as to whether the symptoms associated with AD are a direct result of the plaque formation, or if the

aggregation of Aβ is a secondary result. However, there is no question that the brains of patients who display signs of AD at time of death contain abnormally high amounts of Aβ plaque.

NMR was shown to be a useful analytical tool for the *in vitro* analysis of Aβ. Pulsed-field-gradient NMR (pfg-NMR) is particularly useful as it allows for the determination of diffusion coefficients. By subjecting the sample to a gradient magnetic field, the nuclei of an analyte can be spatially marked along an axis. Any movement along that axis results in signal attenuation. The signal attenuation was plotted against an array of the gradient strength and diffusion coefficients were calculated. This work involved altering sample conditions and measuring the diffusion of Aβ with the intent of finding a trigger for the aggregation of the peptide. The diffusion of Aβ(25-35), an 11 residue fragment of the Aβ peptide, was examined over a range of temperatures, pH, and in solutions with common biological metal ions.

CHAPTER 1
INTRODUCTION

Overview of Nuclear Magnetic Resonance

Nuclei containing an odd number of protons or neutrons behave as though they are spinning and possess an angular momentum. The concept of nuclear spin angular momentum is rather abstract. It is a property of quantum mechanics and has no macroscopic corollary. The existence of nuclear spin was first suggested by Pauli in 1924[1] and later confirmed experimentally by Rabi in 1939[2]. The math describing nuclear spin angular momentum is similar to that for rotational angular momentum, but it is incorrect to imagine nuclei spinning about their own axis[3]. Nuclear spin angular momentum, p, is quantized in units of the reduced Planck constant, $\hbar$.

$$p = I\hbar = \frac{Ih}{2\pi} \tag{1-1}$$

The nuclear spin quantum number, I, is nucleus-dependent and is either an integer or half-integer. Nuclei which have a non-zero nuclear spin quantum number possess a magnetic moment, μ.

$$\mu = \gamma p \tag{1-2}$$

The magnetogyric ratio, γ, is a nucleus-dependent constant and is typically expressed in units of rad·s^{-1}T^{-1}. Nuclei with a nuclear spin of zero, notably ^{12}C and ^{16}O, are not observable by nuclear magnetic resonance (NMR) techniques as they have no angular momentum and thus no magnetic moment.

A nucleus has $2I + 1$ orientations relative to an arbitrary axis. These orientations are often referred to as spin states, m, where:

$$m = I, I-1, \ldots, -I+1, -I \tag{1-3}$$

Absent an external magnetic field, these spin states are of equal energy and an equal distribution of nuclei exists across all spin states. In the presence of a magnetic field, however, the spin states split in energy with:

$$E = -m\hbar\gamma B \tag{1-4}$$

where B is the applied field, usually expressed in tesla (T). Following Eq. 1-3, a spin-½ nucleus has two possible spin states, +½ and –½. In terms of NMR, these spin states are often referred to as parallel and anti-parallel, or spin-up and spin-down, relative to an applied magnetic field.

Spin-Spin Coupling

The presence of different spin states leads to a phenomenon known as spin-spin coupling. Ramsey and Purcell first suggested that information about the spin of one nucleus is transferred to a neighboring nucleus via the bonding electrons[4]. Consider the case of two spin-½ nuclei (Figure 1-1). The Pauli exclusion principle dictates that the electrons must have opposite spins, so it follows that two states exist for a two-nucleus system. In one, the nuclei are of opposite spins, leading to energetically favorable interactions (Figure 1-1A), and in the other the nuclei are of equal spins and one is the same spin as one of the electrons (Figure 1-1B). When one nucleus undergoes resonance, or changes spin states, the energy of the transition depends on the orientation of the other nucleus[5]. The difference in energy between these two different transitions is very small (of the order of hertz) but results in two spectral lines separated in frequency by what is known as the spin-spin coupling constant, J. It would seem logical that the first state where the nuclei are anti-parallel to one another results in the lowest energy state; however, this is not always the case. The interaction of

nuclear spins across one or more bonds can result in the opposite being true. These two cases are distinguished by the sign of the coupling constant; the first is said to have a positive coupling constant ($J>0$) and the second a negative coupling constant ($J<0$)[5]. The signs of coupling constants are often ignored in NMR spectroscopy, as a change in sign results in no visible change in first-order spectra. However, the sign of the coupling constant is useful when one examines the effect of different functional groups or structural changes on the magnitude of *J*. With no knowledge of the sign, it is impossible to know if an increase in magnitude is the result of a positive *J* becoming more positive or a negative *J* becoming more negative and vice versa. It is also necessary to know the signs of the coupling constants when one tries to simulate non-first-order specta. Additionally, the sign of *J* is of use to theoretical chemists and physicists in terms of molecular modeling and dynamics.

Double-Resonance NMR

Double-resonance NMR utilizes a second weaker rf pulse over a much narrower range of frequencies compared to the initial excitation pulse. The concept of using a spin-decoupling (or spin-tickling) pulse was first suggested by Bloch[6]. Maher and Evans were the first to apply this technique to the determination of the relative signs of coupling constants[7]. They used double-resonance (or double-irradiation) NMR to show that the Tl-H(CH_2) and Tl-H(CH_3) coupling constants in thallium diethyl cation were of opposite signs. The technique was further developed by Freeman and Evans to determine the signs of both proton and fluorine coupling constants in three-spin systems[8-11]. Double-resonance NMR differs from conventional decoupling experiments in that it is usually a homonuclear experiment and the second rf pulse is not strong enough to cause rapid changes in the orientation of the spins to a point that

any coupled nuclei only sense an averaged, or decoupled, state. The pulse only slightly perturbs the spins, hence the term spin-tickling. This causes the resonance line of any transition connected to the tickled transition to be slightly split[5] (Figure 1-2). A more thorough explanation of double-resonance NMR and the signs of coupling constants and their effect on the spectrum is included in chapter two.

Chemical Shift

Another important parameter in NMR is the chemical shift (δ). The magnetic field at a nucleus ($B_{nucleus}$) is not equal to the external magnetic field produced by the superconducting magnet (B_o). Since electrons are magnetic particles, their motion is influenced by the external field as well. As stated by Lenz's law, the motion of a particle induced by a magnetic field is in a such a direction as to oppose the field[5]. The motion of the electrons and other nuclei in the vicinity of the observed nucleus cause local fields that shield the nucleus from the external field so:

$$B_{nucleus} = B_0 - \sigma B_0 = B_0(1-\sigma) \tag{1-5}$$

where σ is the shielding factor. When $B_{nucleus}$ is substituted into the Larmor equation,

$$\omega = \frac{\gamma}{2\pi} B_0 \tag{1-6}$$

it shows the resonance frequency (or chemical shift expressed in hertz), υ, of a particular nucleus is a function of the local fields surrounding that nucleus:

$$\upsilon = \frac{\gamma}{2\pi} B_0(1-\sigma) \tag{1-7}$$

To avoid the ambiguity of the chemical shift being dependent on the strength of the magnetic field of a particular instrument, it is commonly reported in the dimensionless

unit of parts per million (ppm)[5]. The resonance frequency (υ) is compared to that of a reference material (υ_r) and:

$$\delta \equiv \frac{\upsilon - \upsilon_R}{\upsilon_R} \times 10^6 \qquad (1\text{-}8)$$

Since the electron cloud, bond angles, and bond lengths can all be affected by things such as solvent, temperature, and conformational changes, the chemical shift is a powerful tool to help analyze samples at the atomic level.

Pulsed-Field-Gradient NMR

Pulsed-field-gradient (pfg) NMR is a specialized NMR technique which can be used to measure self-diffusion coefficients. The stimulated-echo pfg pulse sequence (pfg-se) was first described by Stejskal and Tanner[12]. With the use of a gradient pulse, the spins can be marked spatially, and upon refocusing by a second gradient pulse, the spin-echo can be observed (Figure 1-3). The time between the two gradient pulses, Δ, is the diffusion time. The second rf pulse, a π (or 180^o) pulse, simply inverts the spins in the xy plane. With the second gradient pulse, of equal strength and duration to the first, the spins are 'unwound.' Absent diffusion, the spins are in the same plane along the z axis and they are refocused without any signal attenuation. However, when diffusion does occur, the spins move along the gradient in the z direction and no longer experience an equal gradient from the second gradient pulse resulting in spin incoherence and a loss of signal (Figure 1-3).

For macromolecules such as peptides, a slightly different pulse sequence called the stimulated-echo pfg (pfg-ste) is used (Figure 1-4). There are two types of nuclear relaxation which result in a return to equilibrium following the rf pulse. T_1 relaxation, also known as spin-lattice or longitudinal relaxation, is the process by which localized

and fluctuating fields cause the angle at which spins precess around the magnetic field to change until thermal equilibrium is restored[3]. T_2 relaxation, also known as spin-spin or transverse relaxation, involves the loss of spin phase coherence due to different nuclei experiencing different magnetic fields and precessing at slightly different frequencies[3]. In liquid NMR, T_1 and T_2 are typically of the same order of magnitude (seconds); however, for large molecules T_2 can be very short (milliseconds). This short T_2 would result in an extreme loss of signal over the diffusion time Δ in the pfg-se sequence. The pfg-ste pulse sequence utilizes two $\pi/2$ (or 90^o) pulses in place of the π pulse in the pfg-se sequence (Figure 1-4). This results in the nuclear magnetization being stored on the z axis for most of Δ and being subjected to only T_1 relaxation effects. The pfg experiment makes it possible to calculate the relative diffusion coefficient, *D*, by acquiring spectra over an array of gradient strengths. More details about pfg NMR and the measurement of *D* can be found in chapter three.

Cyclopropanes

Cyclopropane was first synthesized in 1881[13], and Henderson and Lucas discovered its anesthetic properties in 1929[14]. From the 1960s to the 1980s the chemists at W.R. Grace & Co synthesized dozens of fluorinated cyclopropanes (Figure 1-5) in an attempt to create an effective anesthetic to replace the potentially hazardous ethers and halogenated compounds used at the time. The samples were sent to the University of Florida NMR facility for characterization. The project was later abandoned, but the samples were preserved. Fluorinated cyclopropanes present an interesting research opportunity to analyze via NMR using modern high-field magnets. The strain associated with the small bond angles can have an effect on physical properties, and

the effect of different substituents on the chemical shift and coupling constants of the fluorine can be examined. Also, the results may shed light on the NMR properties of fluorine, which is widely used in pharmaceuticals due to the stability of carbon-fluorine bonds.

Amyloid

Alzheimer's disease (AD) is the most common form of dementia and it is estimated that 4.5 million Americans have AD. This includes more than 10% of the population over 65 and 50% of those over 85[15;16]. It is characterized by a loss of memory and changes in personality and behavior. There is some debate as to the root cause of AD, but the most widely accepted hypothesis presumes that cleavage of the amyloid precursor protein (APP) into neurotoxic amyloid-β (Aβ) peptide results in neurfibrillary tangles and cell death[17;18]. The brain tissue of patients demonstrating symptoms of AD at the time of death contains abnormal amounts of plaques, and the main component of these plaques is the Aβ peptide.

The full biological function of APP, a type I transmembrane protein, is not yet understood; but the mechanism by which APP is cleaved into Aβ has been well characterized. Three enzymes, α-, β-, and γ-secretase, cleave APP in different regions of the protein, with cleavage by β- and γ- resulting in Aβ (Figure 1-6). α-secretase cleaves APP within the Aβ sequence creating a benign soluble peptide , while β-secretase cleaves the protein in the extracellular region creating the N-terminus of Aβ, and γ–secretase cleaves within the cell membrane to create the C-terminus[19]. Aβ can range from 30-42 residues depending on where APP is cleaved; the plaques however are composed mainly of 39-42 residue peptides[20;21]. It has been demonstrated

that in membrane-mimicking environments the peptide adopts a typical transmembrane helical conformation[20;21]; in aqueous solutions the picture is less clear. Initially the peptide adopts a soluble random-coil formation, and upon environmental changes forms a self aggregating β-sheet structure. Aβ is a normal metabolic product of APP processing and is found in all individuals. The trigger that causes the conformational changes and subsequent plaque formation and onset of AD is of great interest[18]. Extensive work has been performed with the amyloid-β peptide and it has been shown that there are two regions of the peptide that form β-sheets, residues 16-24 and 31-40. It has also been shown that the conformational changes which lead to the β-sheets and aggregation can be brought about in vitro by changes in pH and temperature and by the addition of metal ions such as Al^{3+} and Zn^{2+} [20-23].

The primary limitation of the amyloid hypothesis is the lack of a strong correlation between the amount of plaques found in the brain and the degree of symptoms evident at time of death. Oligomers of Aβ remain soluble up to dimer and trimer states before they continue to aggregate and become insoluble plaques. Recent research suggests it is these soluble oligomers, not the plaques themselves, which elicit the toxic effect and lead to eventual cell death. Upon interaction with a membrane the oligomers can create an ion channel which destabilizes the ionic homeostasis and can lead to cell death[20;24;25]. Unfortunately not enough is known about the structure of the peptides in the membrane and how that structure differs from that in an aqueous environment.

Aβ (25-35) (Figure 1-6), containing the kink between the two β-sheet regions and a portion of the second β-sheet area, has been proposed to represent the biologically active region of the peptide; it represents the shortest fragment that exhibits large β-

sheet aggregated structures and retains the toxicity of the full length peptide[21]. The 11-residue peptide has been demonstrated to undergo a conformational change from a soluble random-coil to an aggregated β-sheet structure depending on environmental conditions[21].

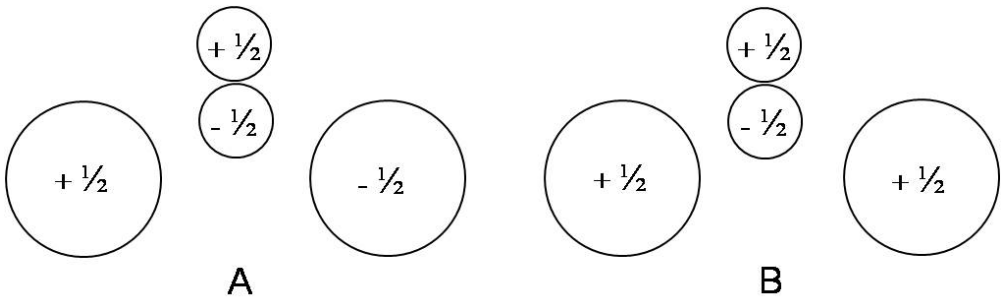

Figure 1-1. Nuclear and electron spins of two spin-½ nuclei. A) The instance where the nuclei are anti parallel. B) The instance where the nuclei are parallel. When the first instance is of lower energy, the coupling constant between the two nuclei is positive. When the second is of lower energy, the coupling constant is negative.

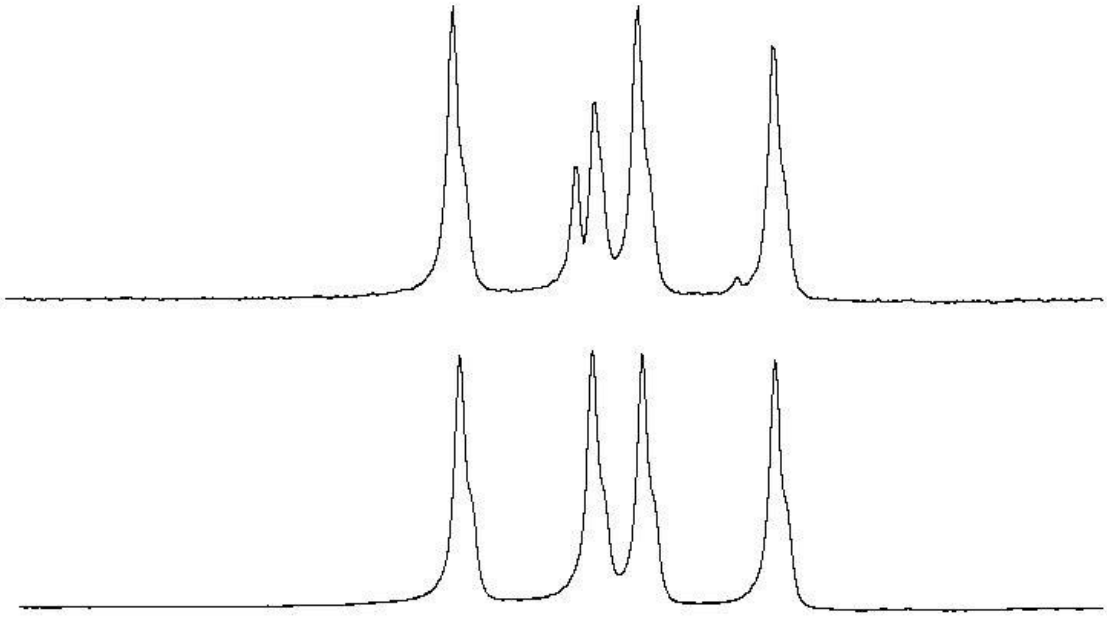

Figure 1-2. An example of the effects of a spin-tickling experiment. The bottom spectrum represents a conventional experiment while the top is from a double-resonance experiment where a spin-tickling pulse was applied to a transition connected to the second peak. Note the splitting of the second peak in the top spectrum.

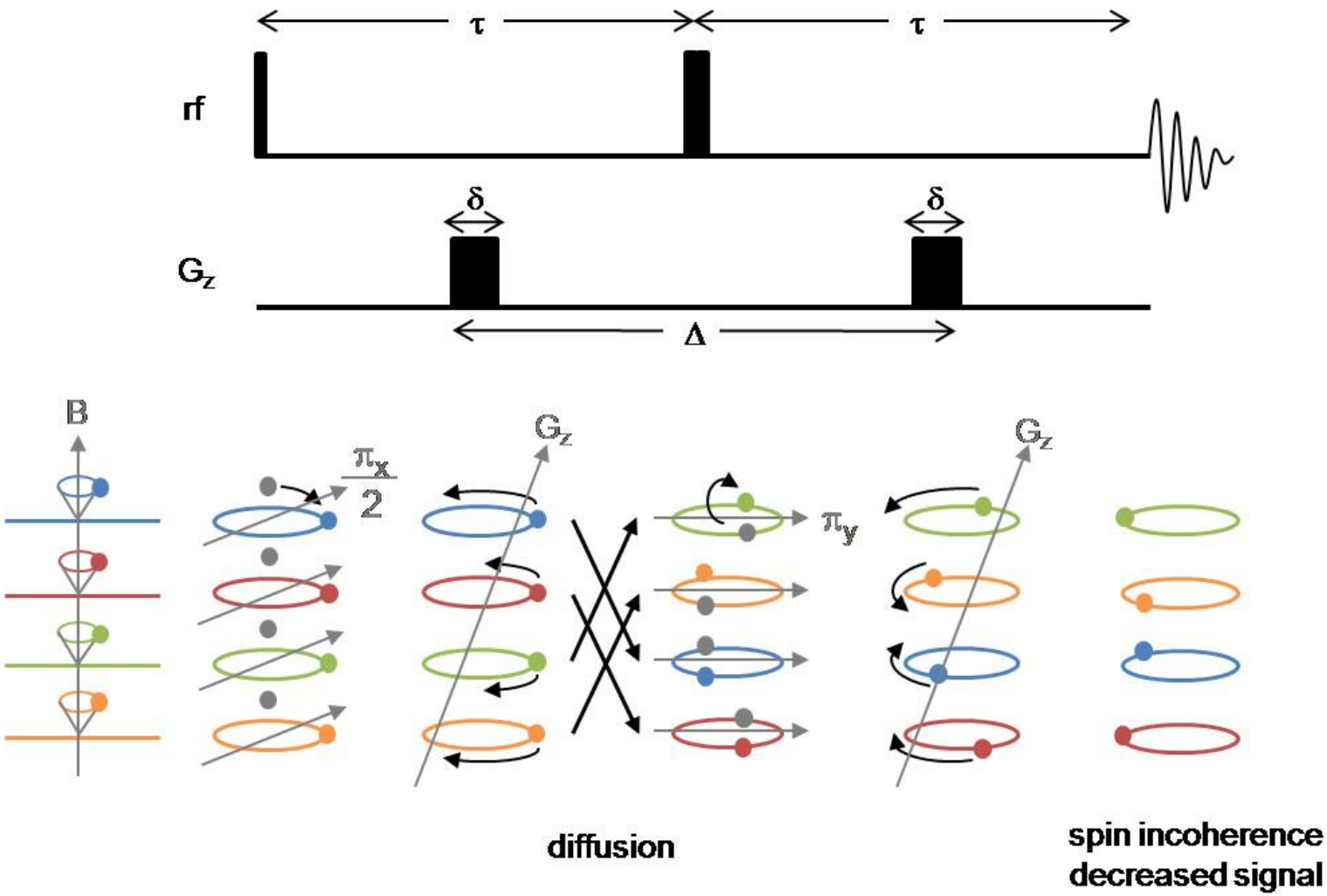

Figure 1-3. The pfg-se pulse sequence. In the absence of diffusion along the axis of the magnetic field, the spins are refocused and the signal is maximum. When the nuclei diffuse along the z axis, they experience a different gradient strength from the second gradient pulse and are not fully refocused, resulting in signal attenuation.

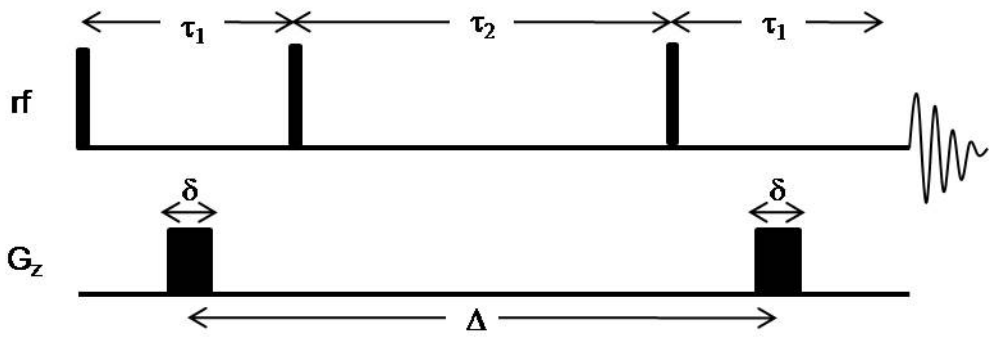

Figure 1-4. The pfg-ste pulse sequence. The 180° inversion pulse is replaced by two 90° pulses to store the nuclear magnetization along the z axis during τ_2 and eliminate T_2 relaxation effects.

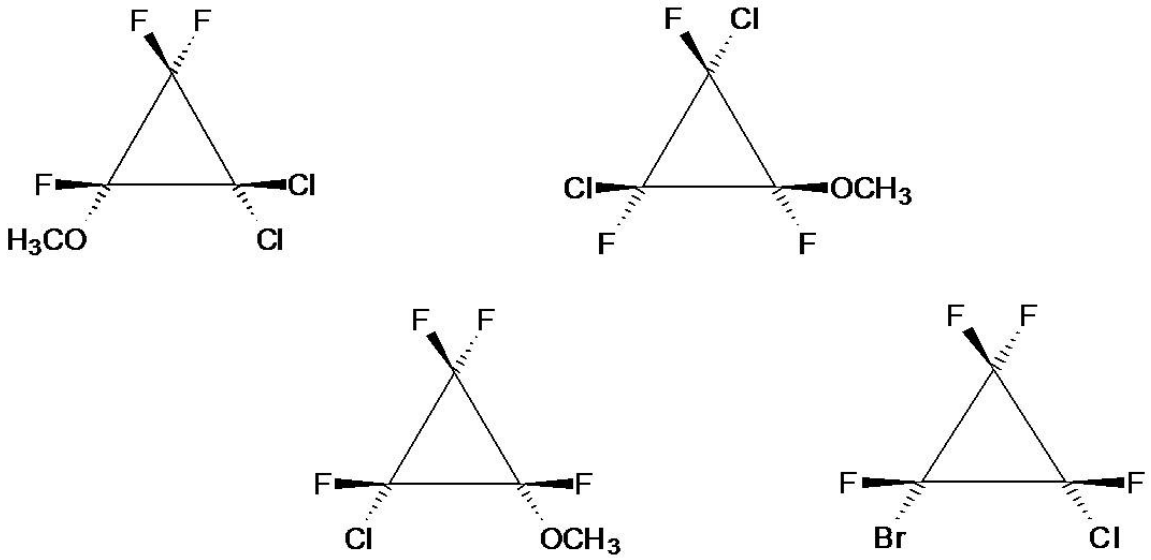

Figure 1-5. Representative cyclopropanes. All the molecules studied have at least three fluorines, and many are ethers.

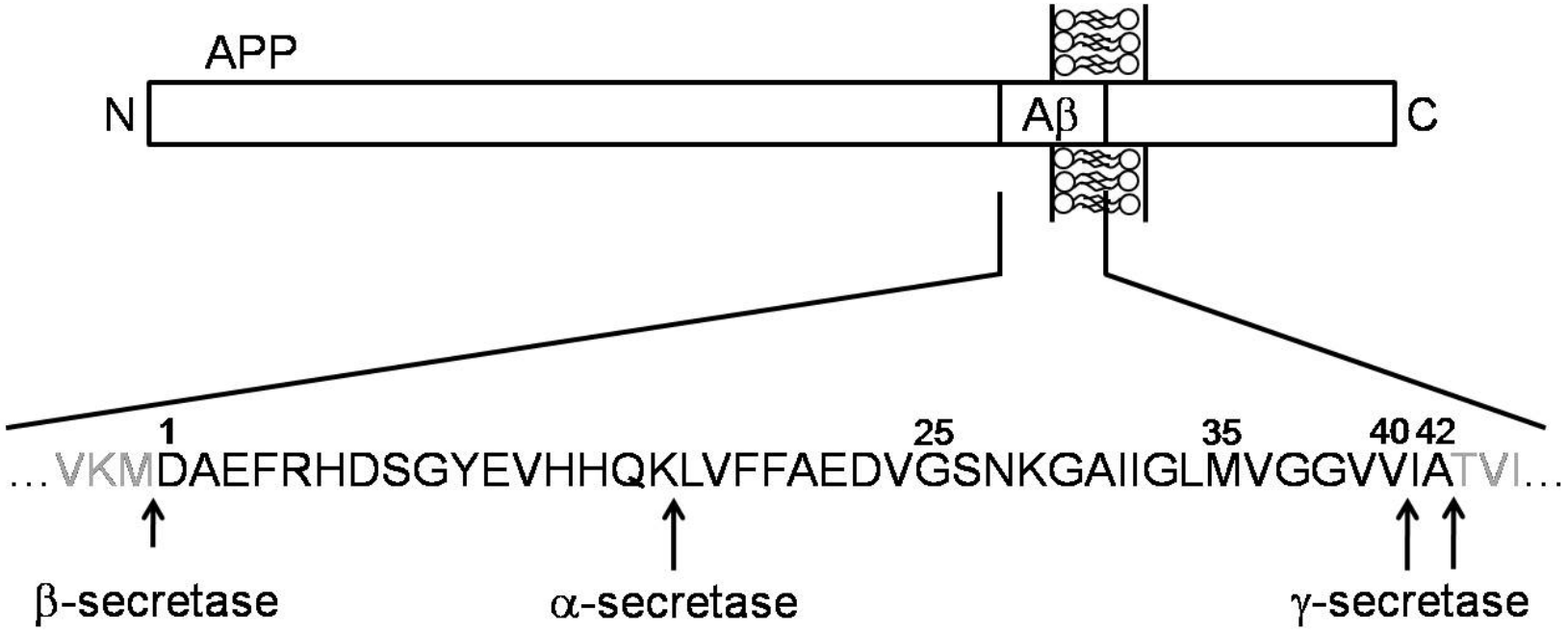

Figure 1-6. The amyloid precursor protein and the positions at which the three enzymes can cleave the protein to produce amyloid beta.

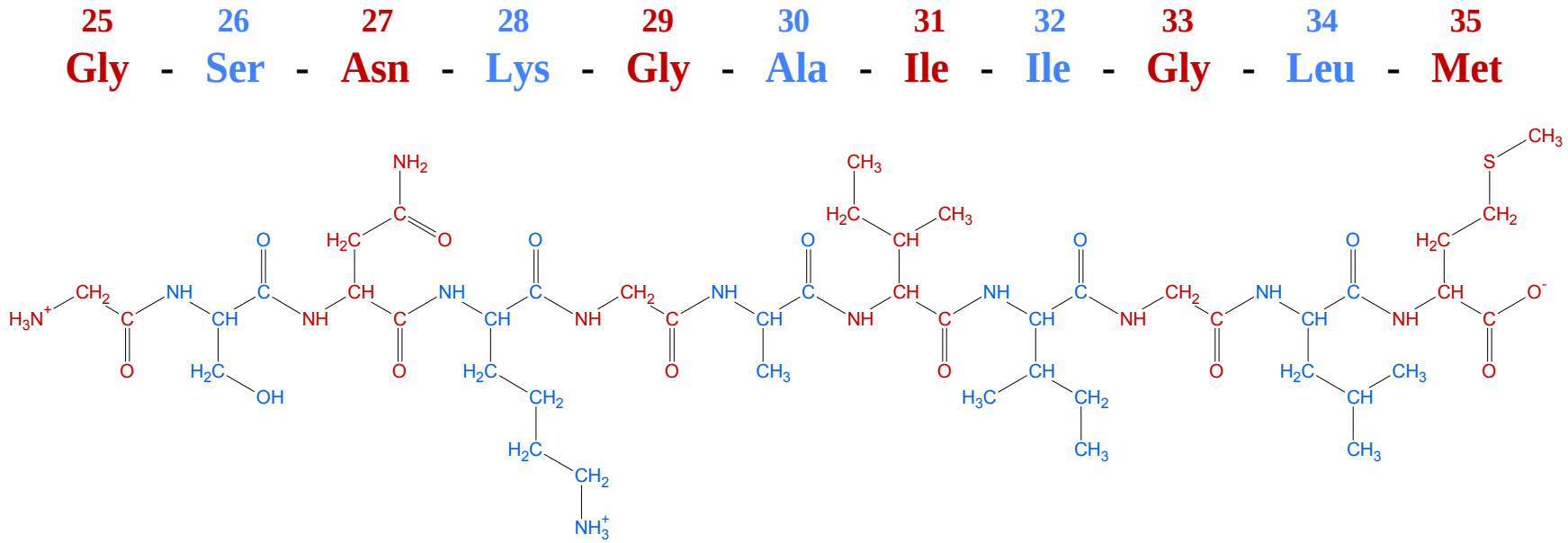

Figure 1-7. The sequence of amyloid beta (25-35).

CHAPTER 2
ANALYSIS OF THE RELATIVE SIGNS OF COUPLING CONSTANTS IN FLUORINATED CYCLOPROPANES

Introduction

Protonated cyclopropanes have been well characterized by NMR[26-32], but little work has been reported on fluorinated cyclopropanes. Sargeant[33] reported the magnitude of fluorine-fluorine coupling constants in various tetra- and pentafluorinated cyclopropanes, and Williamson and Braman[34] reported the signs and magnitudes of the coupling constants in trifluorinated cyclopropanes. Cavalli[35] reported the signs and magnitudes of the coupling constants in tetrafluorinated cyclopropanes and examined the effect of temperature on the magnitude of the coupling constants. In the present work, the signs of the vicinal fluorine-fluorine coupling constants in six fluorinated cyclopropanes were examined using double-resonance ^{19}F NMR and the effect of temperature on the magnitude of the coupling constants in nineteen fluorinated cyclopropanes was examined.

To fully understand the application of double-resonance NMR, a more thorough explanation of the experiment and its effect on the resulting spectrum is necessary. Figure 2-1 shows a theoretical energy level diagram for the transitions associated with a two-spin AM spin system where $J_{AM} = 0$. In the absence of coupling, the transition pairs for each nucleus (for instance $\alpha\alpha \rightarrow \alpha\beta$ and $\beta\alpha \rightarrow \beta\beta$) are of equal energy. This results in a spectrum containing two peaks corresponding to the frequency of each transition pair. However, when the nuclei are coupled together, the energy diagram changes and the spectrum includes four lines (Figure 2-2). The change in energy of an individual energy level depends on the strength of the coupling:

$$\Delta E = J_{AM}(m_A m_M) \qquad (2\text{-}1)$$

Following Eq. 2-1, two of the energy levels in the two spin system will increase by ¼ *J* and two will decrease by ¼ *J*. This results in the frequency of one of the transitions for each nucleus increasing in energy by ½ *J* and the other decreasing by ½ *J* (Figure 2-2). The two pairs of spectral lines corresponding to each nucleus are therefore separated by *J*. The energy-level diagram for a three-spin AMX system (Figure 2-3) is more complex but the effect of coupling remains the same. Up to now the sign of the coupling constant has been ignored, but it is evident from Eq. 2-1 that the sign will affect the energy diagram. Figure 2-4 shows the energy-level diagrams and resultant spectra for four sets of theoretical coupling-constant signs in a three-spin system. The similar transitions are color coded (for instance $\alpha\alpha\alpha \rightarrow \alpha\beta\alpha$ is navy blue across all four diagrams) to demonstrate the effect on the spectrum. The peaks and transitions for the upfield X nucleus are all left light blue for the sake of simplicity. In black and white all the spectra would be identical, and this is the reason the sign of the coupling constant is often ignored. However, it is the variation in position of the colored peaks that is the basis for the application of double-resonance NMR.

In a double-resonance (or spin-tickling) experiment, a weak rf pulse is applied to the frequency of one peak in the spectrum (that is, to one of the transitions in the energy diagram). This pulse results in a splitting of the peaks of any transition connected to the tickled transition. The nature of the splitting depends on the way the two transitions are connected. When the shared energy level lies between the two transitions, it is said to be a progressive connection, and when the shared energy level is above or below both transitions it is said to be a regressive connection (Figure 2-5)[5]. Progressive

connections result in a rather broad splitting while regressive connections result in a relatively sharp splitting (Figure 2-5). When multiple spectra are acquired with the tickling pulse placed on different transitions, the energy level diagram can be pieced together via which transitions are connected. Since changing the signs of the coupling constants results in different transitions being connected, the resulting diagram will only match the theoretical diagram calculated from one set of coupling constant signs.

Experimental

The cyclopropanes used for this research were synthesized decades ago in the laboratories of the Dewey and Almy division of W. R. Grace and Co. The samples were dissolved in deuterated acetone at a concentration of 20% vol. All spectra were acquired on either a Varian Mercury-300 equipped with a Varian ATB probe, or a Varian Inova-500 equipped with a Varian indirect-detection triple-resonance probe. The temperature for the variable temperature experiments was regulated using an FTS Systems XR401 Air-Jet equipped with a TC-84 temperature control unit. Four, eight, or 16 scans were acquired for each experiment. The spectral window was typically set to approximately -130 to -180 ppm (relative to $CFCl_3$) to maximize the digital resolution. The number of points was typically maximized to 128,000, resulting in acquisition times of around 5 seconds. For the double-resonance experiments, the decoupler modulation mode was set to continuous wave and the decoupler power was 1 dB. Double-resonance spectra were acquired with the tickling pulse placed on every transition and the multiple spectra were analyzed until the possible sets of coupling constant signs was narrowed down to one.

Results and Discussion

Temperature Dependence of Coupling Constants

Cavalli reported that an increase in temperature results in both *cis* and *trans* three-bond, or vicinal, coupling constants becoming more positive. Observation of the coupling constants over a range of temperatures would then help establish the sign, with negative coupling constants decreasing in magnitude and positive coupling constants increasing. Table 2-1 shows the change in magnitude of the couplings constants for nineteen cyclopropanes over a range from -20 to 25^{o}C. To simplify analysis and establish stereochemistry, numbers were assigned to each substituent position on the cyclopropyl ring (Figure 2-6). Substituent pairs one and two, three and four, and five and six are on the same carbons, and the odd and even positions are on the same sides of the ring. In general, most of the *cis* coupling constants have a positive temperature coefficient and most of the *trans* have a negative temperature coefficient. This agrees with Cavalli's results from CF_2-CFCl-CFCl where he also found J_{trans} to be negative and J_{cis} to be positive. Surprisingly, all of the $J_{3\text{-}6}$ *trans* couplings, corresponding to a CFCl coupling with a CF(OR), had a positive temperature coefficient. Also of note are the negative $J_{1\text{-}3}$ *cis* couplings found in molecules with a CCl_2. However, this agrees with the work of Williamson and Braman who found both J_{trans} and J_{cis} to be negative in various CF_2-CCl_2-CFX cyclopropanes.

Signs of Coupling Constants

Double-resonance experiments were performed on select cyclopropanes to compare with the results from the temperature study. Figure 2-7 shows the spectrum of CF_2-CFCl-CF($OCCl_3$) with the four highlighted peaks corresponding to one of the isomers. The effect on the spectrum with the application of a spin-tickling pulse to the

most downfield peak is shown in the expansions. A spin-tickling pulse was applied to each peak and a list of the connected transitions was compiled (Table 2-2). For simplicity, only three nuclei were considered at a time, as the energy-level diagram for a four-spin system becomes cumbersome to follow. Thus, two tables similar to Table 2-2 were constructed for each molecule/isomer. The connected transitions were compared to the energy-level diagrams of the four possible combinations of coupling-constant signs (Figure 2-8). The correct signs could typically be ascertained by simple analysis of the results of only one of the spin-tickling spectra. However, to avoid the possibility of misinterpretation of the slight splitting as regressive or progressive, analysis of all of the connected transitions was done, and the correct energy-level diagram was verified.

Analysis of Table 2-3 shows the sign and magnitude of the coupling constants for six cyclopropanes. The signs reported are relative to the two-bond, or geminal, CF_2 coupling constant being positive[10;34]. All but one of the J_{cis} values were found to be positive. This agrees with their positive temperature coefficients and Cavalli's assertion that the coupling constants become more positive with an increase in temperature. The exception is $J_{1\text{-}3}$ for CF_2-$CF(OCH_3)$-CCl_2, this represents a positive coupling constant with a negative temperature coefficient. The J_{trans} values present two deviations from the expected results. The values of $J_{2\text{-}3}$ *trans* were always negative which agree with their negative temperature coefficients. However, the values of $J_{2\text{-}5}$ and $J_{1\text{-}6}$ were found to be positive with negative temperature coefficients and the values of $J_{3\text{-}6}$ were negative with positive temperature coefficients. The last compound in Table 2-3, CFCl-CClF-$CF(OCH_3)$, has no geminal CF_2 to ascertain absolute sign, but the three coupling constants were found to be of the same relative sign. Regardless of the absolute sign,

at least one of the trends found in the other molecules for the signs of the coupling constants between particular substituent positions always having the same sign would be broken. All of these data point to the fact that the sign of coupling constants and their temperature coefficients do not necessarily correlate to bonding geometry and should not be used as the sole basis for assignment.

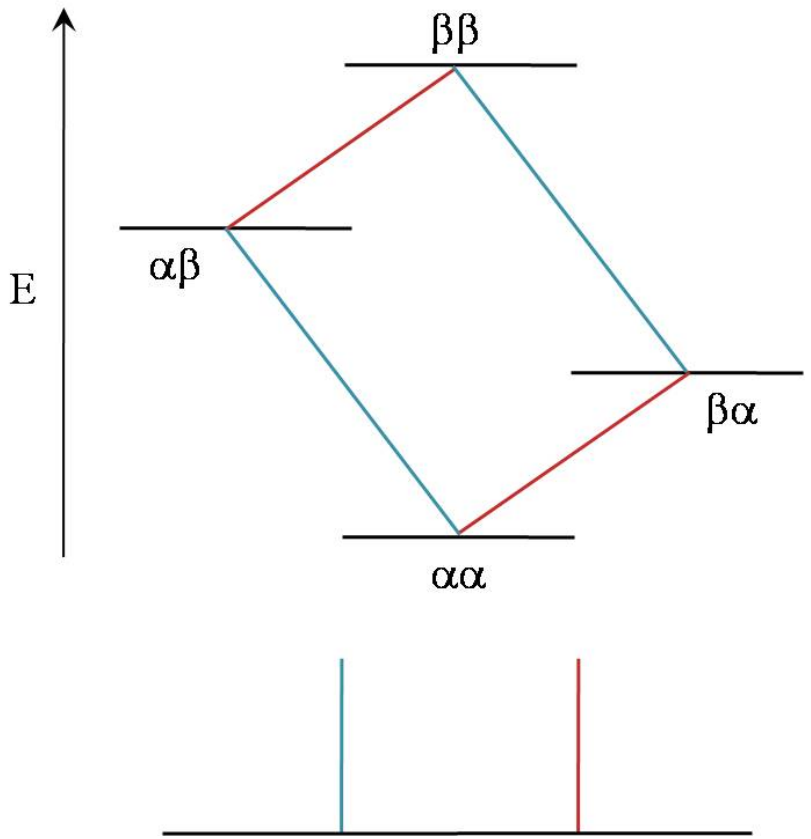

Figure 2-1. A theoretical energy-level diagram and corresponding spectrum for the transitions of a two-spin first-order system with no coupling.

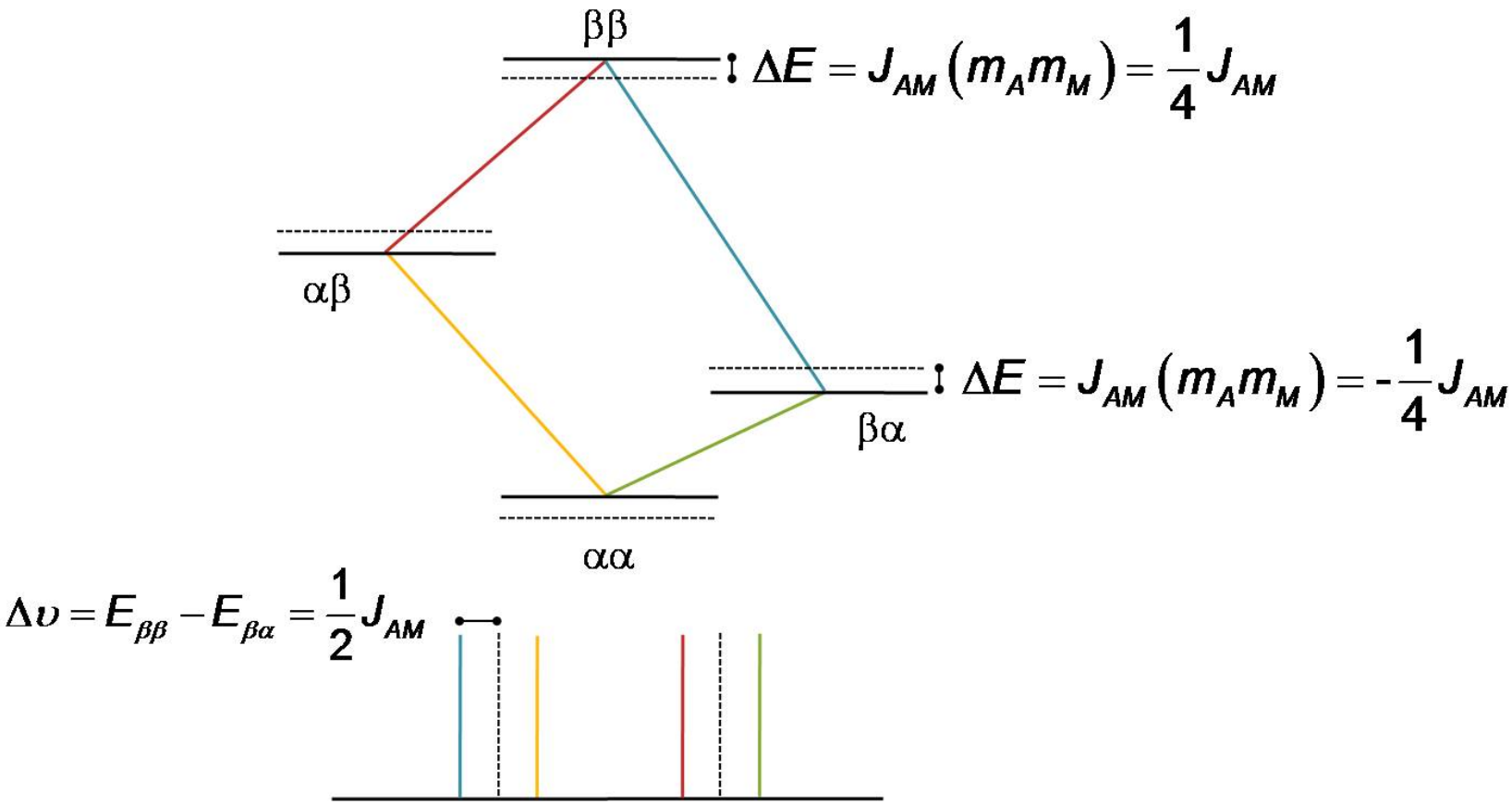

Figure 2-2. A theoretical energy-level diagram and corresponding spectrum for the transitions of a two-spin first-order system with coupling.

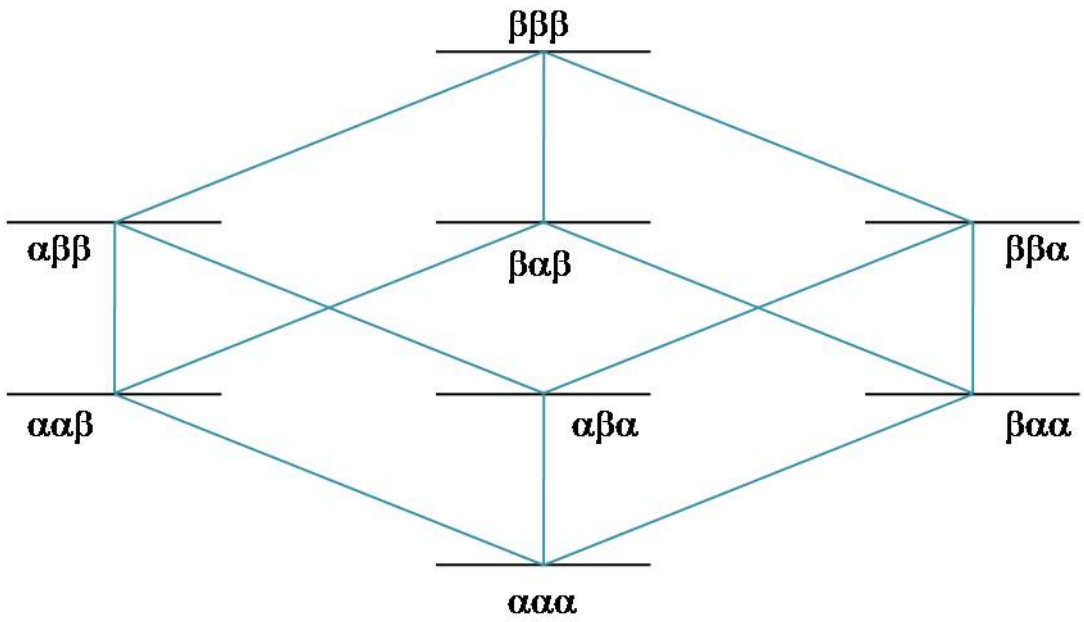

Figure 2-3. A theoretical energy-level diagram for a three-spin system.

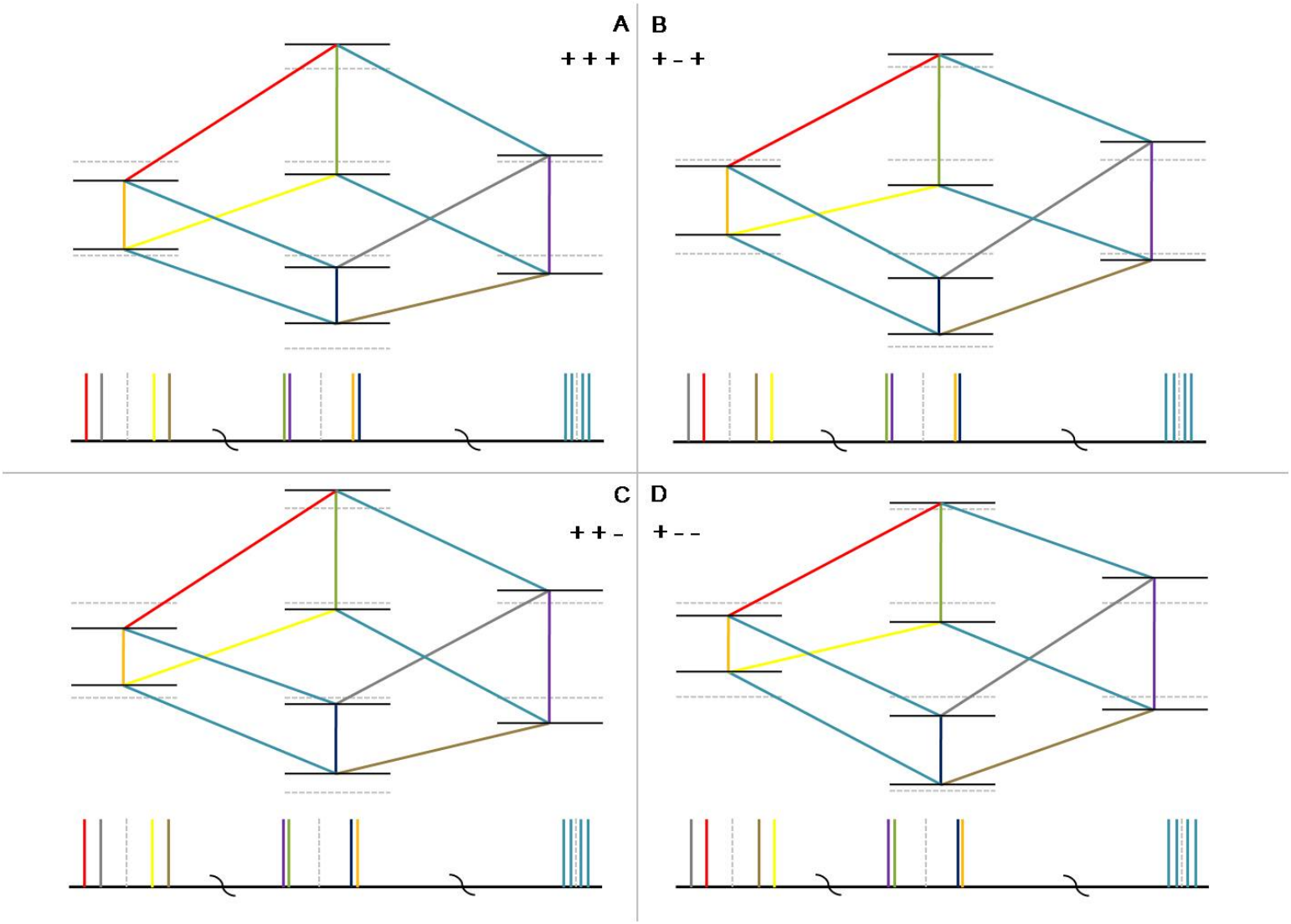

Figure 2-4. The effect of the sign of the coupling constants in a three-spin AMX system on the theoretical spectrum. J_{AM} is assumed to always be positive. A) all coupling constants are positive. B) J_{AX} is negative and J_{MX} is positive. C) J_{AX} is positive and J_{MX} is negative. D) both J_{AX} and J_{MX} are negative.

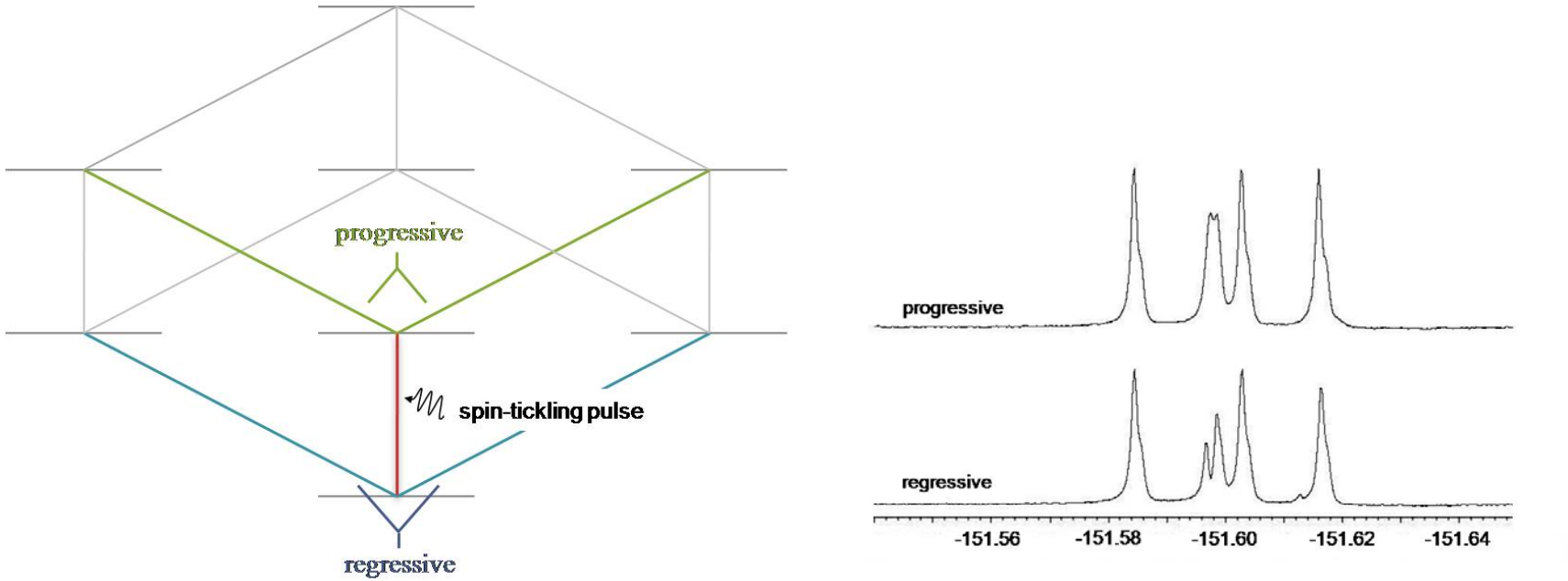

Figure 2-5. The difference between progressively and regressively connected transitions and their effect on the spectrum of a double-irradiation experiment.

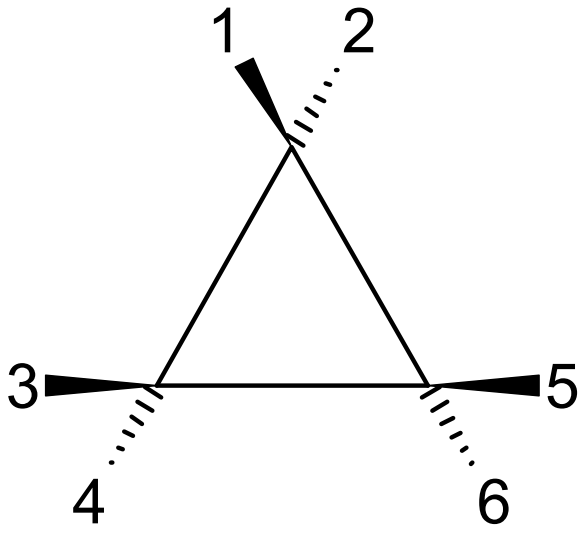

Figure 2-6. The numbering scheme assigned to the substituent positions of the cyclopropane.

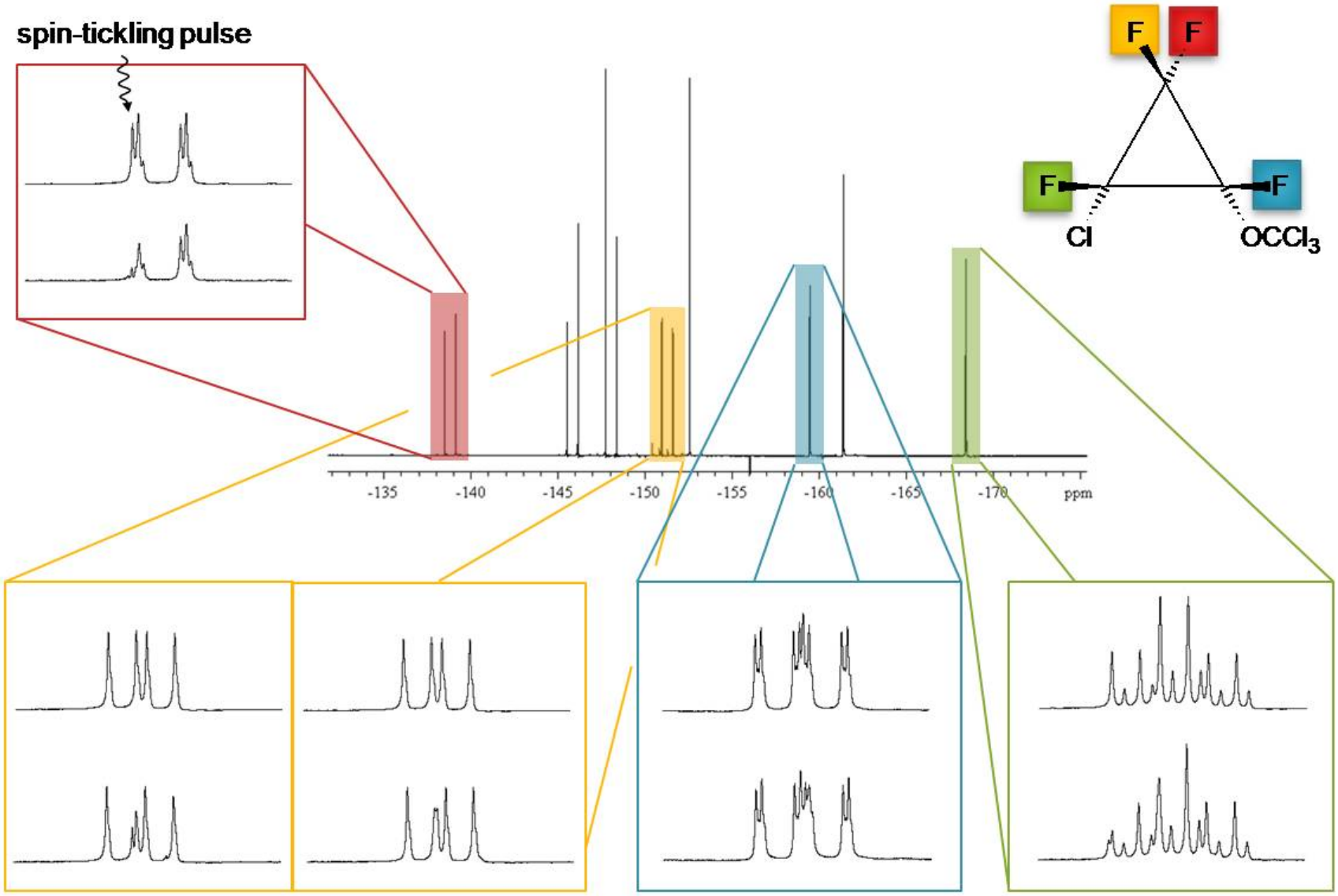

Figure 2-7. The effect of a spin-tickling experiment on the ^{19}F spectrum of CF_2-CFCl-CF($OCCl_3$).

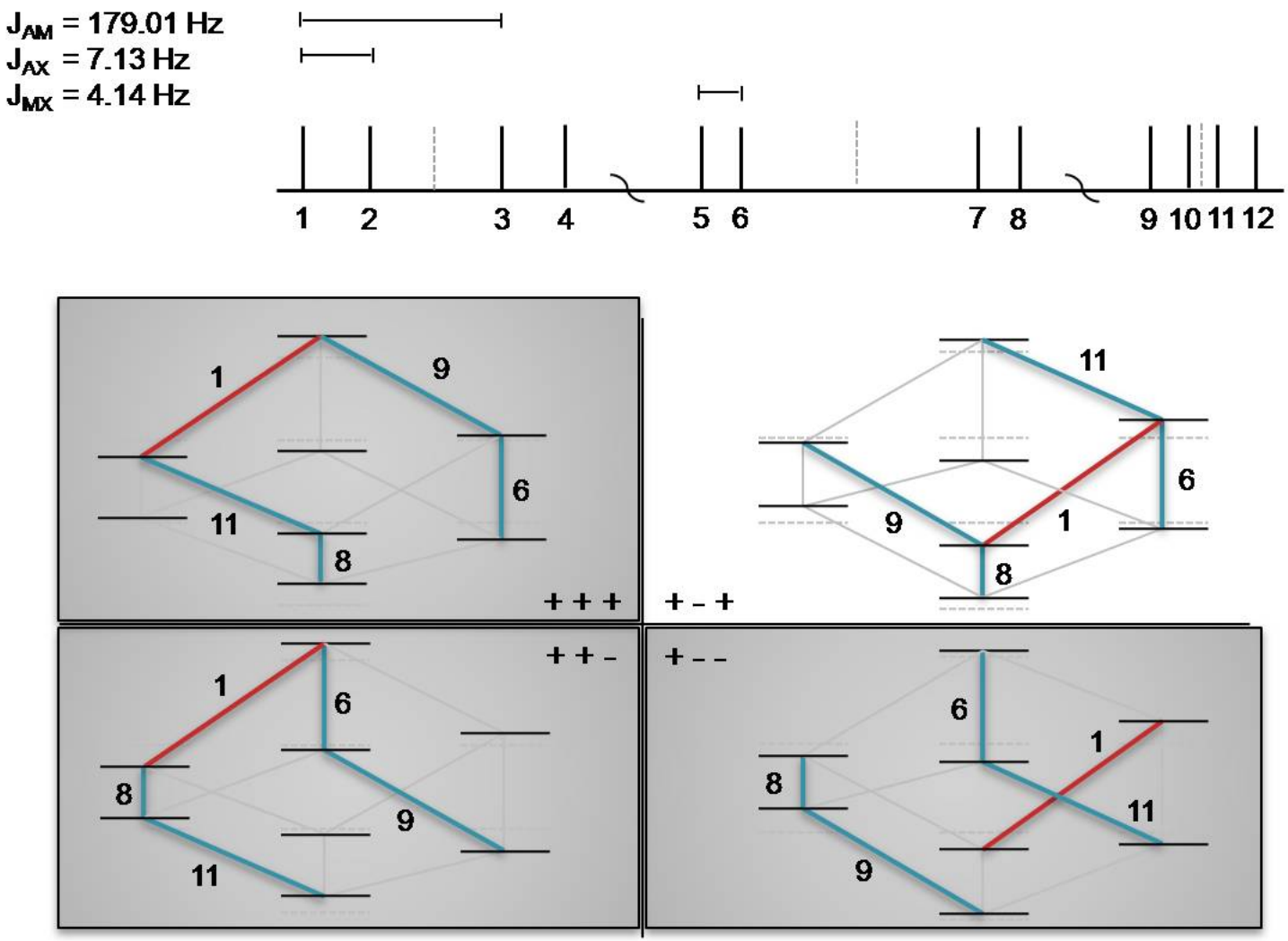

Figure 2-8. The possible sets of coupling-constant signs and their corresponding energy-level diagrams for CF_2-CFCl-CF($OCCl_3$). The labeled transitions correspond to the results in the first row of Table 2-2.

Table 2-1. The change in magnitude of the vicinal fluorine-fluorine coupling constants (Hz) with a change in temperature from -20°C to 25°C.

	cis			*trans*		
Compound[†]	*ΔJ(1-3)*	*ΔJ(1-5) or ΔJ(2-6)*	*ΔJ(3-5)*	*ΔJ(2-3)*	*ΔJ(1-6) or ΔJ(2-5)*	*ΔJ(3-6)*
CF_2 - CFCl - CFCl	+ 0.54	+ 0.54		- 0.13	- 0.13	
CF_2 - CFCl - $CF(OCH_3)$	+ 0.85	+ 0.47	+ 0.59	- 0.09	0	
CF_2 - CFCl - $C(OCH_3)F$	+ 0.51	nr[a]		- 0.23	+ 0.07	+ 0.22
CF_2 - CFCl - $CF(OCHCl_2)$	+ 0.61	+ 0.36	+ 0.69	- 0.07	- 0.11	
CF_2 - CFCl - $C(OCHCl_2)F$	+ 0.35	+ 0.33		- 0.06	- 0.09	+ 0.39
CF_2 - CFCl - $CF(OCCl_3)$	+ 0.42	+ 0.51	+ 0.39	- 0.12	- 0.05	
CF_2 - CFCl - $C(OCCl_3)F$	+ 0.65	+ 0.19		- 0.07	nr	+ 0.22
CF_2 - CFCl - $CF(OCHF_2)$	+ 0.48	+ 0.39	+ 0.39	- 0.06	- 0.15	
CF_2 - CFCl - $C(OCHF_2)F$	+ 0.35	+ 0.20		- 0.17	- 0.06	+ 0.29
CF_2 - CFCl - $CF(OCH_2F)$	+ 0.27	+ 0.78	+ 0.47	- 0.06	- 0.09	
CF_2 - CFCl - $C(OCH_2F)F$	+ 0.45	+ 0.23		- 0.15	0	+ 0.06
CF_2 - CFCl - $CF(OCF_2Cl)$	+ 0.45	+ 0.50	+ 0.39	- 0.14	- 0.06	
CF_2 - CFCl - $C(OCF_2Cl)F$	+ 0.45	+ 0.23		- 0.09	+ 0.11	+ 0.15
CF_2 - $CF(CH_3)$ - CCl_2	0			- 0.49		
CF_2 - $CF(CF_3)$ - CCl_2	- 0.94			- 0.65		
CF_2 - $CF(OCH_3)$ - CCl_2	- 0.30			+ 0.18		
CFCl - CFCl - $CF(OCH_3)$	+ 0.52					
CFCl - CFCl - $C(OCH_3)F$					+ 0.04	
CFCl - CClF - $CF(OCH_3)$		+ 0.08		- 0.07[b]	- 0.39	

[a]not resolved, [b]*ΔJ(1-4),* [†]The substituent positions 1-6 on the ring are defined in Figure 2-6. The chemical formula is written in such a way that the positions 1 and 2 are on the first carbon in sequential order, positions 3 and 4 on the second carbon, and 5 and 6 on the third

Table 2-2. List of the connected transitions for CF_2-CFCl-$CF(OCCl_3)$.

Double-resonance peak[†]	Connected transitions	
	Regressive	Progressive
1	6, 9	8, 11
2	5, 9	7, 11
3	8, 10	6, 12
4	7, 10	5, 12
5	2[a]	4[a]
6	1, 12	3, 11
7	4, 9	2, 10
8	3[a]	1[a]
9	1, 7	2, 8
10	3, 8	4, 7
11	2, 5	1, 6
12	4, 6	3, 5

[a]The effect of some spin-tickling pulses could not be resolved due to complication from coupling with the fourth fluorine in the spin system or overlap with peaks resulting from the isotope effect. [†]The peak numbering scheme can be found in Figure 2-8.

Table 2-3. The sign and magnitude of the vicinal fluorine-fluorine coupling constants (Hz) in fluorinated cyclopropanes.

Compound[†]	*cis*			*trans*		
	J(1-3)	*J(1-5) or J(2-6)*	*J(3-5)*	*J(2-3)*	*J(1-6) or J(2-5)*	*J(3-6)*
CF_2 - CFCl - $CF(OCH_3)$	+ 6.54	+ 5.73	+ 3.80	- 5.13	+ 2.85	
CF_2 - CFCl - $C(OCH_3)F$	+ 6.87	nr[a]		- 5.85	+ 2.40	- 4.37
CF_2 - CFCl - $CF(OCCl_3)$	+ 4.14	+ 5.71	+ 7.17	- 7.13	+ 0.86	
CF_2 - CFCl - $C(OCCl_3)F$	+ 1.81	+ 1.44		- 7.06	nr	- 7.16
CF_2 - $CF(OCH_3)$ - CCl_2	+ 2.50			- 5.50		
CFCl - CClF - $CF(OCH_3)$		2.28[c]		11.93[b,c]	4.43[c]	

[a]Not resolved, [b]*J(1-4)*, [c]The compound contains no CF_2 to ascertain absolute sign. [†]The substituent positions 1-6 on the ring are defined in Figure 2-6. The chemical formula is written in such a way that the positions 1 and 2 are on the first carbon in sequential order, positions 3 and 4 on the second carbon, and 5 and 6 on the third.

CHAPTER 3
ANALYSIS OF THE AGGREGATION OF AMYLOID BETA (25-35)

Introduction

There is a great deal of research involving Alzheimer's Disease and the amyloid beta peptide. While the current trend entails utilizing the whole 40-42 residue peptide, it is not uncommon to find recent articles involving Aβ(25-35)[36-42]. In fact, Aβ(25-35) is often used as a model for the behavior of the full length peptide because it retains both the physical and biological properties, and is easier to synthesize and derivatize due to its relatively short 11 amino acid sequence[43].

The genesis of this research goes back to observations made during earlier work in this laboratory. Similar samples prepared by previous researchers appeared to show reversible aggregation upon placement in and removal from the refrigerator. Samples were stored in the refrigerator and when removed for analysis they appeared cloudy and viscous. Thought to be ruined, they were left on the laboratory bench to be discarded. Upon warming to room temperature they became clear and liquid. This process was repeated with similar results. No quantitative analysis was performed. The goal of the current research was to use NMR to analyze the effects of temperature and other sample conditions such as concentration on the apparent aggregation. We also hoped to measure the oligomerization equilibrium and estimate the size and shape of the oligomers.

Experimental

The synthetic Aβ(25-35) peptide was obtained from Dr. John West at Florida A&M University. A 1 mM stock solution was made using 16.6 mg peptide and deionized water with the pH adjusted to 3.4 using deuterium chloride. Attempts to make samples

using unadjusted pH water were unsuccessful. All samples made with water from pH 5-7 became very viscous gels within five minutes and were unsuitable for liquid NMR analysis. Samples of concentrations greater than 1 mM were made on an individual basis using low-pH deionized water. Unless otherwise noted, deuterated water was added to all samples such that H_2O:D_2O was 90%:10% volume to volume.

All experiments were performed on a Varian Inova-500 MHz spectrometer equipped with a Varian indirect-detection pulsed-field-gradient probe. All standard proton spectra were acquired using the presat pulse sequence to suppress the water peak. A saturation delay of 1.00 second and a saturation power of 15 dB was used. The acquisition time was 2.90 seconds and the recycle delay was 1.00 second. Depending on the concentration of the sample, either 64 or 128 scans were acquired. For the pulsed-field-gradient experiments, the gradient was arrayed from 20-60 G/cm using either 10 or 15 steps with intervals such that the squares of the gradient strengths were linearly spaced. Either 16 or 32 scans were acquired for each step. The gradients were applied for 1250 μs with a diffusion time of 0.10 seconds. The two-dimensional experiments were all acquired with an acquisition time of 0.36 seconds, a recycle delay of 1.00 second, and a mixing time of 150 ms. The TOCSY (or total correlation spectroscopy) experiments were acquired using the tnTOCSY pulse sequence with a saturation delay of 1.00 second and a saturation power of 10 dB, the number of increments was either 256 or 400, and 32 scans were acquired for each increment. The ROESY (or rotating frame nuclear Overhauser effect spectroscopy) experiments were acquired using the tnROESY pulse sequence with a saturation delay

of 1.00 second and a saturation power of either 2 or 5 dB; the number of increments was either 512 with 20 scans per increment, or 768 with 16 scans per increment.

Gradient Calibration

The strength of the gradient pulses had to be calibrated using a compound with a known diffusion coefficient. The acquisition software generates an array of the experimental parameter *dac_p1* (dac units). This value is sent to a digital-to-analog converter and is translated to an actual gradient strength, *G* (gauss/cm), by multiplication with another parameter, *grad_p_coef* ((gauss/cm)/dac units):

dac_p1 × *grad_p_coef* = *gradient strength*, *G* (3-1)

By observing the signal intensity of a reference compound over an array of *dac_p1*, the appropriate value of *grad_p_coef* can be calculated with Eq. 3-2 using the expected diffusion coefficient.

$$\ln(A_i) = \ln(A_0) + D(-\gamma^2\delta(\Delta - \frac{1}{3}\delta))G_i^2 \quad (3\text{-}2)$$

Equation 3-2 relates the observed intensity, *A*, and the gradient strength, *G*, to the diffusion coefficient, *D*. The diffusion time, Δ, and the length of the gradient pulses, δ, are both experimental parameters; and γ, as previously noted is the magnetogyric ratio.

Lysozyme from chicken egg white was obtained from Sigma-Aldrich. A 10 mg/mL lysozyme solution in D_2O was used to calibrate the gradient strength. A value of 11.0 × 10^{-7} cm^2/s [44] corrected by a factor of 1.23 for the increased viscosity of D_2O[45;46] was used for the diffusion coefficient of lysozyme. The intensity of three regions in the lysozyme spectrum was observed over a range of fifteen gradient strengths from 20 to 60 G/cm. The natural log of these three sets of intensities was plotted against the square of the gradient strength (Figure 3-1) and a linear regression was applied. From

Eq. 3-2, the slope of the line is proportional to the diffusion coefficient. Using the known value for the diffusion coefficient, the expected slope can be calculated with Eq. 3-3.

$$m = D \times \left[-\gamma^2 \delta^2 \left(\Delta - \frac{\delta}{3} \right) \right] \tag{3-3}$$

The value of *grad_p_coef* was adjusted, changing the values of G^2 in Figure 3-1, so that the average slope of the three regression lines equaled the expected slope.

The calibration was verified using bovine serum albumin obtained from Sigma-Aldrich. A 10 mg/mL solution was prepared in D_2O. The intensities of the peaks corresponding to the methyl side-chain protons in alanine, isoleucine, and leucine were observed over a range of fifteen gradient strengths from 20 to 60 G/cm. The natural log of these sets of intensities was plotted against the square of the gradient strength (Figure 3-2). A linear regression was applied to the three data sets and the slopes were used to calculate *D* using Eq. 3-3. The average measured diffusion coefficient, corrected by a factor of 1.23 for the increased viscosity of D_2O, was $6.09 \times 10^{-7} \pm 3 \times 10^{-9}$ cm^2/s compared to the literature value of 5.8×10^{-7} cm^2/s [47;48].

Temperature Regulation

The standard method of regulating the temperature of the sample in an NMR spectrometer is not appropriate for diffusion measurements. A coil, slightly below the sample (Figure 3-3), intermittently heats the nitrogen flowing into the probe to regulate the temperature. This can result in a temperature gradient across the sample from top to bottom. Since the diffusion coefficient is calculated based on movement of nuclei along the z axis, the presence of a temperature gradient must be avoided. A temperature gradient will result in convective flow and lead to additional displacement of spins along the z axis and to an overestimation of the diffusion coefficient[49-52].

To avoid convection, the temperature of the nitrogen flowing into the probe was regulated upstream using an external variable-temperature unit (Figure 3-3), and the heating coil in the probe was disabled. To account for thermal conduction over the longer flow path of the nitrogen, the regulator on the external unit had to be set below the desired sample temperature when running below room temperature and above the desired temperature when running above room temperature. The samples were left to equilibrate for a minimum of thirty minutes after the temperature readings from both the external control unit and the thermocouple in the probe were stable. The temperature remained constant to a tenth of a degree celsius during all experiments.

Chemical Shift Referencing

When reporting chemical shift data it is imperative to use a suitable standard compound as a reference. This is especially true with biomolecular NMR where it is common to make assumptions about the secondary structure of peptides and proteins based on chemical shifts. Unfortunately there is a wide array of reference compounds, many of which have chemical shifts that vary with changes in pH, temperature, and solvent composition[53-56]. For this work all reported chemical shifts are relative to internal 2,2-dimethyl-2-silapentane-5-sulfonic acid (DSS). The chemical shift of DSS has been shown to be insensitive to changes in solvent, temperature, and pH[55].

Results and Discussion

Chemical Shift Evaluation and Assignment

To verify the sequence of the synthetic peptide was correct, all peaks had to be assigned to their respective residues and the order the residues are connected had to be analyzed. The reasons for this are two-fold. Due to an error in synthesis, we have two versions of the solid Aβ(25-35) peptide, one with the correct sequence and one

missing an isoleucine. To ensure the proper peptide was used, the sequence needed to be verified. Also, to analyze any changes in chemical shifts, it was necessary to know which peaks belong to which residues.

The peaks were assigned using a combination of proton, TOCSY, and ROESY spectra. Due to significant overlap, as is typical with biomolecular NMR, it was impossible to assign and calculate chemical shifts for many peaks using only the proton spectra (Figure 3-4). Assignment was done following the procedure known as the sequential assignment strategy developed by Wüthrich *et al.*[57] and further outlined by Cavanagh *et al.*[58]. Since each residue represents an individual spin system, a peptide of *N* residues has *N* distinct backbone-based spin systems[58]. The first stage of assignment typically involves a two-dimensional scalar correlation experiment such as COSY or TOCSY. Each type of amino acid gives rise to a characteristic peak pattern based on its side-chain protons. Analysis starts in the fingerprint region of the spectrum, where the cross peaks resulting from the correlation of the alpha and side chain protons to the amide protons can be observed (Figure 3-5). Distinct horizontal or vertical lines, depending on which fingerprint region is used, connect the peaks of each individual residue at the chemical shift of the amide proton for that residue. Examination of the peak pattern yields a straight-forward assignment of which amino acid the peaks represent.

The amide protons of the asparagine side chain are not part of the same spin system as the backbone amide and alpha protons. In the same that way each residue forms an individual spin system isolated by the backbone amide bonds, the amide bond in the asparagine side chain isolates the amide protons. However, these protons

appear at distinctive chemical shifts, 6.8 and 7.5 ppm (Figure 3-5), and the only overlap is with the amine proton of the lysine side chain, which is easily distinguished by its correlation to the other lysine protons. Also, the asparagine side chain amide protons show correlation with each other via chemical exchange, making the assignment apparent.

Analysis of the TOCSY spectrum helps assign each peak to a particular residue but yields little information about the placement of the residue in the peptide sequence. Determination of the sequence and discrimination of degenerate residues is step two of the sequential assignment strategy[57;58].

Assignment of Duplicate Residues

The second stage of the sequential assignment strategy involves distinguishing the duplicate glycine and isoleucine residues of Aβ(25-35), and requires the use of nuclear Overhauser enhancement and exchange spectroscopy (NOESY). Two-dimensional NOESY spectra yield cross peaks for nuclei in close spatial proximity[57]. The assignment of ambiguous residues, and verification of the whole peptide sequence itself, is established by observing cross peaks (off-diagonal peaks) between the amide and alpha protons of neighboring residues $\left({}^1\mathrm{H}_i^{\mathrm{N}} - {}^1\mathrm{H}_{i-1}^{\alpha}\right)$.

While the intensity of the cross peak, for a given experimental mixing time, is relative to the distance between two nuclei, there are limits to that intensity imposed by the spectrometer frequency, ω_o, and the molecular correlation time τ_c[58;59]. The homonuclear nuclear Overhauser enhancement, as a function of τ_c, ranges from 0.5 for small molecules to -1 for macromolecules (Figure 3-6)[5]. Unfortunately, at the frequency

of modern high field spectrometers, the correlation time of peptides (on the order of nanoseconds) corresponds to the range where the NOE is nearly zero.

Rotating frame Overhauser effect spectroscopy (ROESY) was developed by Bothner-By *et al.*. to overcome this problem[59]. Originally termed CAMELSPIN (cross-relaxation appropriate for minimolecules emulated by locked spins), ROESY has the advantage that the rotating frame Overhauser effect (ROE) is positive for all correlation times, with a minimum of 0.38 for small molecules and a maximum of 0.68 for macromolecules[58;59]. Therefore, ROESY is useful in the examination of peptides, or any molecules with similar correlation times, where the laboratory frame NOEs are nearly zero[58].

ROESY was used to differentiate glycine-29 and glycine-33 (the assignment of glycine-25 was apparent due to its placement at the N-terminus of the peptide), and isoleucine-31 and isoleucine-32. Figure 3-7 shows an expansion of the alpha-amide region above the diagonal of the ROESY spectrum of 0.69 mM Aβ(25-35) in 80% D_2O and 20% d_3-TFE acquired with a mixing time of 150 ms. Many ${}^1H_i^N$-${}^1H_{i-1}^{\alpha}$ cross peaks can be seen, but the cross peak at the chemical shift of an ambiguous glycine amide proton (8.35 ppm) and the lysine-28 alpha proton (4.28 ppm) was used to assign glycine-29. Similarly, the cross peaks between the isoleucine-31 amide proton (7.96 ppm) and alanine-30 alpha proton (4.34 ppm), and glycine-33 amide proton (8.27 ppm) and isoleucine-32 alpha proton (4.17 ppm) were used to assign the isoleucines and remaining glycine respectively. A cross peak can also been seen at the chemical shift of the isoleucine-32 amide (8.00 ppm) and isoleucine-31 alpha (4.17 ppm) protons, further confirming the assignment of the two isoleucines. Figure 3-8 presents a similar

picture, this time an expansion of the alpha-amide region below the diagonal, of the ROESY spectrum of 6.5 mM Aβ(25-35) in 90% H_2O and 10% D_2O. However, this spectrum better demonstrates some of the difficulties in assigning peptide spectra. Of note, the alpha protons of glycine-29 and glycine-33 are not resolvable, nor are the amide and alpha protons of isoleucine-31 and isoleucine-32. The cross peak at the chemical shift of the glycine-29 amide proton (8.39 ppm) and lysine-28 alpha proton (4.29 ppm) was used to distinguish the glycines. The combination of the TOCSY and ROESY spectra was used to assign each peak and verify the peptide was in fact the known Aβ(25-35) sequence.

Chemical Shift Results

Complete assignments of Aβ(25-35) at two concentrations in 90% H_2O and 10% D_2O are shown in Tables 3-1 and 3-2. There are many ways to analyze and interpret peptide chemical shifts[60-64], but perhaps the most straight-forward approach is the $\Delta\delta$ technique developed by Dalgarno *et al.*[60]. The $\Delta\delta$ technique utilizes the finding that alpha protons shift upfield for residues in α-helix regions and downfield for β-sheet regions[60;65-67]. The chemical shift of the alpha protons is very dependent on the orientation of the C^{α}-H bond axis relative to the adjacent C=O bond axis[68]. As a result, the chemical shifts of the alpha protons can be used to estimate local secondary structure. This technique relies on the comparison of observed chemical shifts to known random-coil shifts (Eq. 3-4).

$$\Delta\delta = \delta_{RC} - \delta_{Obs} \tag{3-4}$$

It has been shown that the alpha protons can shift by as much as 1 ppm from their expected random-coil chemical shift[60;67] and that the mean shifts in helices and sheets

differ by as much as 0.8 ppm with little overlap[64]. Many tables of random-coil chemical shifts can be found in literature[53-55;69;70]. For this work, the table suggested by Wishart and Nip[69] was used.

Figure 3-9 shows the $\Delta\delta$ plot for the alpha protons of 6.71 mM Aβ(25-35) in 90% H_2O and 10% D_2O at 2.53. All of the chemical shifts are very near their expected random-coil chemical shift, with the largest $\Delta\delta$ shift being 0.06 ppm for the N-terminal glycine. This indicates the observable Aβ(25-35) in a solution of 90% H_2O and 10% D_2O adopts a random-coil conformation. This also validates our chemical-shift calculation and assignment method. The results (not shown) for the alpha protons of 3.47 mM Aβ(25-35) in similar sample conditions were comparable, with the largest $\Delta\delta$ shift being -0.06 for the serine-26 proton. It should, however, be noted that the alpha protons for glycine-25 and asparagine-27 were not observed due to solvent exchange and overlap with the solvent peak, respectively.

Effect of TFE

2,2,2-trifluoroethanol (TFE) has been shown to mimic the lipid environment of the cell membrane and promote α-helices[71]. It has also been shown that TFE does not promote new structures in small peptides, but rather stabilizes helices inherent to the entire protein[72]. An α-helical Aβ structure has been suggested as an intermediate on the way from a mostly unstructured peptide to β-sheet-rich Aβ fibrils[73-77].

Deuterated TFE (d_3-TFE) was used as a co-solvent and the chemical shifts were again measured. Table 3-3 shows the complete assignment of 0.69 mM Aβ(25-35) in 80% H_2O and 20% d_3-TFE. The results are remarkably similar to the chemical shifts found in a mixture of H_2O and D_2O except for the amide protons. This is most likely due

to the sensitivity of the amide protons to the change in hydrogen bonding with the addition of TFE. A mixture of TFE and water has a reduced capacity for forming hydrogen bonds compared to just water[76]. There is also little change in the $\Delta\delta$ plot (Figure 3-10) compared to Aβ in just water, with the largest shift from the expected random-coil value being -0.07 for both serine-26 and leucine-34. All of the chemical shifts for the alpha protons after the addition of 20% d_3-TFE are within 0.03 ppm of the results without TFE except for methionine-35, which changed by 0.07 ppm. This is most likely a result of its position on the C-terminus, and the sensitivity of the carboxylic acid to the change in hydrogen bonding. These results, indicating soluble Aβ(25-35) remains a random-coil even in the presence of low concentrations of TFE, contradict previously published results. Using circular dichroism and NMR, Lee *et al.*. found Aβ(25-35) has a random-coil structure in water and adopts a helical structure from isoleucine-31 to methionine-35 in the presence of TFE[78]. This is perhaps a result of the higher TFE content in their solvent. They published the full assignment of chemical shifts for 1 mg Aβ(25-35) in 0.4 mL of 1:1 (vol/vol) d_3-TFE:H_2O at pH 4.0. Surprisingly, virtually all of their chemical shifts for each proton (including the side chain protons) on every residue are significantly more downfield (as much as 0.11 ppm and on average 0.06 ppm) than the results found here, contradicting the thought that the protons of helical residues shift upfield.

Kohno *et al.*. also concluded that the C-terminal region (lysine-28 through methionine-35) of Aβ(25-35) adopted a helical conformation in a membrane mimicking environment[79]. They published the chemical shift results for 2 mM Aβ(25-35) in 90% H_2O and 10% D_2O at pH 4.0 with 250 mM LiDS-d_{25}. Their alpha proton chemical shifts

for serine-26 and asparagine-27 were similar to the results found here, but lysine-28 through methionine-35 were all shifted upfield, as expected for helical regions, by an average of 0.11 ppm. Sticht *et al.*. examined 2.5 mM Aβ(1-40) with 40% TFE at pH 2.8[80]. Their chemical shift results were similar to those published by Kohno *et al.*., and they concluded Aβ forms a helix from lysine-28 to valine-40.

The absence of a C-terminus helix in this work is presumably the result of the relatively low percentage of TFE used. A mixture of 80% H_2O and 20% TFE was chosen due to the prohibitive cost of d_3-TFE. This conclusion is supported by the work of D'Ursi *et al.*[21]. They examined Aβ(25-35) with varying ratios of hexafluoroisopropanol (HFIP), another membrane-mimicking solvent, and water. They found that Aβ(25-35) adopted a random-coil conformation up to 40% HFIP and the helix content increased almost linearly up to 80% HFIP.

Effect of metal ions

Transition metals, such as Cu(II) and Zn(II), have been implicated in the development of Alzheimer's disease[81-83]. They are found in elevated concentrations in amyloid plaques[22;84;85] and have been shown to promote or even induce aggregation[86-90]. The current consensus in the literature suggests the binding site is near the N-terminus of amyloid peptide, with the histidine-6,13, and 14 side chains, the N-terminus itself, and the carboxylate groups of aspartic acid-1 and glutamic acid-11 being potential ligands[85-87;91]. Interestingly, Aβ(25-35) has no known metal binding sites, but aggregates more readily than other fragments and maintains the toxicity of the full length peptide.

Copper(II) and zinc(II) were added at various molar ratios and the chemical shifts of Aβ(25-35) were measured (Tables 3-4 through 3-7). All of the results are remarkably similar, and comparison to the results with no metal (Table 3-3) reveals little change. The largest shift was 0.05 ppm for the amide protons of the N-terminal glycine-25 in the sample with 3:1 zinc-to-peptide molar ratio. These protons readily exchange with the solvent and in some instances were not even observed. The comparatively large shift could easily be a result of error in chemical-shift calculation due to the small signal-to-noise ratio of the peak. The mean shift for all the metal samples compared to the sample with no metal was 0.0009 ppm, an insignificant amount. The lack of any observed changes in chemical shift indicates there was no change in the peptide with addition of the metal ions.

The spectra were also examined for line broadening. Gaggelli *et al.* observed large chemical-shift variations and selective line broadening for the previously mentioned ligand protons with the addition of Zn(II) to a membrane mimicking solution of Aβ(1-28)[87]. Similar results have also been observed with Aβ(1-40), Aβ(1-28), and Aβ(1-16)[92-95]. Not surprisingly, no broadening was observed. This confirms the chemical shift result, that there is no specific binding of Aβ(25-35) with the metal ions.

This defies the qualitative observation on the disposition of the samples. Figure 3-11 shows a picture of three samples made at the same time with similar sample conditions, 1.84 ± 0.06 mM Aβ(25-35) in 90% H_2O and 10% D_2O. The samples which appear cloudy include a 3:1 molar ratio of Cu(II) or Al(III) and the sample which appears clear has no added metal ions. The appearance of the samples indicates some sort of interaction between the peptide and the metal ions. When this observation is combined

with the lack of change in the NMR data, it suggests some of the peptide aggregated into a high-order oligomer that was unobservable via liquid NMR and the peptide remaining in solution was unchanged. The presumed equilibrium of the peptide (Figure 3-12) includes soluble monomer and low-order oligomers along with unobservable insoluble high-order oligomers. Since all of the spectra include fairly well resolved and sharp peaks, it is assumed we observed random-coil monomer and once aggregation was triggered it went all the way to high-order oligomers. This is confirmed by the fact that the only observable change between spectra of clear samples and cloudy samples acquired under identical conditions was a decrease in signal intensity (Figure 3-13).

Effect of temperature

The effect of temperature on the chemical shifts of the amine protons was also examined. The temperature dependence of the chemical shifts of amine protons has a somewhat dubious past when used as the only evidence for suggesting peptides exist in particular conformations, but they are often used to support the findings of other techniques. The amine protons of random-coil peptides have been shown to display $\Delta\delta/\Delta T$ values of -7.8 ± 1.2 ppb/^{o}C in aqueous solutions[70;96], while the amine protons of structured peptides typically display a less negative (<-4 ppb/^{o}C) temperature dependency[97;98]. The change in the chemical shifts of the amine protons of 2.82 mM Aβ(25-35) in 90 H_2O and 10% D_2O was linear in the observed range of 5 to 65^{o}C (Figure 3-14) and the average $\Delta\delta/\Delta T$ value was -7.6 ppb/^{o}C with the lowest being -5.8 ± 0.1 ppb/^{o}C for alanine-30 (Table 3-8). These results further suggest the presence a random-coil peptide.

Diffusion Results

In the absence of aggregation, a plot of log *D* versus 1/*T* should follow the Arhhenius relationship and have a linear slope[99]:

$$\ln(D_i) = \ln(D_0) - \left(\frac{E_a}{RT_i} \right) \tag{3-5}$$

To verify experimental setup and parameters, the diffusion coefficient of the same lysozyme sample used to calibrate the gradient strength was acquired in five degree increments over a range of 5-55^{o}C (Figure 3-15). Ilyina *et al.* reported lysozyme does not aggregate at this concentration over this temperature range[47]. The linearity of the data in Figure 3-15 confirms this.

All diffusion data reported here is the result of integrating the peaks corresponding to the side-chain methyl protons on the leucine and isoleucines (Figure 3-16). The diffusion coefficient of 2.82 mM Aβ(25-35) was measured in five degree increments from 5-70^{o}C (Figure 3-17). To further verify what appears to be a deviation from linearity around 22^{o}C (or 3.39×1000/K), data were measured approximately every 2.5^{o}C from 5^{o}C to 25^{o}C. A linear regression was applied over the whole range of temperatures and a second linear regression was applied from 25-70^{o}C and the residuals were plotted (Figure 3-17). The parabolic behavior of the residuals from the regression applied over the whole range of temperatures indicates the data are not linear. Additionally, a linear regression was applied to the lower temperatures (22^{o}C to 5^{o}C, or 3.39×1000/K to 3.60×1000/K) and the upper-95%-confidence-limit slope (-2.40) was compared to the lower-95%-confidence-limit slope of the regression applied to the higher temperatures (-2.10). The change in linearity over the two temperature ranges appears to be statistically significant. This could be the result of the peptide self

aggregating or a conformational change which increased the hydrodynamic radius at lower temperatures.

The effect of concentration on the diffusion over a range of temperatures was examined. The diffusion coefficients of three concentrations of the peptide were measured from 5-55^{o}C (Figure 3-18, Table 3-9). There appears to be no dependence of the diffusion on concentrations in the mM range. All of the values are in good agreement and, if nothing else, validate the reproducibility of the experiment. The diffusion was also measured at two pH values with a concentration of 2.82 mM (Figure 3-19, Table 3-10). There were slight differences at lower temperatures, but all of the values were within error of one another. As previously mentioned, attempts to make samples with pH values closer to neutral were unsuccessful and the solutions quickly turned to viscous gels unsuitable for diffusion measurements. While there is no mention of similar observations about neutral pH samples becoming highly viscous, the common trend in literature is to use pH values around four[21;78;79]. The diffusion was measured with the addition of Zn(II) at a 3:1 molar ratio as well (Figure 3-20, Table 3-11). There were slight differences at higher temperatures, but the low temperature values were all in good agreement.

In an attempt to observe a change in the measured *D*, samples of 50 and 100 μM were made. The diffusion coefficients of these samples were measured at 25^{o}C and compared with the higher millimolar concentration samples (Figure 3-21). There appears to be no change from 50μM up to 6.75mM. Additionally, formic acid has been shown to dissolve protein aggregates and help in the analysis of peptides that are not easily solvated[100]. 2.3 mg of the raw amyloid powder was dissolved in formic acid. The

solution was left to sit for 15 minutes and the formic acid was blown to leave slightly wet crystals. The resulting solid was then dissolved in 90% H_2O and 10% D_2O and the *D* of the resulting 2.6 mM solution was measured at 25°C (Figure 3-21). This resulted in no change of the observed diffusion coefficient.

The lack of any significant difference in the measured *D* over all the different sample conditions, combined with the chemical shift result, suggests low-order soluble oligomers were never observed. The signal that was observed must have been from monomeric peptide and the aggregation that occurred resulted in high order oligomers which could not be detected using liquid NMR. Systematic error, such as that which could result from not allowing sufficient time to equilibrate the temperature of the sample, is ruled out because the lysozyme data, which was acquired under similar conditions, did not deviate from linearity at lower temperatures. The observation of visible aggregation accompanied by no change in the diffusion coefficient is supported by the recently published findings of researchers working with the whole 40 residue amyloid-beta peptide[101]. Filippov *et al.* noted that "it is surprising that the visually observed state of the sample and the self-diffusion do not completely correspond to one another." They came to a similar conclusion: "In the course of peptide aggregation, no signal attributed to dimers arises, while the aggregation itself is easy to observe visually." They also noted that it has previously been found that the low-order oligomers are not stable intermediate products in the course of Aβ aggregation[102;103].

Collectively, the NMR data presented in this chapter indicate that the visible aggregates (Figure 3-11) are too large to be observed by high-resolution NMR spectra acquired under the given conditions due to their excessively short T_2 relaxation times[104].

Furthermore, the lack of any change in the diffusion coefficient under conditions which induce visible aggregates also indicates that it is unlikely any significant amounts of low-order oligomers such as dimers and trimers are formed. While the low-order oligomers could result in peaks unseen upon visual inspection of the spectra, they would affect the diffusion measurements. The signal intensities, *A* values, used to calculate *D* (Eq. 3-2) represent the total intensities across a given chemical shift range. If low-order oligomers were present, the calculated *D* would represent a weighted average of the diffusion coefficients based on the relative concentrations of the monomer and low-order oligomers. However, as is shown in the following, this possibility is excluded by the close agreement between the observed diffusion coefficient and the theoretically predicted value for monomeric Aβ(25-35).

The diffusion coefficient of a particle is related to its size by the Stokes-Einstein equation:

$$D = \frac{k_B T}{6\pi\eta r_H} \tag{3-6}$$

where k_B is the Boltzmann constant, T is temperature, η is solvent viscosity, and r_H is hydrodynamic radius. The r_H of a peptide is given by[105;106]:

$$r_H = \left[\frac{3M(V_2 + \delta_1 V_1)}{4N_0}\right]^{\frac{1}{3}} \tag{3-7}$$

where M is mass, V_1 and V_2 are the specific volumes of the particle and solvent, δ_1 is the solvent fraction bonded to the particle, and N_o is Avogadro's number. The self-diffusion coefficient of a particle with mass M is given by[101]:

$$D = \frac{k_B T}{6\pi\eta\Phi}\left[\frac{4\pi N_0 \rho}{3M(V_2 + \delta_1 V_1)}\right]^{\frac{1}{3}} \tag{3-8}$$

where Φ is the form factor and ρ is particle density. When calculating D, the following assumptions were made: the monomer has a globular conformation, particles are spherical (Φ=1), and the effects of interparticle interactions can be ignored[101]. The expected diffusion coefficient for Aβ(25-35) at 25°C was calculated using the following values from the literature, ρ = 1300 kg/m^3 [104], η = 9.088$_2$ × 10^{-4} kg/m·s (the viscosity of water corrected for the 10% volume fraction of D_2O), and δ_1 = 0.328[107]. The calculated diffusion coefficient was 2.71 × 10^{-6} cm^2/s, which compares very well with the experimentally determined value of 2.69 × 10^{-6} cm^2/s. This result is consistent with the absence of any liquid-NMR-observable low-order oligomers.

A minimum mass for the non-observable high-order oligomers was estimated using an assumed maximum observable spectral line width. The full-width-at-half-maximum NMR line width, $\Delta\nu_{FWHM}$, for a nucleus dominated by spin-spin relaxation due to dipolar interactions, as would be expected for protons in the visible aggregates, is given by:

$$\Delta\upsilon_{FWHM} = \frac{1}{\pi T_2} \tag{3-9}$$

where[3]:

$$T_2^{-1} = \frac{3}{20} b^2 \left[3J(0) + 5J(\omega) + 2J(2\omega)\right] \tag{3-10}$$

The normalized spectral density function J is given by[3]:

$$J(\omega) = \frac{\tau_c}{1 + \omega^2 \tau_c^2} \tag{3-11}$$

where τ_c is the rotational correlation time. The dipolar coupling constant, *b*, from eq. 3-10 is given by[3]:

$$b = -\frac{\mu_0}{4\pi}\frac{\hbar\gamma^2}{r^3} \tag{3-12}$$

where *r* is the distance between the spins. For this work a distance of 0.2 nm was used, corresponding to a $b/2\pi$ (for conversion from radians to Hz) of -15.012 kHz [3]. The rotational correlation time, τ_c, is given by[108]:

$$\tau_c = \left[2(D_x + D_y + D_z)\right]^{-1} \tag{3-13}$$

According to the Perrin ellipsoidal shape approximation[109;110], the diffusion tensor elements D_x, D_y, and D_z are given by:

$$D_l = \frac{k_B T}{f_l} \tag{3-14}$$

where:

$$f_x = \frac{16\pi\eta(a_y^2 + a_z^2)}{3(a_y^2 Q + a_z^2 R)} \tag{3-15}$$

$$f_y = \frac{16\pi\eta(a_x^2 + a_z^2)}{3(a_z^2 R + a_x^2 P)} \tag{3-16}$$

$$f_z = \frac{16\pi\eta(a_x^2 + a_y^2)}{3(a_x^2 P + a_y^2 Q)} \tag{3-17}$$

Here, a_x, a_y, and a_z are the semi-axes of a general ellipsoid. The parameters *P*, *Q*, and *R* are the following ellipsoidal integrals:

$$P = \int_0^\infty \frac{1}{\sqrt{(a_x^2 + s)^3(a_y^2 + s)(a_z^2 + s)}}\,ds \tag{3-18}$$

$$Q = \int_0^\infty \frac{1}{\sqrt{(a_y^2 + s)^3 (a_z^2 + s)(a_x^2 + s)}} ds \tag{3-19}$$

$$R = \int_0^\infty \frac{1}{\sqrt{(a_z^2 + s)^3 (a_x^2 + s)(a_y^2 + s)}} ds \tag{3-20}$$

Combining equations 3-9, 3-10, 3-13, and 3-14 relates aggregate size to spectral line width.

Three geometric models were used to estimate line width, a 2D beta-sheet topology, a spherical model, and an ellipsoidal model. In all the models *n* is the number of monomer units in the aggregate, the length of the distended Aβ(25-35) monomer was assumed to be 4.4 nm in length and 1 nm in thickness. The hydration layer was taken to be 2.8 nm per side[104]. Approximating the 2D beta-sheet as an ellipsoid with a constant thickness in the y axis, the dimensions (in cm) along the x, y, and z axis increase with *n* as:

$$a_z = 44 \times 10^{-8}$$

$$a_y = (10.0 + 2 \times 2.28) \times 10^{-8}$$

$$a_x(n) = (10.0 \times n + 2 \times 2.28) \times 10^{-8}$$

For the ellipsoid model where a_x=a_y:

$$a_z = 44 \times 10^{-8}$$

$$a_x(n) = a_y(n) = (10.0 \times n^{\frac{1}{2}} + 2 \times 2.28) \times 10^{-8}$$

For the spherical model the hydrodynamic radius was taken to be 0.886 nm (from eq. 3-7). The volume of the monomer (in cm^3) is given by:

$$V_m = \frac{4}{3} \pi (8.86 \times 10^{-8})^3$$

Taking the volume of the oligomer to be proportional to *n*:

$$V = V_m n$$

The radius increases with *n* as:

$$a_x(n) = a_y(n) = a_z(n) = \left(\frac{3nV_m}{4\pi} \right)^{\frac{1}{3}}$$

In all three models, a line width of over 100 Hz is obtained after only around 10 monomer units (giving a total mass of ~10 kDa) have aggregated (Figure 3-22).

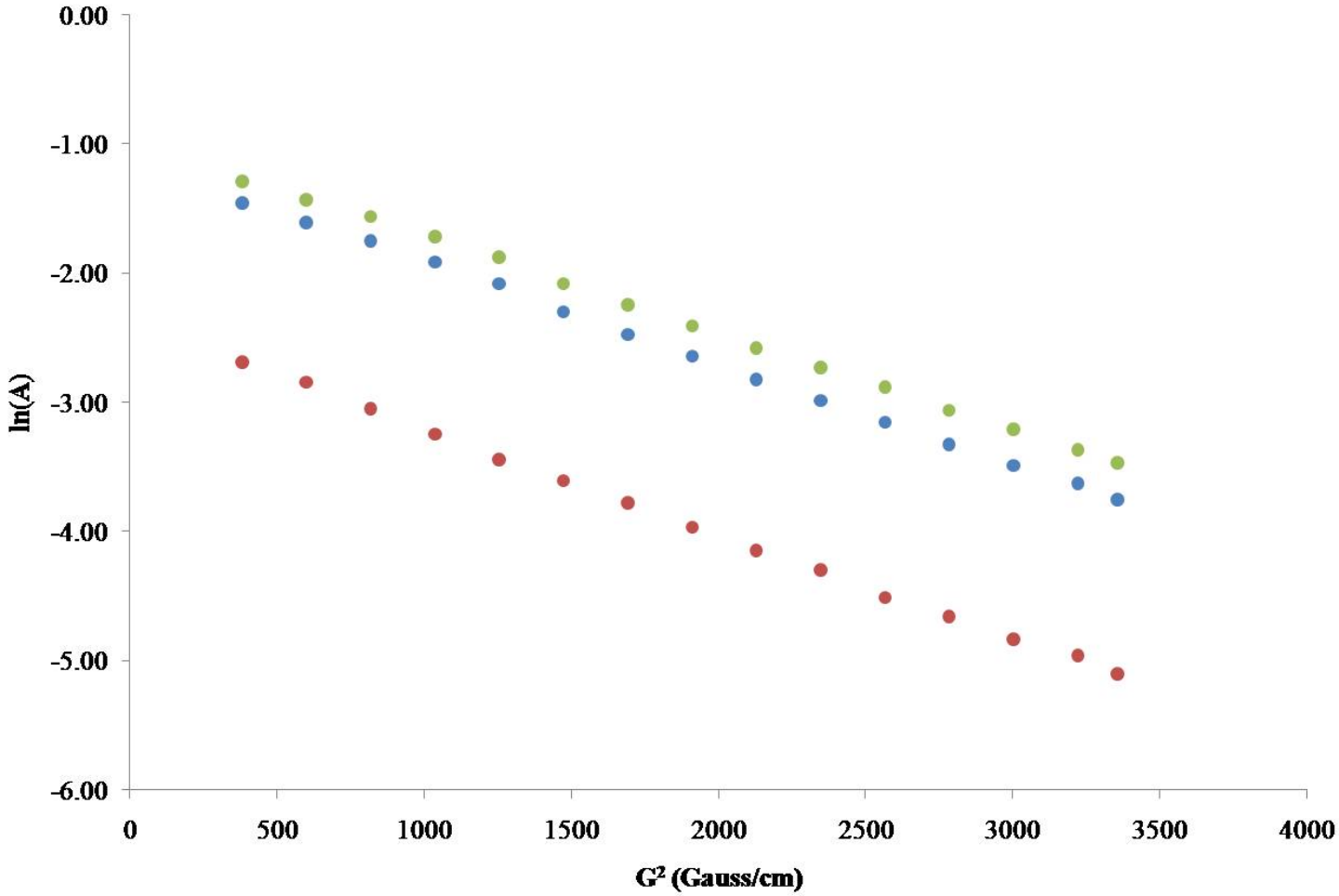

Figure 3-1. Amplitude of 10 mg/mL lysozyme signal for three spectral regions over a range of gradient strengths.

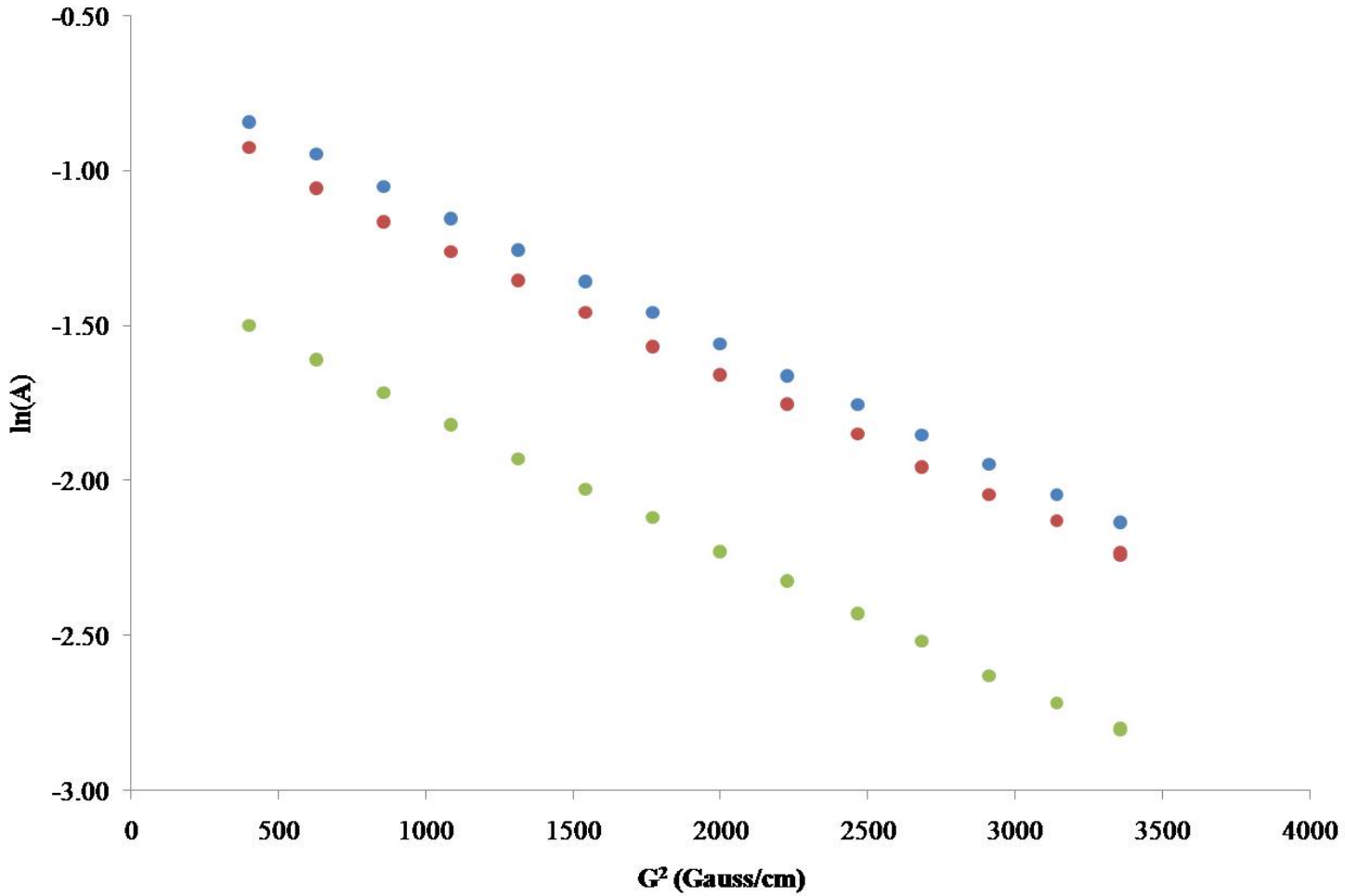

Figure 3-2. Amplitude of 10 mg/mL BSA signal for three spectral regions over a range of gradient strengths.

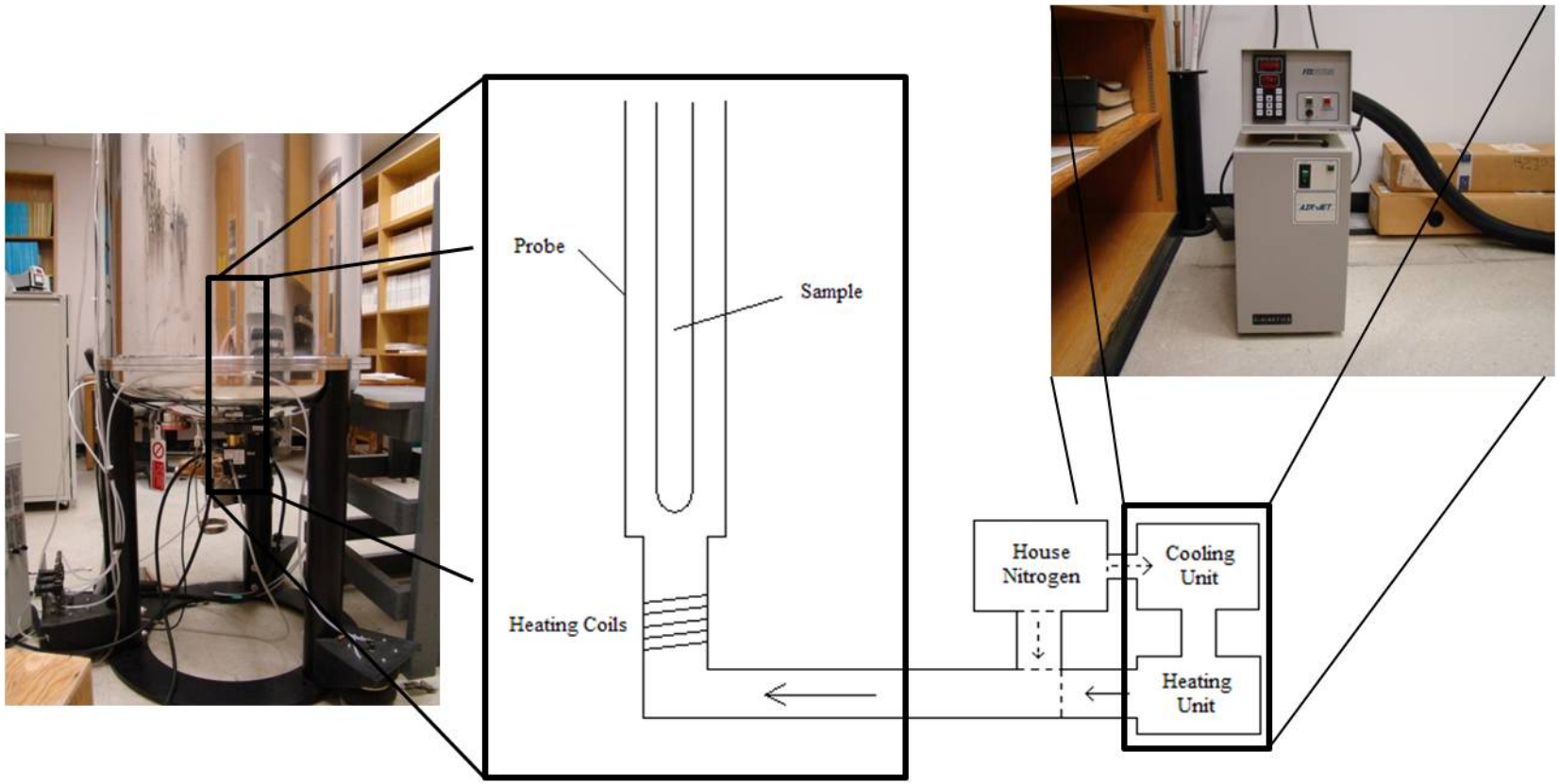

Figure 3-3. Diagram of external variable-temperature unit used to regulate the sample temperature.

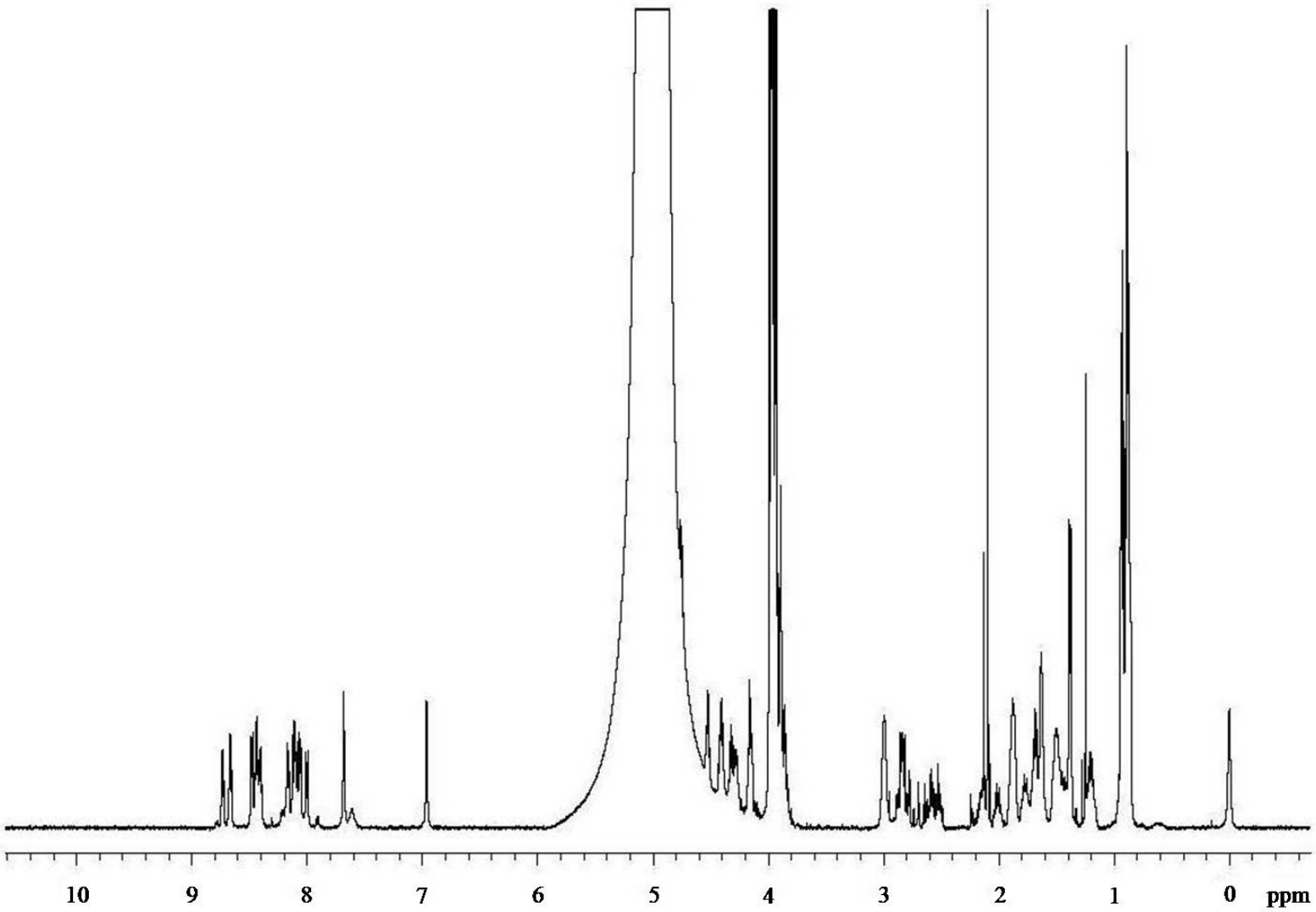

Figure 3-4. ^{1}H spectrum of 0.69 mM Aβ(25-35) in 80% H_2O and 20% d_3-TFE at 10°C referenced to internal DSS. Spectrum represents 256 scans acquired with the presat pulse sequence. Spectrum has been baseline corrected and processed with 0.5 Hz line broadening.

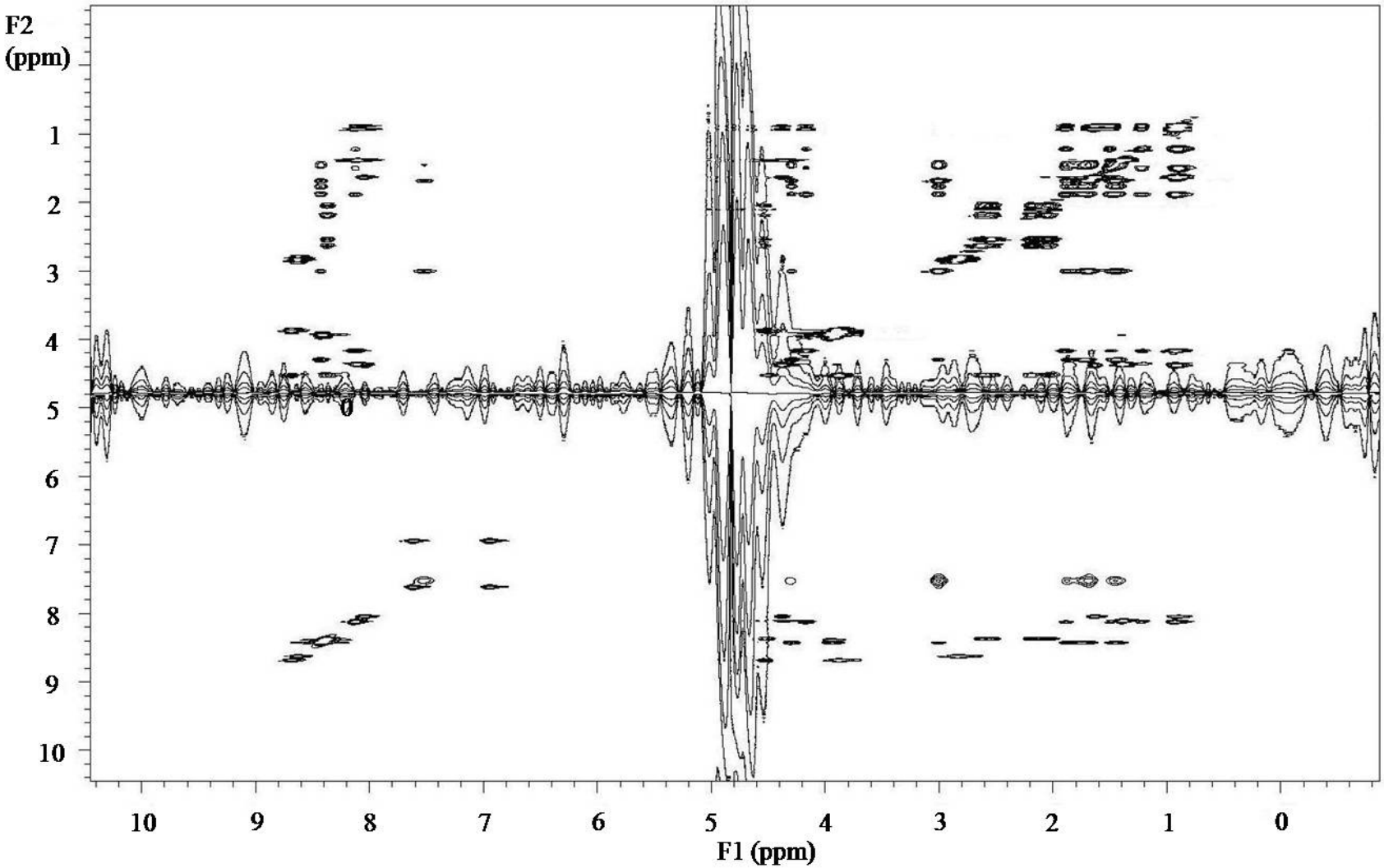

Figure 3-5. TOCSY spectrum of 6.71 mM Aβ(25-35) in 90% H_2O and 10% D_2O at 25°C. Processed with a Gaussian weighting function in both dimensions such that the signal decays to zero before the end of the fid.

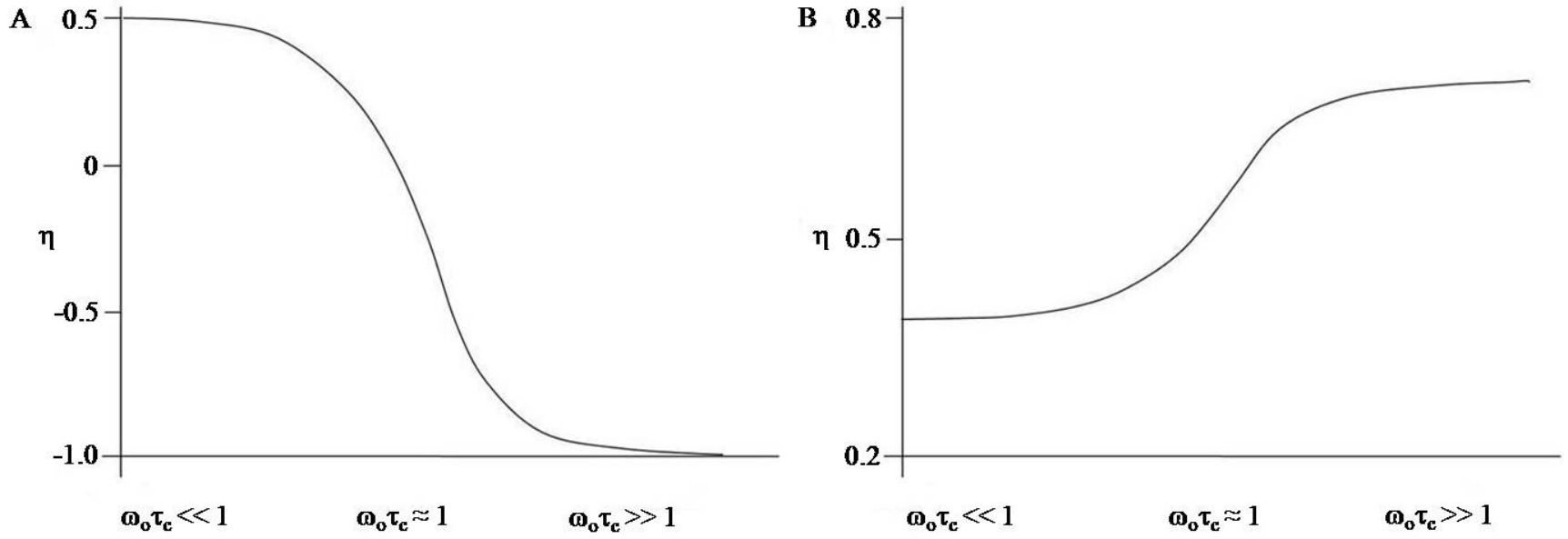

Figure 3-6. Dependence of the homonuclear nuclear Overhauser enhancement (η) on the spectrometer frequency (ω_o) and correlation time (τ_c) for A) NOESY and B) ROESY.

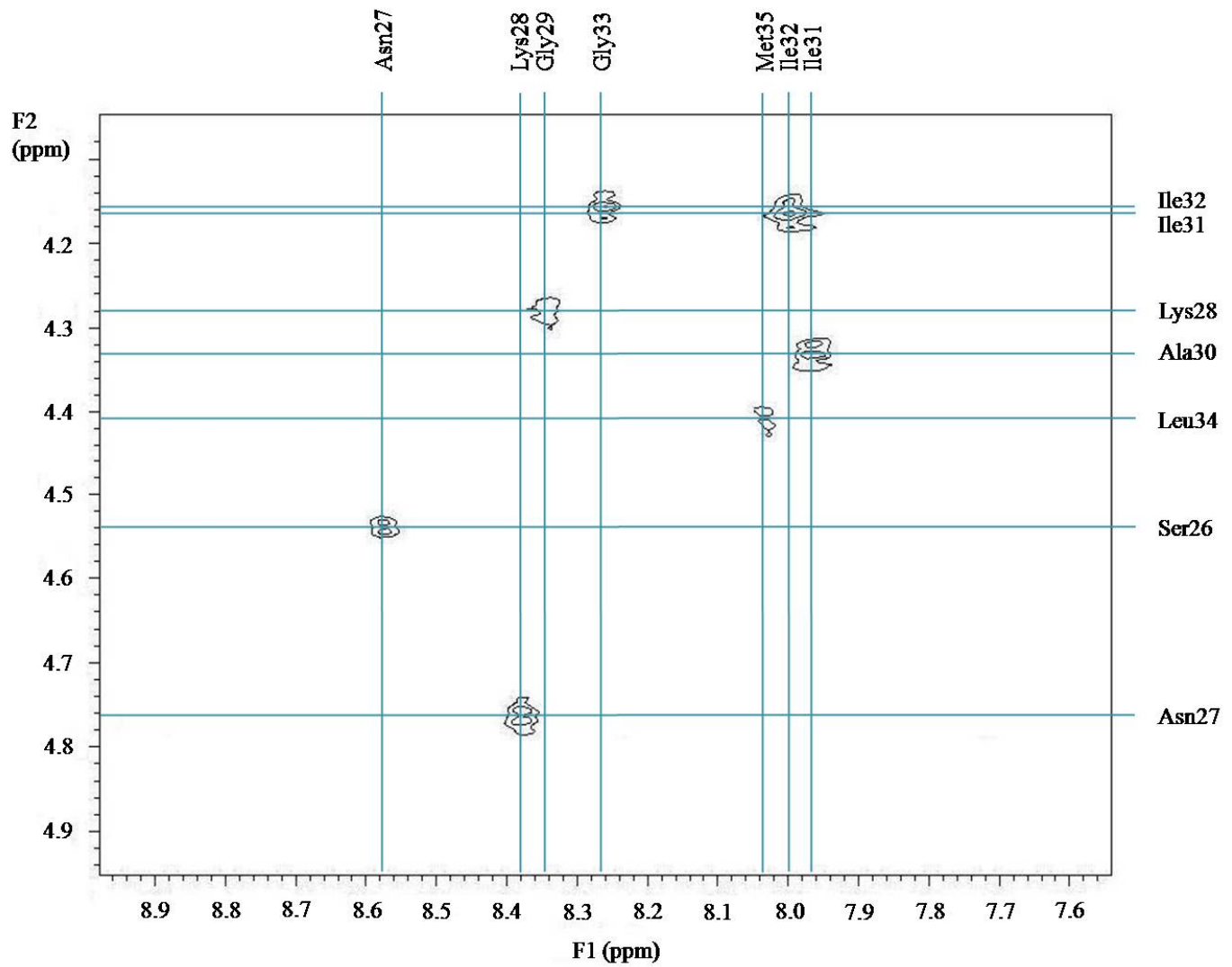

Figure 3-7. Expansion of the ROESY spectrum of 0.69 mM Aβ(25-35) in 80% H_2O and 20% d_3-TFE. Shows a portion of the amide-proton region in the f_1 dimension (x axis) and a portion of the alpha-proton region in the f_2 dimension (y axis).

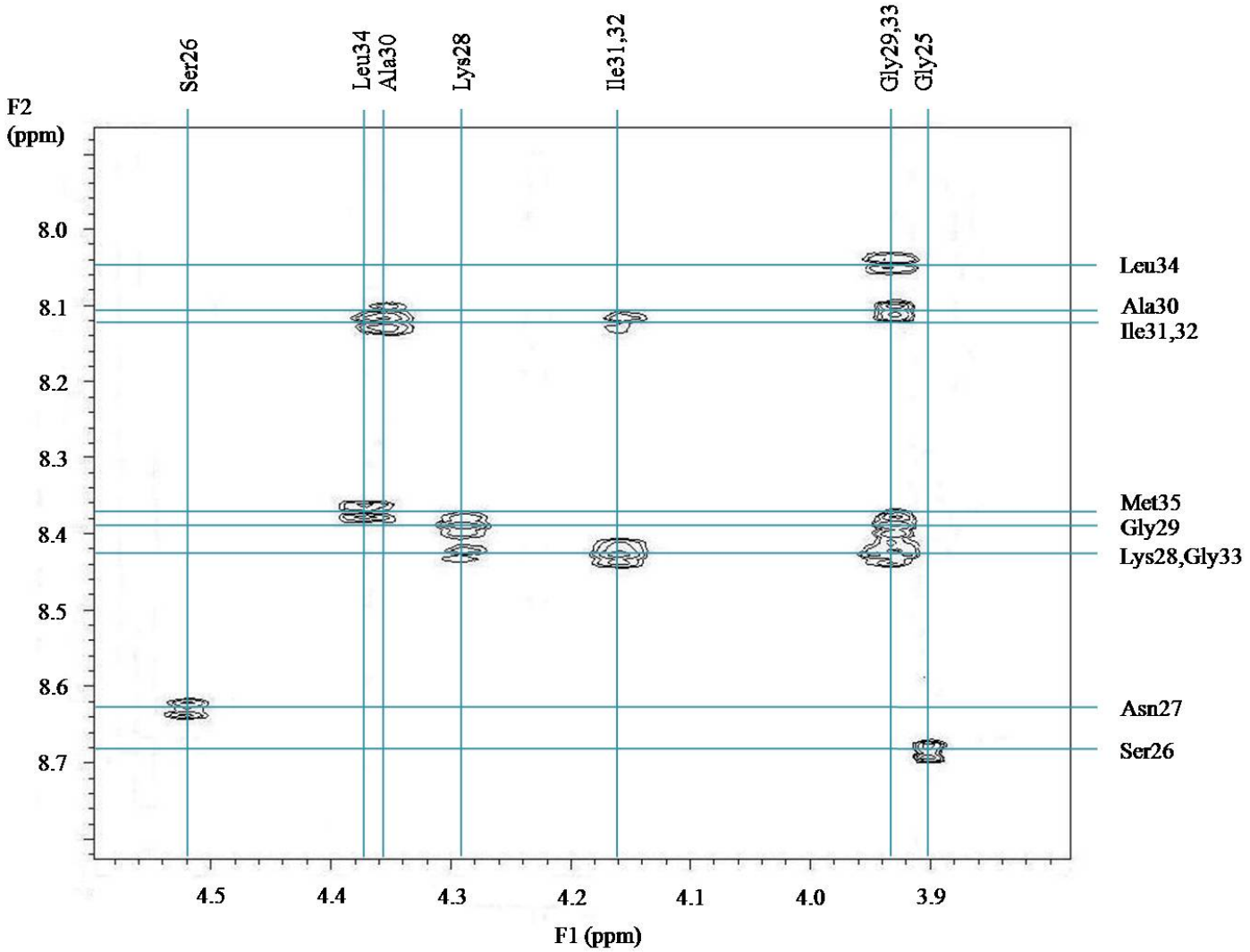

Figure 3-8. Expansion of the ROESY spectrum of 6.71 mM Aβ(25-35) in 90% H_2O and 10% D_2O. Shows a portion of the alpha proton region in the f_1 dimension (x axis) and a portion of the amide proton region in the f_2 dimension (y axis).

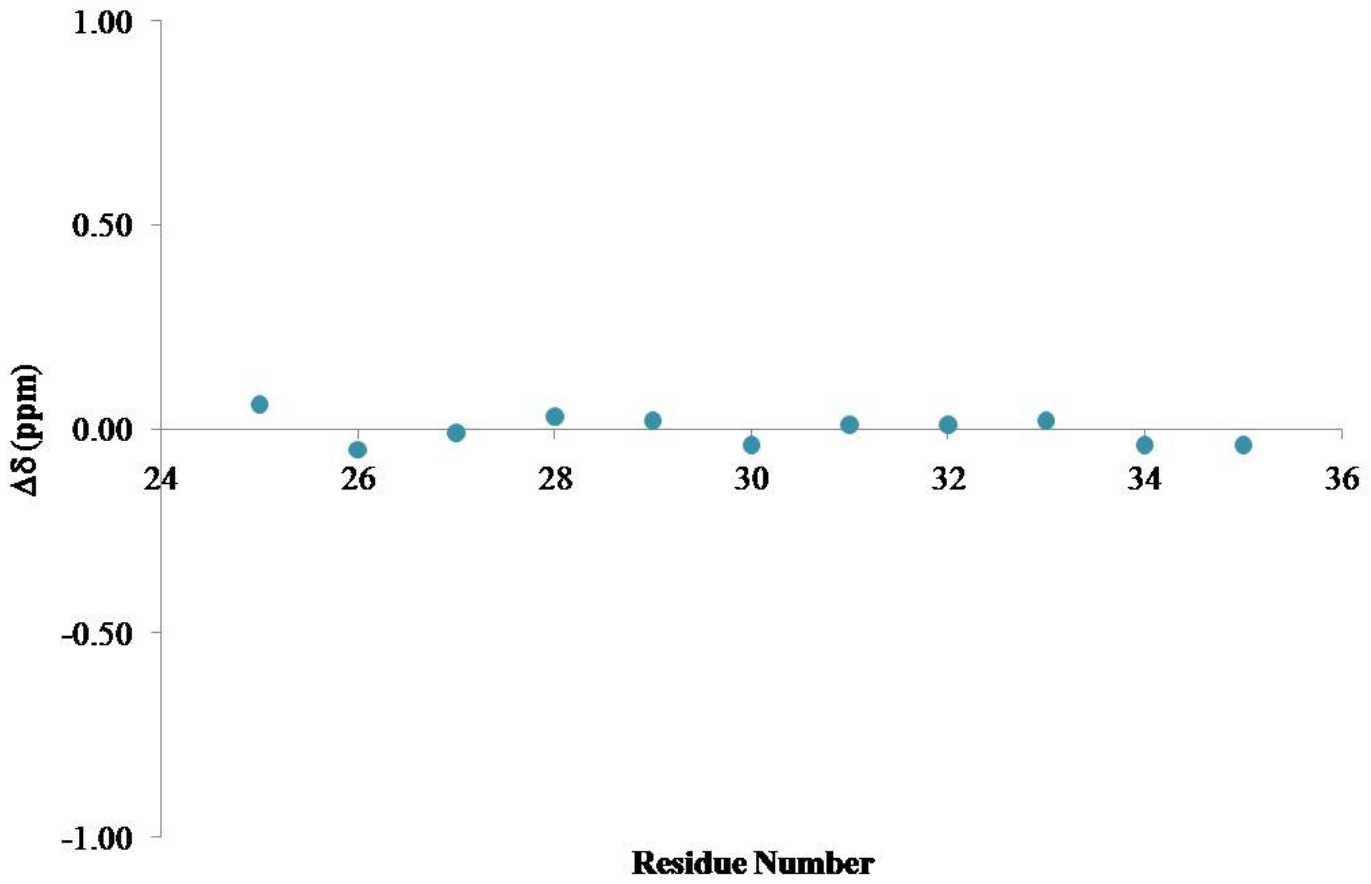

Figure 3-9. $\Delta\delta$ plot for the alpha protons of 6.71 mM Aβ(25-35) in 90% H_2O and 10% D_2O at pH 2.53 compared to random-coil chemical shifts.

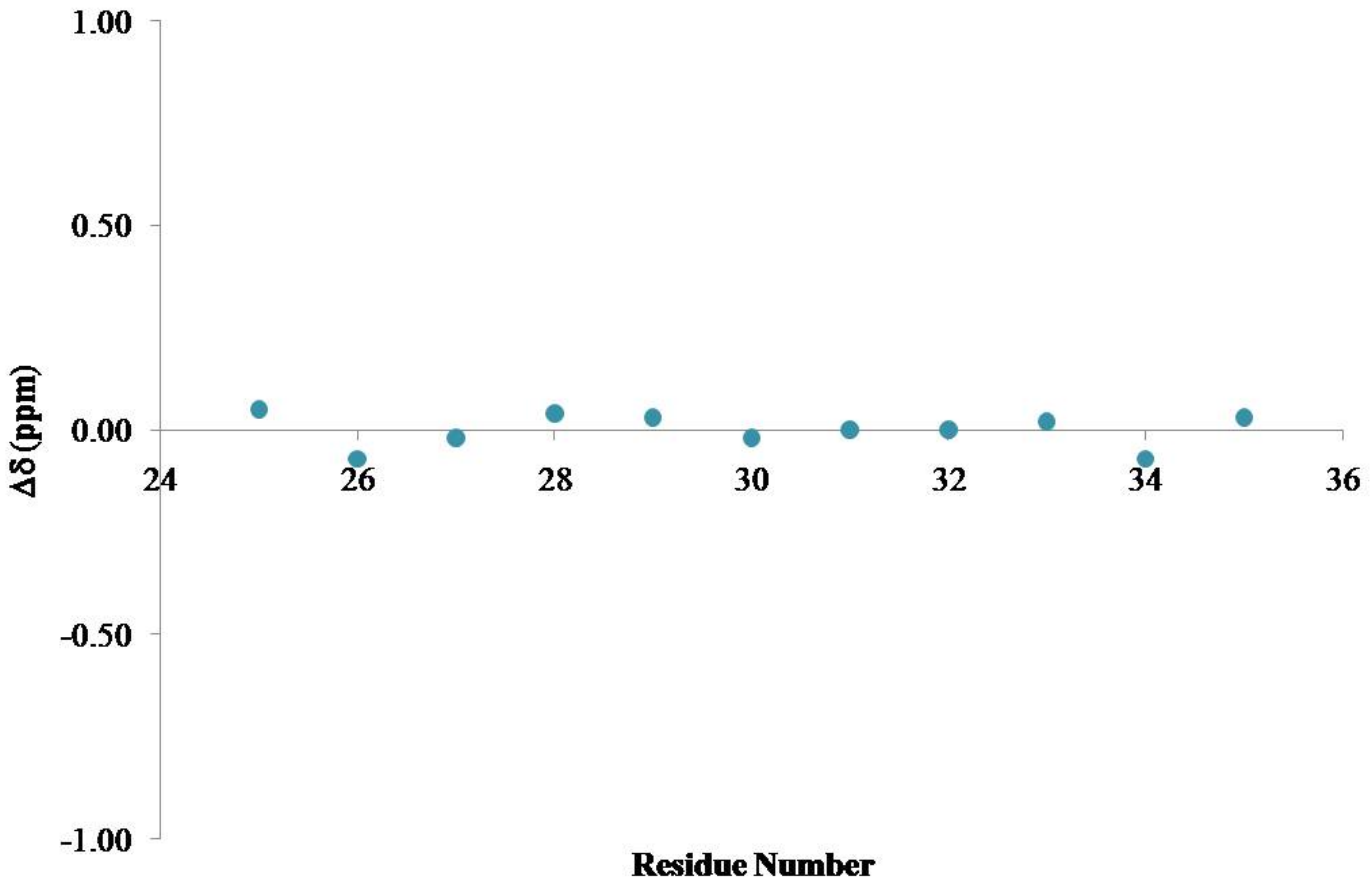

Figure 3-10. $\Delta\delta$ plot for the alpha protons of 0.69 mM Aβ(25-35) in 80% H_2O and 20% d_3-TFE at pH 3.23 compared to random-coil chemical shifts.

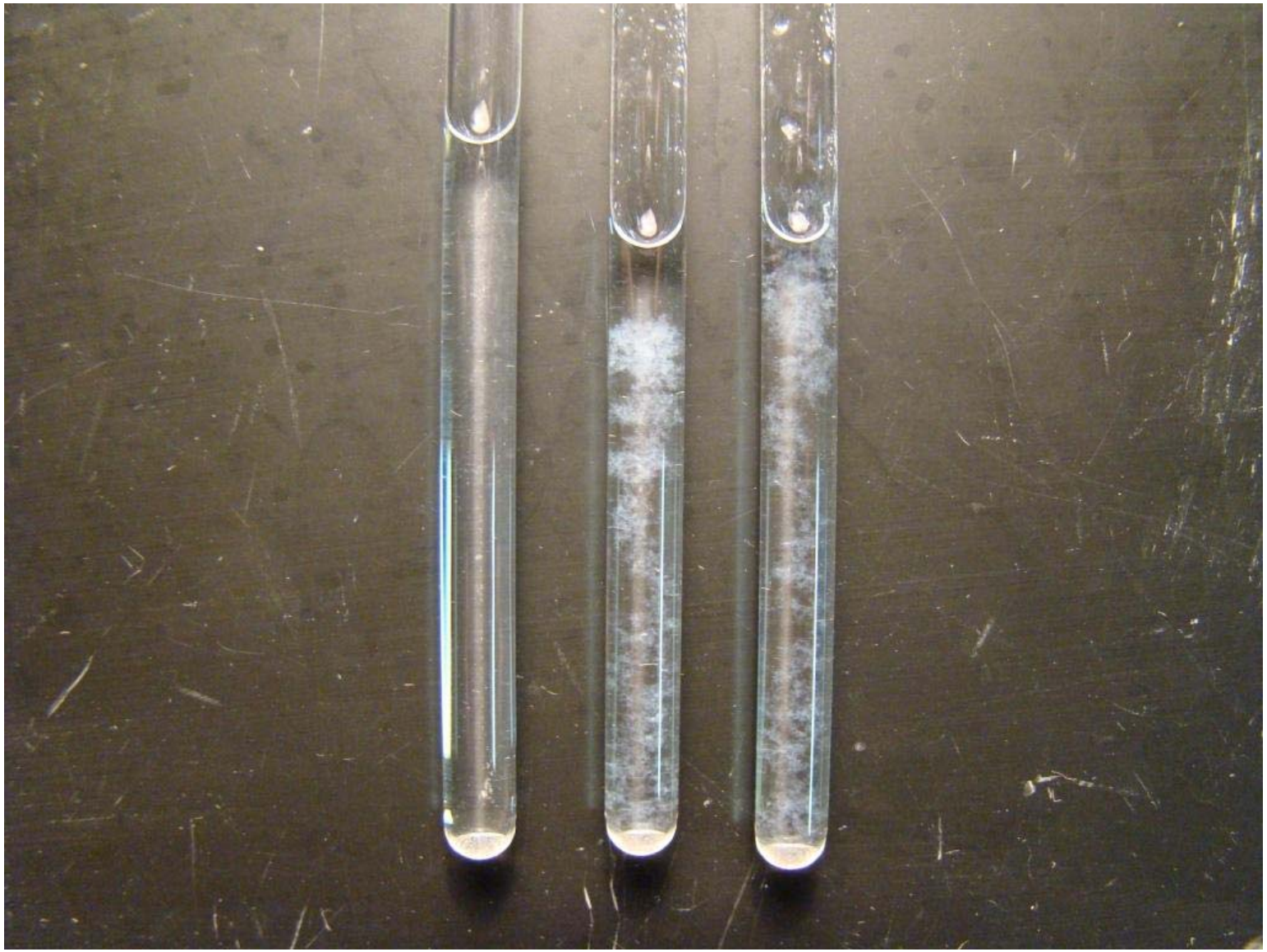

Figure 3-11. Two visibly cloudy Aβ(25-35) samples and one clear sample.

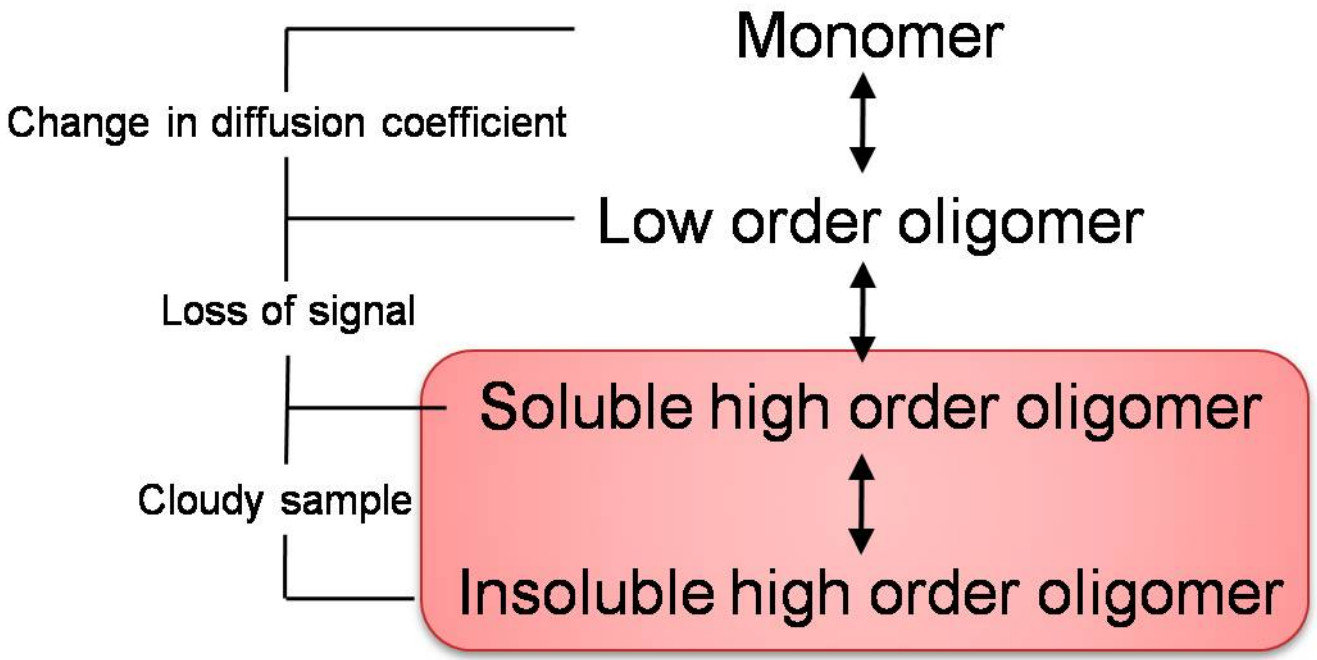

Figure 3-12. The equilibrium of Aβ(25-35) in solution, and the effect of each transition. The high order oligomers are not observable by solution phase NMR.

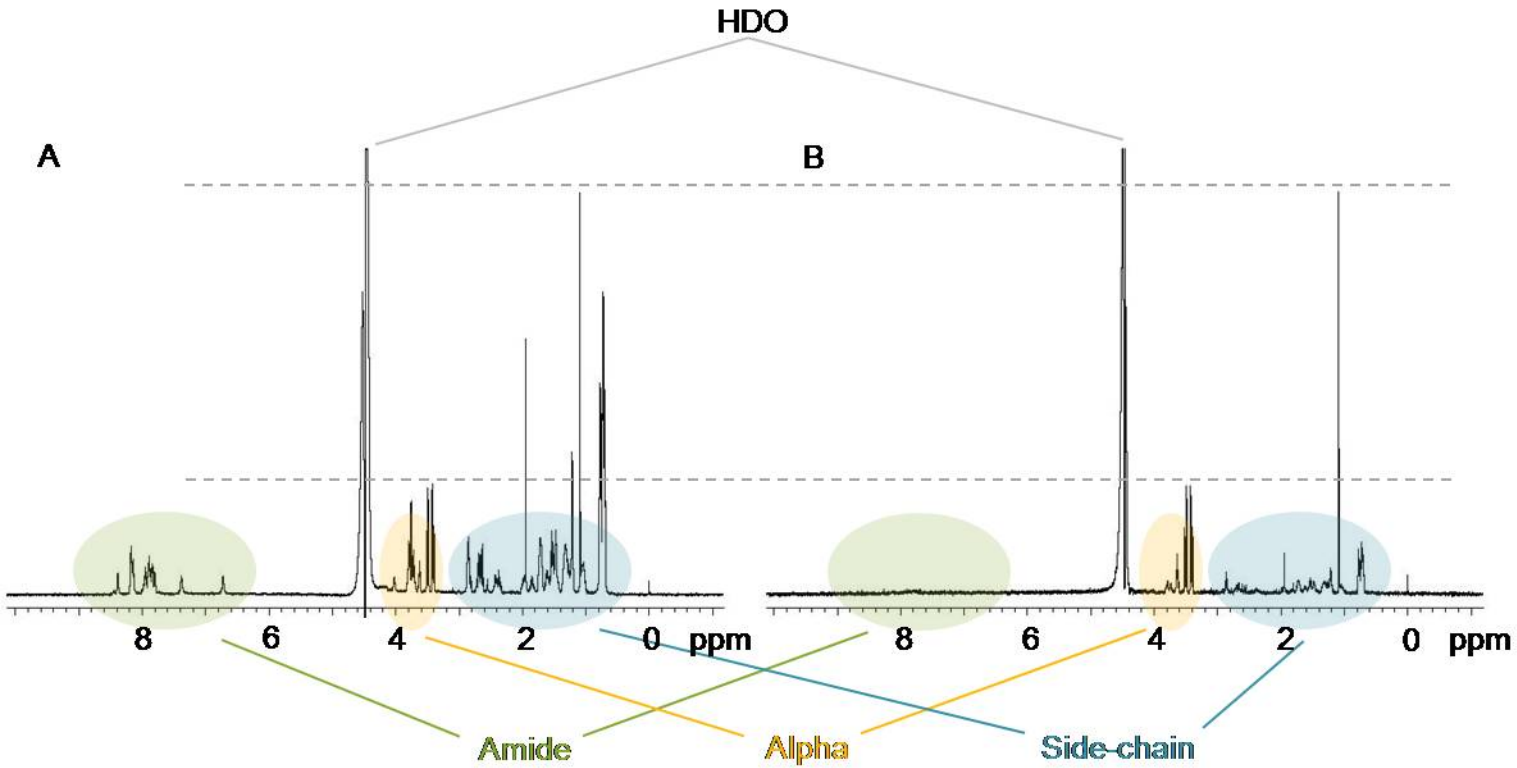

Figure 3-13. Two spectra showing the decrease in Aβ(25-35) signal intensity of the samples with visible aggregation. The intensities of the spectra were normalized using the peaks at 1.1 and 3.5 ppm which represent an unknown impurity present in the solid peptide as received. A) 3.26 mM Aβ(25-35), no visible aggregation. B) 3.13 mM Aβ(25-35) with 5:1 molar ratio of Zn(II), visible aggregation.

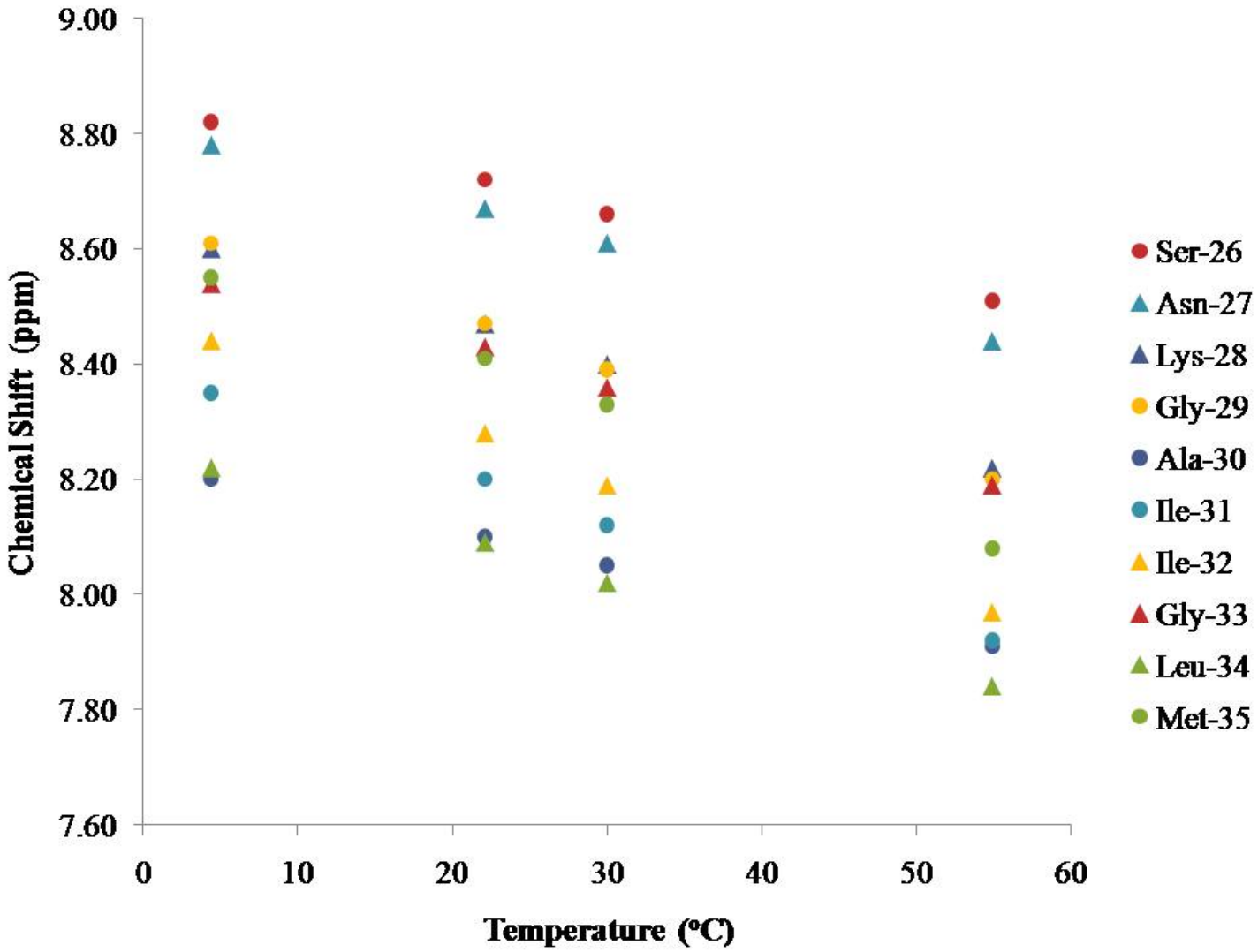

Figure 3-14. The chemical shifts of the amide protons of 1.88 mM Aβ(25-35) in 90% H_2O and 10% D_2O over a range of temperatures. Glycine-25 was not observable due to solvent exchange.

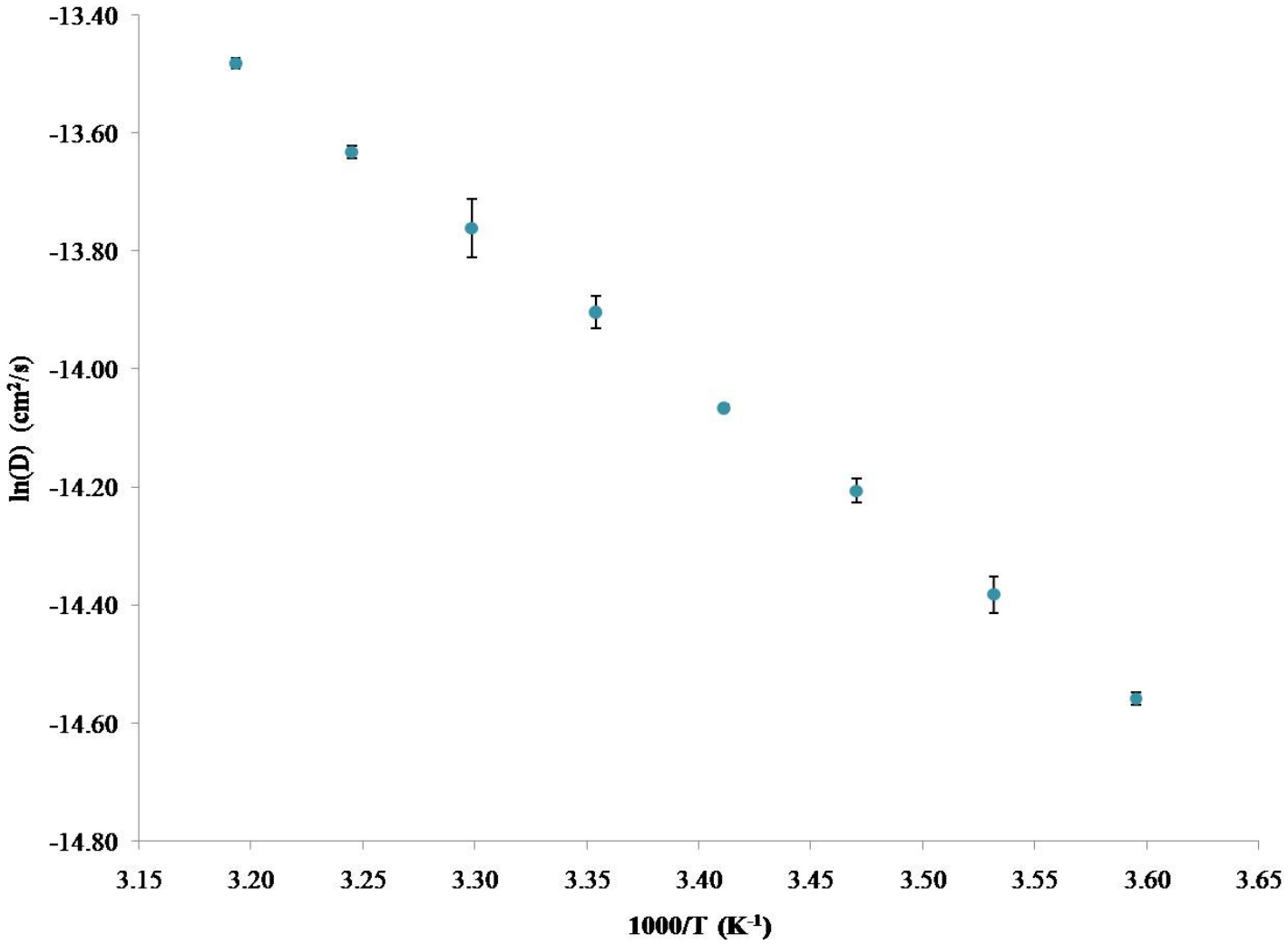

Figure 3-15. Diffusion of lysozyme over a range of temperatures. Error bars represent standard deviation of the mean (n=3).

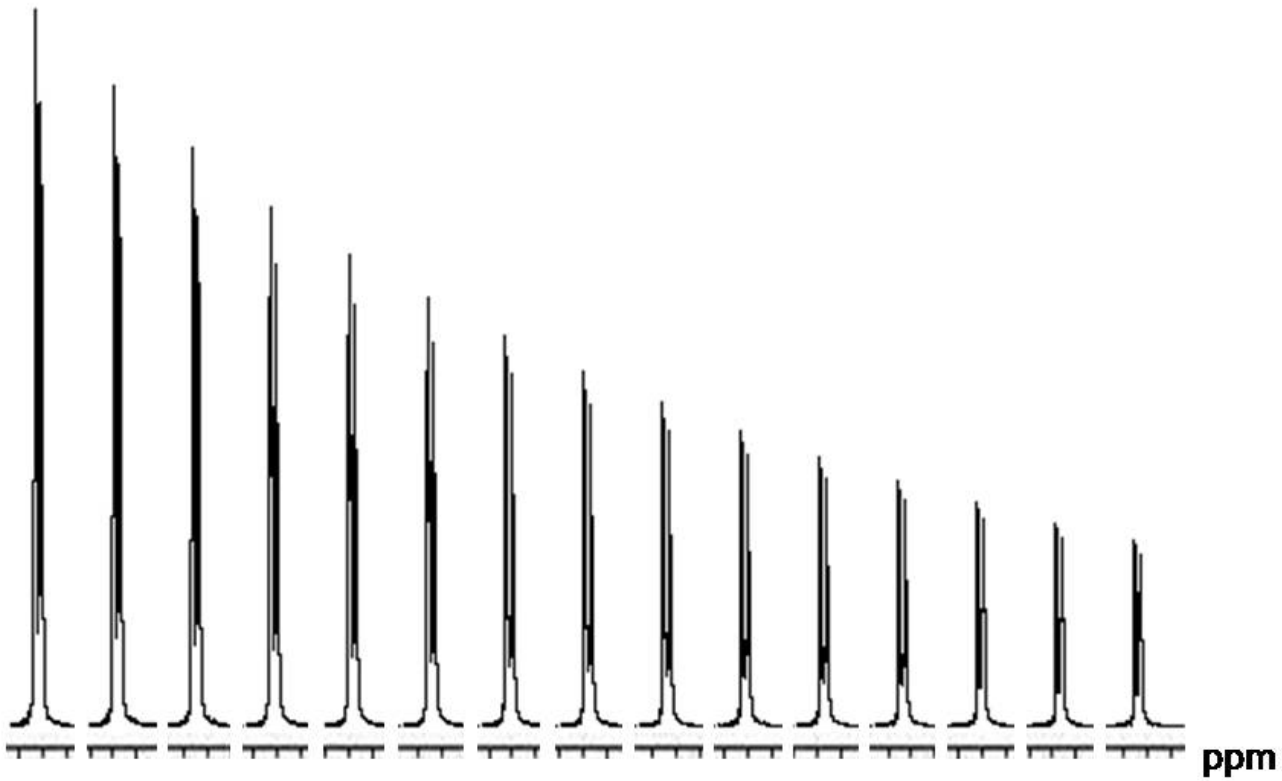

Figure 3-16. Typical results from a pfg experiment. The methyl peaks displayed with relative intensity over 15 gradient strengths.

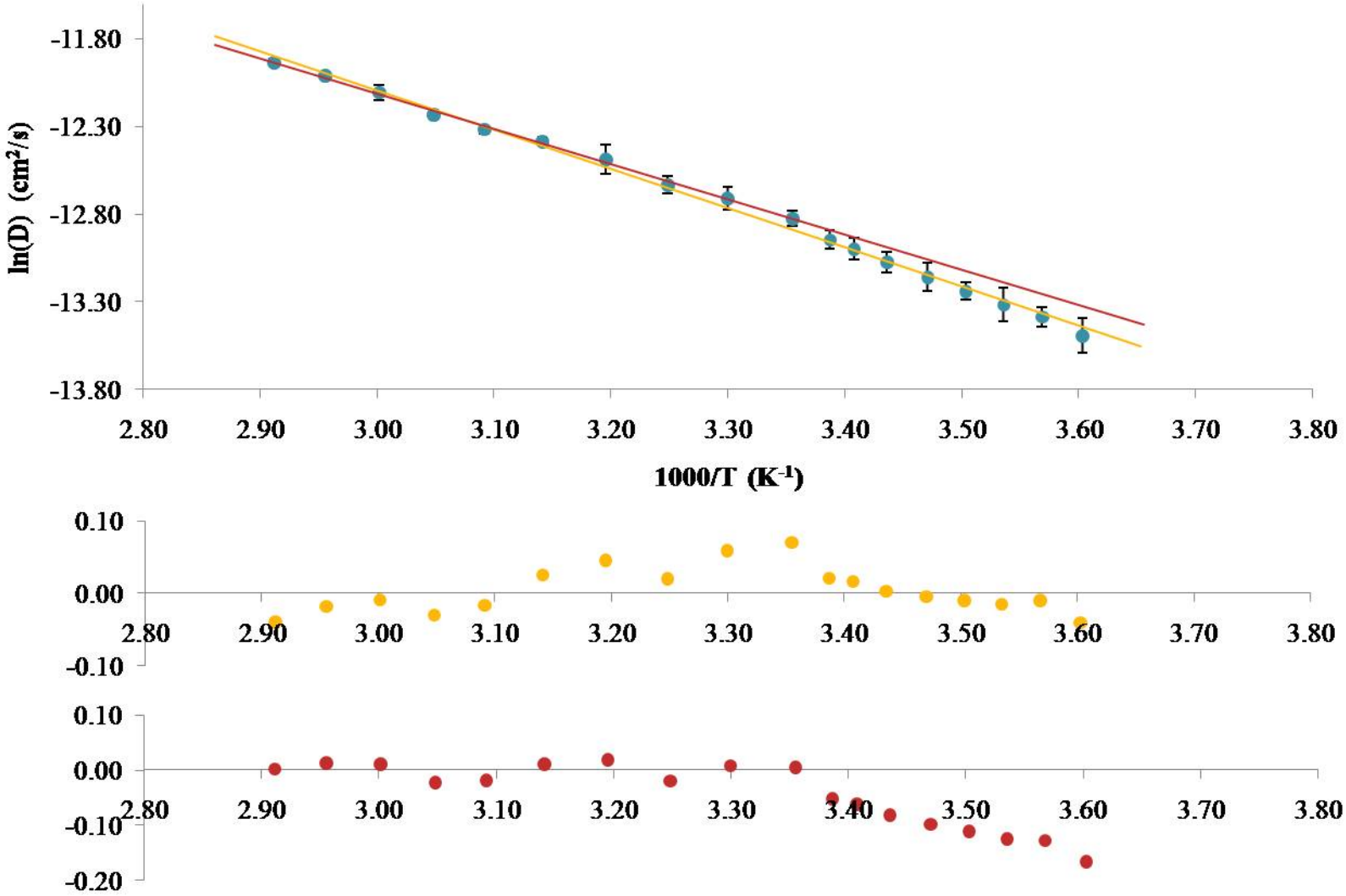

Figure 3-17. Diffusion of 2.82 mM Aβ (25-35) over a range of temperatures with linear regression applied over all temperatures (yellow) and from 25-70°C (red). The error bars represent standard deviation of the mean (n=3). The plots below represent the residuals resulting from the corresponding regression.

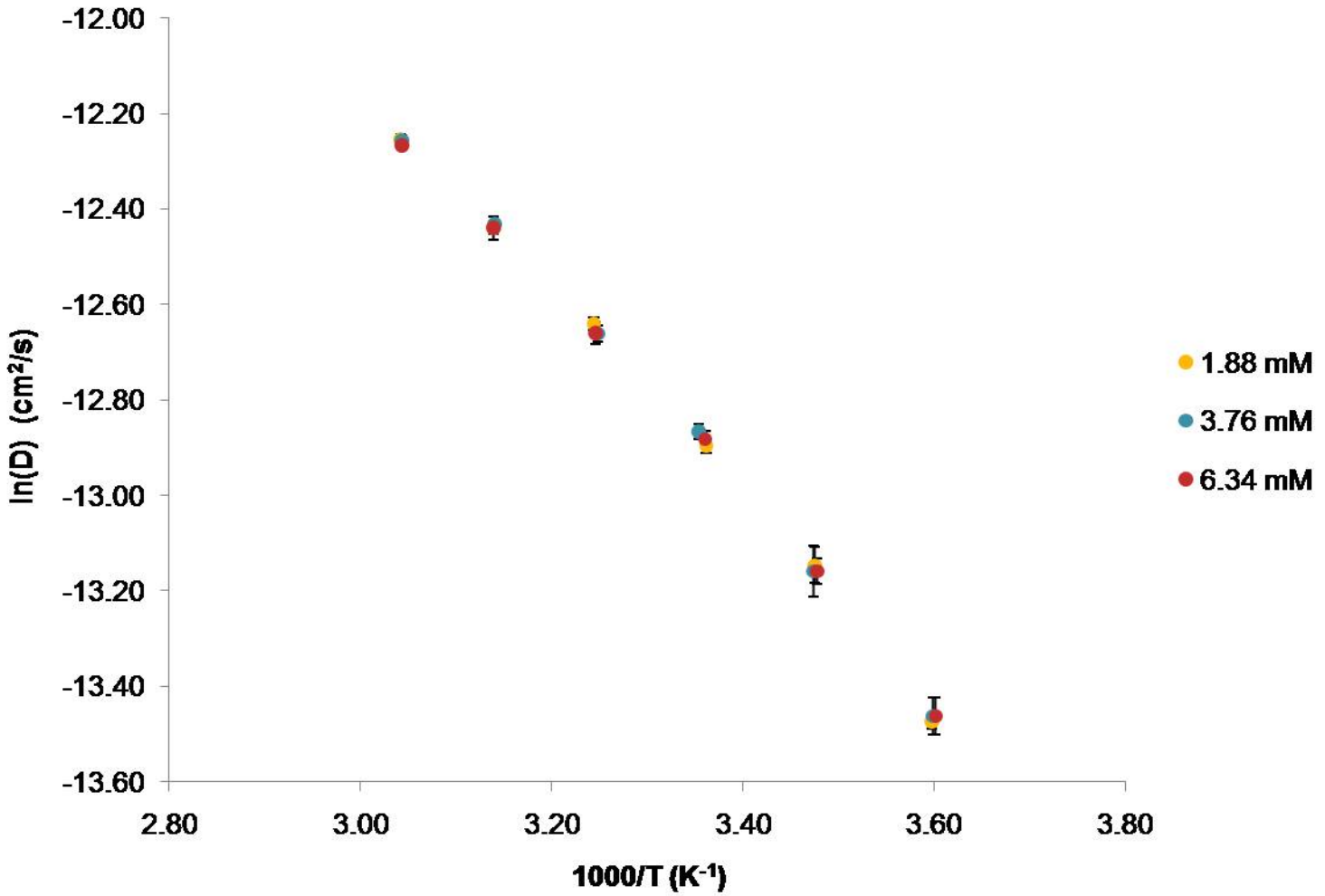

Figure 3-18. The diffusion coefficient of Aβ(25-35) for three concentrations in 90% H_2O and 10% D_2O from 5-55°C. The error bars represent standard deviation of the mean (n=3).

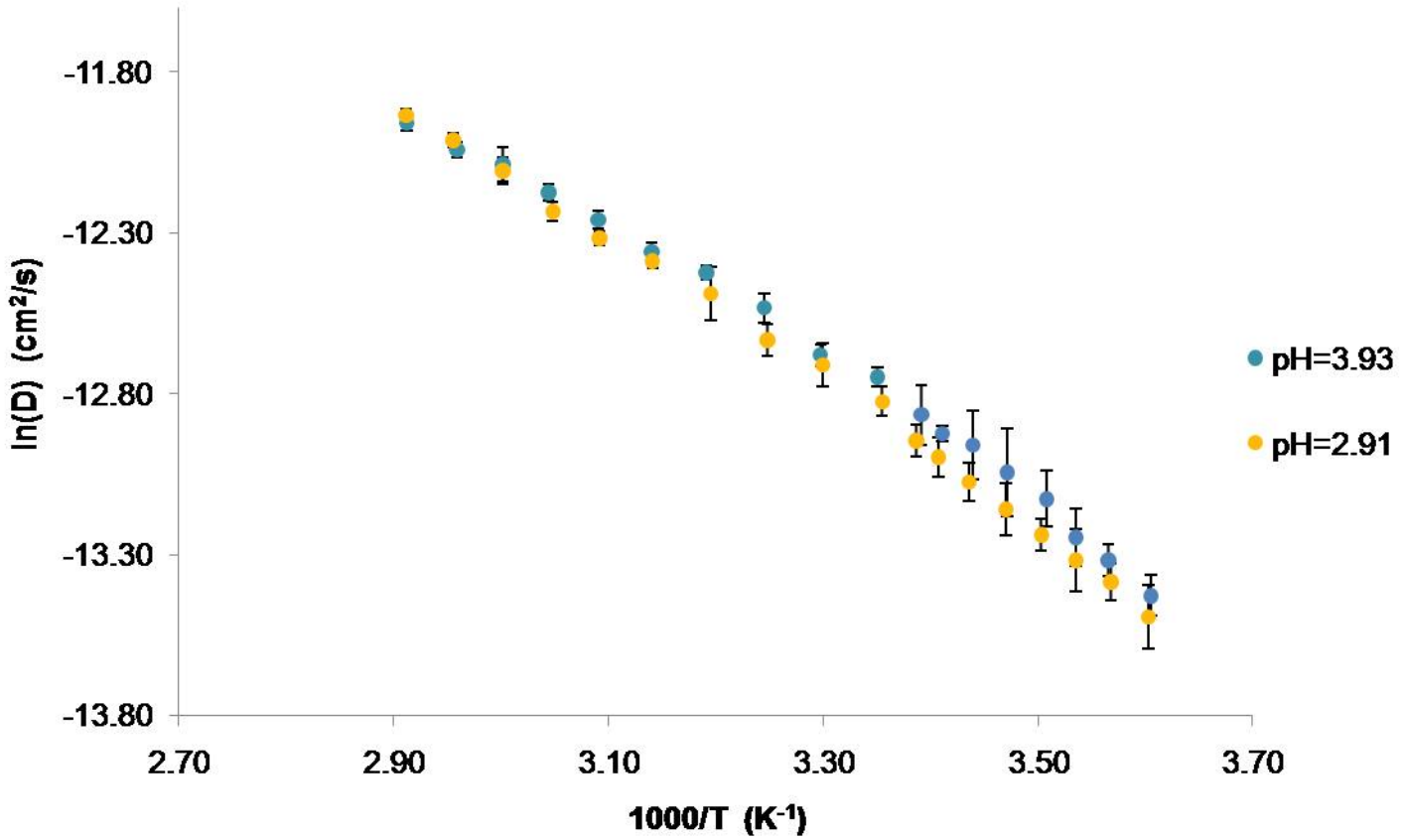

Figure 3-19. The diffusion coefficient of 2.82 mM Aβ(25-35) with a change in pH over a range of temperatures. The error bars represent the standard deviation of the mean (n=3).

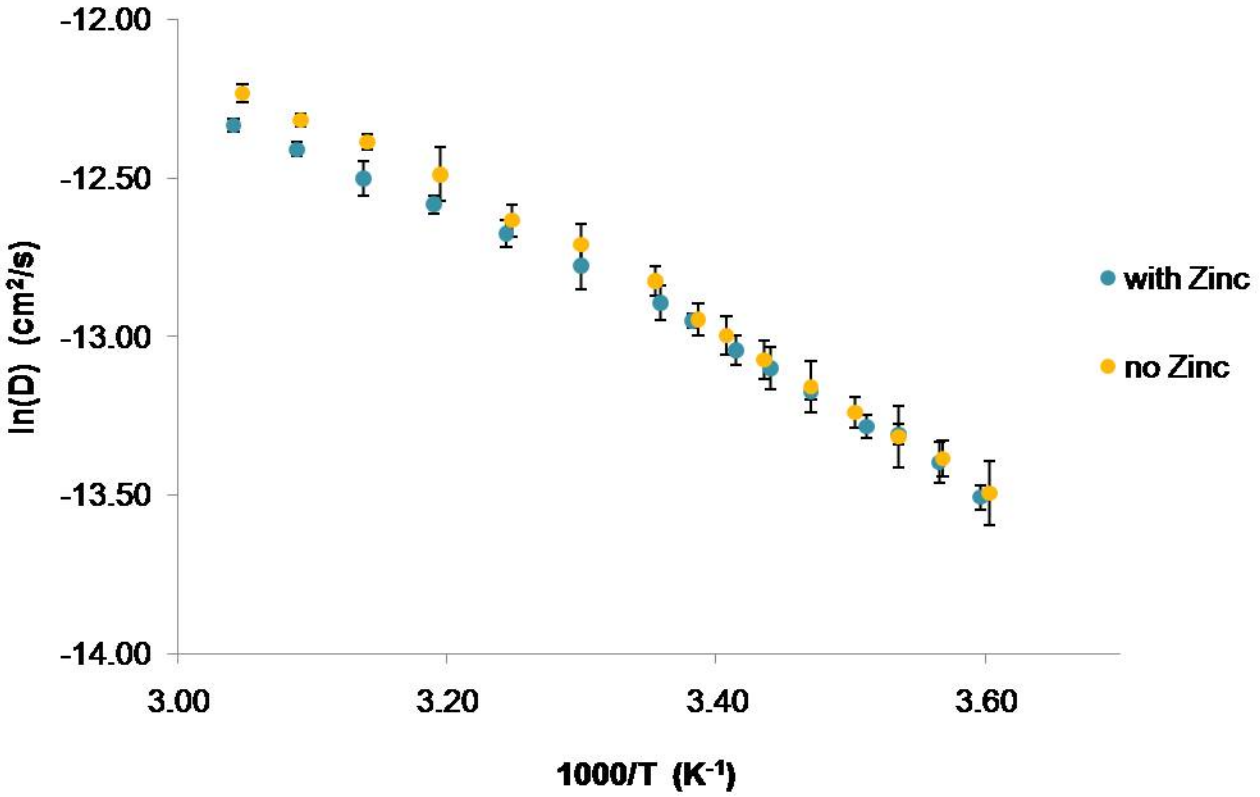

Figure 3-20. The diffusion coefficient of Aβ(25-35) with the addition of 3:1 molar ratio Zn(II) over a range of temperatures. The error bars represent standard deviation of the mean (n=3).

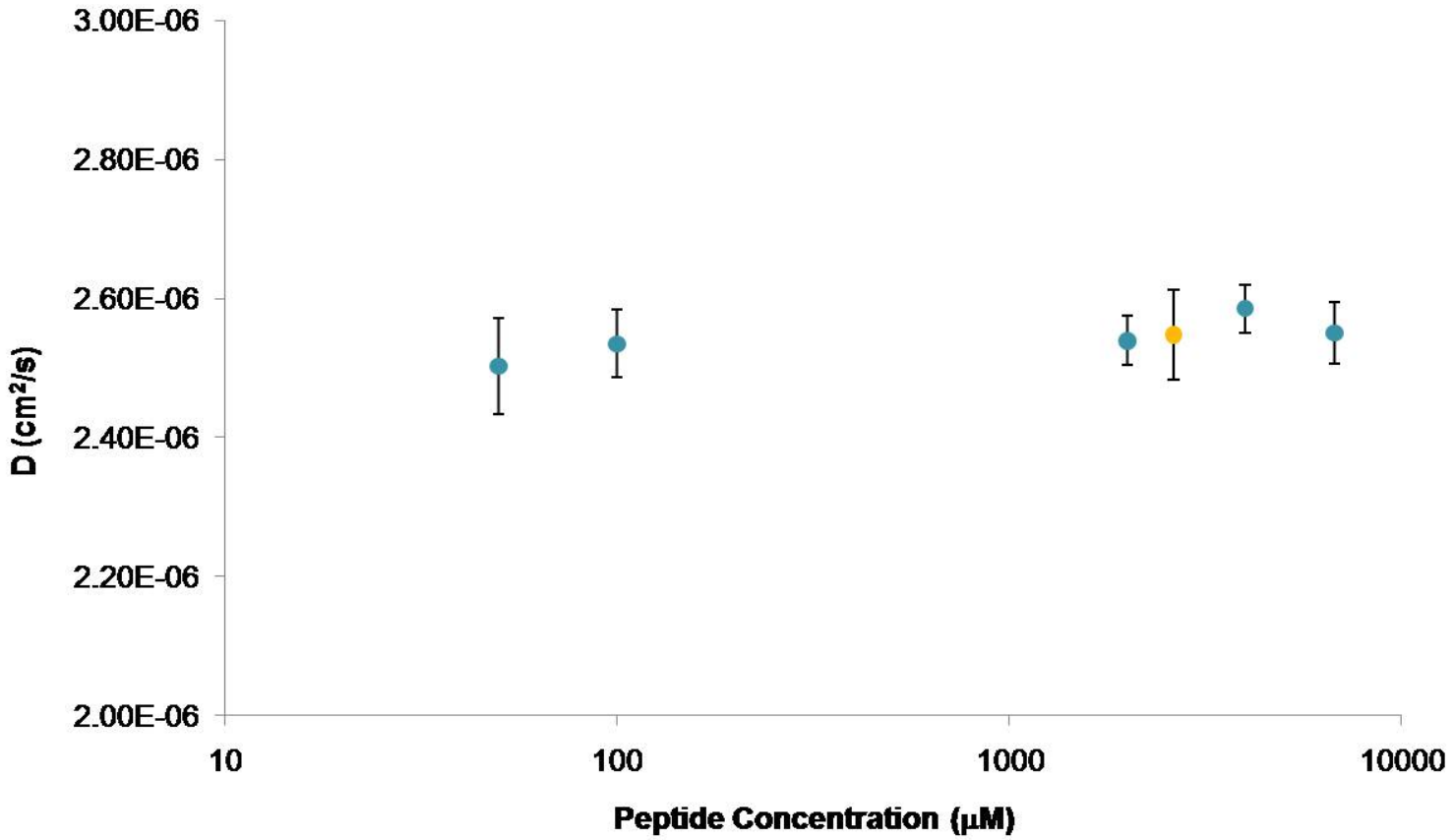

Figure 3-21. The diffusion coefficient of Aβ(25-35) at 25°C over a large range of concentrations. The error bars represent standard deviation of the mean (n=3). The yellow point corresponds to the diffusion coefficient measured after dissolving the peptide in and blowing off formic acid followed by dissolving in a 90% H_2O and 10% D_2O.

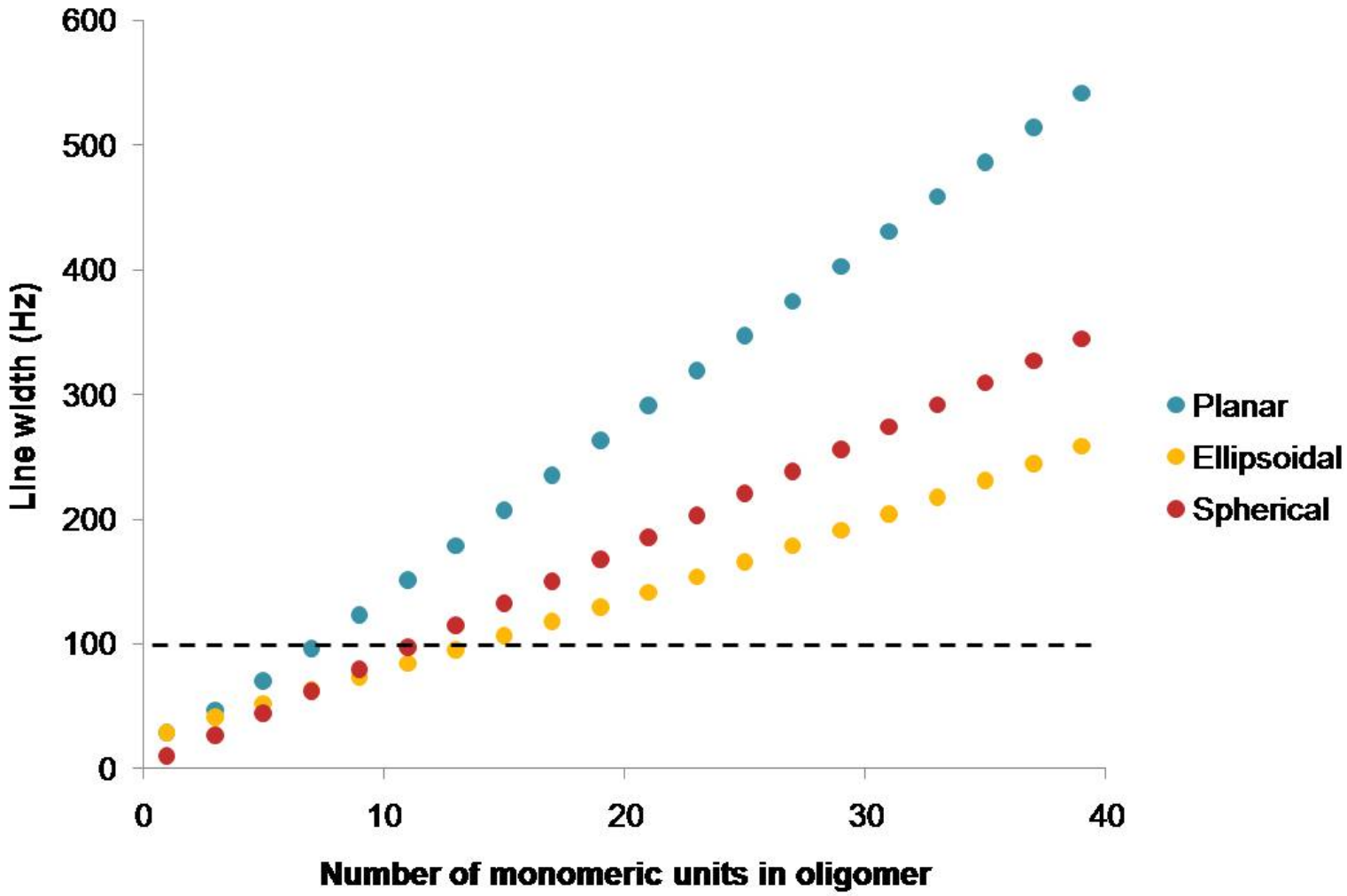

Figure 3-22. The calculated line widths over a range of degrees of oligomerization for three geometric models.

Table 3-1. Chemical shifts (ppm) of 6.71 mM Aβ(25-35) in 90% H_2O and 10% D_2O at pH 2.53

Residue	H^N	H^α	H^β	H^γ	H^δ	H^ε	other	
Gly-25	8.05[a]	3.90						
Ser-26	8.68	4.52	3.89, 3.85					
Asn-27	8.63	4.75[a]	2.85, 2.80				γNH_2	7.61, 6.94
Lys-28	8.43	4.29	1.87, 1.77	1.45	1.68	3.00	εNH_3^+	7.52
Gly-29	8.39	3.94						
Ala-30	8.11	4.36	1.38					
Ile-31	8.12	4.16	1.88	1.50, 1.22	0.87[a]		γCH_3	0.89[a]
Ile-32	8.12	4.16	1.88	1.50, 1.22	0.92[a]		γCH_3	0.93[a]
Gly-33	8.42	3.94						
Leu-34	8.05	4.38	1.62	1.63	0.93, 0.88[a]			
Met-35	8.37	4.52	2.18, 2.05	2.63, 2.53		2.10		

[a]Chemical shift could not be accurately determined from ^1H spectrum due to overlap or solvent exchange, value was determined from TOCSY spectrum with an error of ± 0.02 ppm.

Table 3-2. Chemical shifts (ppm) of 3.47 mM Aβ(25-35) in 90% H_2O and 10% D_2O at pH 2.60

Residue	H^N	H^α	H^β	H^γ	H^δ	H^ε	other	
Gly-25	N.O.	N.O.						
Ser-26	8.69	4.53[a]	3.89, 3.85					
Asn-27	8.64	N.O.	2.85, 2.80				γNH_2	7.61, 6.94
Lys-28	8.43	4.30[a]	1.87, 1.77	1.45	1.68	3.00	εNH_3^+	7.52
Gly-29	8.43	3.94						
Ala-30	8.07	4.32[a]	1.37					
Ile-31	8.17	4.16	1.85	1.49, 1.20	0.87[a]		γCH_3	0.89[a]
Ile-32	8.23	4.16	1.86	1.49, 1.20	0.91[a]		γCH_3	0.92[a]
Gly-33	8.39	3.94						
Leu-34	8.07	4.32[a]	1.63	1.63	0.93, 0.88[a]			
Met-35	8.37	4.51[a]	2.18, 2.03	2.62, 2.54		2.10		

[a]Chemical shift could not be accurately determined from ^1H spectrum due to overlap or solvent exchange, value was determined from TOCSY spectrum with an error of ± 0.02 ppm. N.O. = not observed due to solvent exchange or overlap with solvent peak.

Table 3-3. Chemical shifts (ppm) of 0.69 mM Aβ(25-35) in 80% H_2O and 20% d_3-TFE at pH 3.23

Residue	H^N	H^α	H^β	H^γ	H^δ	H^ε	other
Gly-25	8.14[a]	3.91					
Ser-26	8.65	4.54	3.90, 3.87[a]				
Asn-27	8.58	4.76[a]	2.87, 2.82				γNH_2 7.60, 6.89
Lys-28	8.38	4.28	1.89, 1.78	1.46	1.70	3.01	εNH_3^+ 7.57[a]
Gly-29	8.35	3.93[a]					
Ala-30	7.98	4.34	1.39				
Ile-31	7.96	4.17	1.90	1.51, 1.20	0.90[a]		γCH_3 0.91[a]
Ile-32	8.00	4.17	1.89	1.51, 1.22	0.94[a]		γCH_3 0.96[a]
Gly-33	8.27	3.94[a]					
Leu-34	7.88	4.41	1.64	1.64	0.96, 0.89[a]		
Met-35	8.05	4.45[a]	2.17, 2.03	2.60, 2.54		2.10	

[a]Chemical shift could not be accurately determined from ^1H spectrum due to overlap or solvent exchange, value was determined from TOCSY spectrum with an error of ± 0.02 ppm.

Table 3-4. Chemical shifts (ppm) of 0.69 mM Aβ(25-35) in 80% H_2O and 20% d_3-TFE at pH 3.19 with 1:1 molar ratio of Zn^{2+}

Residue	H^N	H^α	H^β	H^γ	H^δ	H^ε	other
Gly-25	8.15[a]	3.92[a]					
Ser-26	8.65	4.54	3.91, 3.86[a]				
Asn-27	8.58	4.76[a]	2.87, 2.82				γNH_2 7.60, 6.89
Lys-28	8.38	4.29	1.89, 1.78	1.45	1.70	3.01	εNH_3^+ 7.57[a]
Gly-29	8.35	3.93[a]					
Ala-30	7.98	4.34	1.39				
Ile-31	7.96	4.16	1.90	1.51, 1.21	0.90[a]		γCH_3 0.91[a]
Ile-32	8.00	4.16	1.88	1.51, 1.22	0.92[a]		γCH_3 0.94[a]
Gly-33	8.26	3.95[a]					
Leu-34	7.88	4.41	1.64	1.64	0.94, 0.89[a]		
Met-35	8.06	4.46	2.18, 2.04	2.60, 2.53		2.10	

[a]Chemical shift could not be accurately determined from ^1H spectrum due to overlap or solvent exchange, value was determined from TOCSY spectrum with an error of ± 0.02 ppm.

Table 3-5. Chemical shifts (ppm) of 0.60 mM Aβ(25-35) in 80% H_2O and 20% d_3-TFE at pH 3.24 with 3:1 molar ratio of Zn^{2+}

Residue	H^N	H^α	H^β	H^γ	H^δ	H^ε	other
Gly-25	8.09[a]	3.88					
Ser-26	8.65	4.54[a]	3.90, 3.87[a]				
Asn-27	8.58	4.76[a]	2.87, 2.82				γNH_2 7.60, 6.89
Lys-28	8.38	4.29	1.89, 1.79	1.47	1.70	3.01	εNH_3^+ 7.58[a]
Gly-29	8.35	3.94[a]					
Ala-30	7.98[a]	4.34	1.40				
Ile-31	7.97[a]	4.17	1.89	1.51, 1.21	0.90[a]		γCH_3 0.91[a]
Ile-32	8.00[a]	4.17	1.89	1.51, 1.21	0.92[a]		γCH_3 0.93[a]
Gly-33	8.27	3.95[a]					
Leu-34	7.88	4.41	1.64	1.64	0.94, 0.89[a]		
Met-35	8.01[a]	4.42	2.16, 2.02	2.59, 2.54		2.10	

[a]Chemical shift could not be accurately determined from ^1H spectrum due to overlap or solvent exchange, value was determined from TOCSY spectrum with an error of ± 0.02 ppm.

Table 3-6. Chemical shifts (ppm) of 0.69 mM Aβ(25-35) in 80% H_2O and 20% d_3-TFE at pH 3.23 with 0.1:1 molar ratio of Cu^{2+}

Residue	H^N	H^α	H^β	H^γ	H^δ	H^ε	other
Gly-25	8.13[a]	3.91					
Ser-26	8.65	4.54[a]	3.92, 3.86[a]				
Asn-27	8.58	4.76[a]	2.87, 2.82				γNH_2 7.60, 6.89
Lys-28	8.38	4.29	1.90, 1.79	1.47	1.70	3.01	εNH_3^+ 7.57[a]
Gly-29	8.34	3.93[a]					
Ala-30	7.98	4.34[a]	1.39				
Ile-31	7.97	4.17	1.89	1.51, 1.21	0.87[a]		γCH_3 0.91[a]
Ile-32	8.00	4.17	1.89	1.51, 1.22	0.90[a]		γCH_3 0.94[a]
Gly-33	8.26	3.95[a]					
Leu-34	7.88	4.42[a]	1.64	1.64	0.94, 0.89[a]		
Met-35	8.04	4.44[a]	2.17, 2.04	2.60, 2.54		2.10	

[a]Chemical shift could not be accurately determined from ^1H spectrum due to overlap or solvent exchange, value was determined from TOCSY spectrum with an error of ± 0.02 ppm.

Table 3-7. Chemical shifts (ppm) of 0.69 mM Aβ(25-35) in 80% H_2O and 20% d_3-TFE at pH 3.08 with 1:1 molar ratio of Cu^{2+}

Residue	H^N	H^α	H^β	H^γ	H^δ	H^ε	other
Gly-25	8.14[a]	3.88[a]					
Ser-26	8.65	4.55	3.91, 3.87				
Asn-27	8.57	4.76	2.88, 2.83				γNH_2 7.60, 6.89
Lys-28	8.38	4.29	1.89, 1.79	1.47	1.70	3.02	εNH_3^+ 7.57[a]
Gly-29	8.34	3.94					
Ala-30	7.98	4.34	1.40				
Ile-31	7.96	4.18	1.89	1.52, 1.22	0.87[a]		γCH_3 0.90[a]
Ile-32	8.04	4.18	1.89	1.52, 1.22	0.90[a]		γCH_3 0.93[a]
Gly-33	8.26	3.96					
Leu-34	7.87	4.42	1.64	1.64	0.94, 0.90[a]		
Met-35	8.05	4.45	2.20, 2.02	2.58[a]		2.11	

[a]Chemical shift could not be accurately determined from ^1H spectrum due to overlap or solvent exchange, value was determined from TOCSY spectrum with an error of ± 0.02 ppm.

Table 3-8. Temperature dependence of the amide chemical shifts of 2.82 mM Aβ(25-35) in 90% H_2O and 10% D_2O.

Residue[†]	$\Delta\delta/\Delta T$ (ppb/°C)
Ser-26	-6.2 ± 0.2
Asn-27	-6.8 ± 0.1
Lys-28	-7.6 ± 0.1
Gly-29	-8.2 ± 0.2
Ala-30	-5.8 ± 0.1
Ile-31	-8.5 ± 0.2
Ile-32	-9.3 ± 0.2
Gly-33	-7.0 ± 0.2
Leu-34	-7.6 ± 0.1
Met-35	-9.4 ± 0.4

[†]Glycine-25 was not observable due to solvent exchange.

Table 3-9. The diffusion coefficients of three concentrations of Aβ(25-35) in 90% H_2O and 10% D_2O from 5-55°C.

	Diffusion Coefficient × 10^6 (cm^2/s)		
Temperature (°C)	1.88 mM	3.76 mM	6.34 mM
5	1.41 ± 0.02	1.42 ± 0.05	1.42 ± 0.06
15	1.95 ± 0.07	1.93 ± 0.11	1.93 ± 0.05
25	2.51 ± 0.04	2.58 ± 0.04	2.54 ± 0.04
35	3.24 ± 0.04	3.17 ± 0.06	3.18 ± 0.07
45	3.96 ± 0.05	3.99 ± 0.03	3.96 ± 0.10
55	4.76 ± 0.06	4.76 ± 0.04	4.71 ± 0.03

Table 3-10. The diffusion coefficients of two pH values of 2.82 mM Aβ(25-35) in 90% H_2O and 10% D_2O from 5-70°C.

	Diffusion Coefficient × 10^6 (cm^2/s)	
Temperature (°C)	pH = 2.91	pH = 3.93
5	1.38 ± 0.14	1.47 ± 0.09
7	1.54 ± 0.09	1.65 ± 0.08
10	1.65 ± 0.16	1.77 ± 0.16
12	1.78 ± 0.09	1.99 ± 0.17
15	1.93 ± 0.16	2.16 ± 0.29
18	2.10 ± 0.13	2.35 ± 0.25
20	2.27 ± 0.14	2.44 ± 0.06
22	2.39 ± 0.12	2.59 ± 0.24
25	2.69 ± 0.12	2.91 ± 0.09
30	3.02 ± 0.20	3.11 ± 0.10
35	3.26 ± 0.16	3.60 ± 0.16
40	3.77 ± 0.32	4.02 ± 0.09
45	4.17 ± 0.10	4.29 ± 0.12
50	4.47 ± 0.09	4.74 ± 0.13
55	4.86 ± 0.14	5.16 ± 0.13
60	5.52 ± 0.23	5.63 ± 0.30
65	6.07 ± 0.13	5.89 ± 0.13
70	6.56 ± 0.12	6.40 ± 0.15

Table 3-11. The diffusion coefficients 2.82 mM Aβ(25-35) in 90% H_2O and 10% D_2O with and without zinc from 5-55°C.

	Diffusion Coefficient × 10^6 (cm^2/s)	
Temperature (°C)	no Zinc	Zinc
5	1.38 ± 0.14	1.36 ± 0.05
7	1.54 ± 0.09	1.52 ± 0.10
10	1.65 ± 0.16	1.66 ± 0.06
12	1.78 ± 0.09	1.70 ± 0.06
15	1.93 ± 0.16	1.90 ± 0.05
18	2.10 ± 0.13	2.05 ± 0.13
20	2.27 ± 0.14	2.16 ± 0.10
22	2.39 ± 0.12	2.38 ± 0.05
25	2.69 ± 0.12	2.51 ± 0.13
30	3.02 ± 0.20	2.82 ± 0.21
35	3.26 ± 0.16	3.12 ± 0.13
40	3.77 ± 0.32	3.43 ± 0.10
45	4.17 ± 0.10	3.72 ± 0.20
50	4.47 ± 0.09	4.08 ± 0.09
55	4.86 ± 0.14	4.40 ± 0.08

CHAPTER 4
CONCLUSION

The coupling constants of fluorinated cyclopropanes were examined. In general it was found that three-bond *cis* couplings were positive and three-bond *trans* couplings were negative. However, when one of the fluorines was geminal to an oxygen, the *trans* couplings were found to be positive. Additionally, the effect of temperature on the magnitude of the coupling constants was examined. The previously reported trend that the coupling constants increase in magnitude with increasing temperature was found to be violated in multiple instances. The signs of the coupling constants should not be used to determine relative geometry of fluorines in cyclopropanes, and the change in magnitude of coupling constants with a change in temperature cannot reliably be used to predict the correct sign of the coupling constants.

The aggregation of amyloid beta (25-35) was examined extensively with different sample conditions. The chemical shifts were measured and compared to compiled tables of known random-coil chemical shifts. In all sample conditions the observable peptide was found to maintain a random-coil conformation. The chemical shifts of the amide protons were measured over a range of temperatures and again the values indicated the peptide exists as a random-coil under the sample conditions used. Pulsed-field-gradient NMR was used to measure the diffusion coefficient of the peptide. There was little change with many changes in sample conditions. The pH was adjusted from approximately three to four with little effect on the measured diffusion coefficient despite the observation that samples made at near neutral pH rapidly turned to a very viscous gel. Zinc was added to the solution and, although the samples became visibly cloudy, there was still no change in the observed diffusion coefficient. Finally, the

peptide was dissolved in formic acid. The formic acid was blown off and the resulting solid dissolved in water. This too resulted in no change of the observed diffusion coefficient. Despite the samples visibly aggregating, the observed diffusion coefficient never changed. This indicates we only observed monomeric peptide in solution and the aggregation resulted in large unobservable high-order oligomers.

Suggestions for future work include increasing the ratio of trifluoroethanol. Other researchers have observed alpha helical structures in samples with as high as 50% TFE or other membrane mimicking solvents. Additionally, acquiring ROESY spectra with an array of mixing times might result in the observation of NOE peaks between non-neighboring residues. However, this would demand a great deal of instrument time even at relatively high concentrations. Another possible study would be measuring the diffusion coefficient from day to day over a long period of time to see if there are any changes as the sample settles.

LIST OF REFERENCES

(1) Pauli, W. *Naturwissenschaften* **1924**, *12*, 741-743.

(2) Rabi, I. I.; Millman, S.; Kusch, P.; Zacharias, J. R. *Physical Review* **1939**, *55*, 0526-0535.

(3) Levitt, M. H. *Spin Dynamics*; John Wiley & Sons Ltd: New York, NY, 2001.

(4) Ramsey, N. F.; Purcell, E. M. *Physical Review* **1952**, *85*, 143-144.

(5) Becker, E. D. *High resolution NMR - theory and chemical applications*; Academic Press: San Diego, CA, 2000.

(6) Bloch, F. *Physical Review* **1954**, *96*, 944.

(7) Maher, J. P.; Evans, D. F. *Proceedings of the Chemical Society of London* **1961**, 208.

(8) Freeman, R.; Anderson, W. A. *Journal of Chemical Physics* **1962**, *37*, 2053-2073.

(9) Freeman, R.; Whiffen, D. H. *Molecular Physics* **1961**, *4*, 321-325.

(10) Evans, D. F. *Molecular Physics* **1962**, *5*, 183-187.

(11) Evans, D. F. *Discussions of the Faraday Society* **1962**, 139-142.

(12) Stejskal, E. O.; Tanner, J. E. *Journal of Chemical Physics* **1965**, *42*, 288-292.

(13) Freund, A. *Monatshefte fur Chemie / Chemical Monthly* **1882**, *3*, 625-635.

(14) Lucas, G. H. W.; Henderson, V. E. *Canadian Medical Association Journal* **1929**, *21*, 173-175.

(15) Dimakopoulos, A. C. *Curr.Alzheimer Res.* **2005**, *2*, 19-28.

(16) Campiglia, P.; Esposito, C.; Scrima, M.; Gomez-Monterrey, I.; Bertamino, A.; Grieco, P.; Novellino, E.; D'Ursi, A. M. *Chemical Biology & Drug Design* **2007**, *69*, 111-118.

(17) Hardy, J. A.; Higgins, G. A. *Science* **1992**, *256*, 184-185.

(18) Selkoe, D. J. *Alzheimers Disease: A Compendium of Current Theories* **2000**, *924*, 17-25.

(19) Esler, W. P.; Wolfe, M. S. *Science* **2001**, *293*, 1449-1454.

(20) Danielsson, J.; Andersson, A.; Jarvet, J.; Graslund, A. *Magnetic Resonance in Chemistry* **2006**, *44*, S114-S121.

(21) D'Ursi, A. M.; Armenante, M. R.; Guerrini, R.; Salvadori, S.; Sorrentino, G.; Picone, D. *Journal of Medicinal Chemistry* **2004**, *47*, 4231-4238.

(22) Ricchelli, F.; Drago, D.; Filippi, B.; Tognon, G.; Zatta, P. *Cellular and Molecular Life Sciences* **2005**, *62*, 1724-1733.

(23) Jarvet, J.; Damberg, P.; Bodell, K.; Eriksson, L. E. G.; Graslund, A. *Journal of the American Chemical Society* **2000**, *122*, 4261-4268.

(24) Kayed, R.; Head, E.; Thompson, J. L.; McIntire, T. M.; Milton, S. C.; Cotman, C. W.; Glabe, C. G. *Science* **2003**, *300*, 486-489.

(25) Quist, A.; Doudevski, L.; Lin, H.; Azimova, R.; Ng, D.; Frangione, B.; Kagan, B.; Ghiso, J.; Lal, R. *Proceedings of the National Academy of Sciences of the United States of America* **2005**, *102*, 10427-10432.

(26) Graham, J. D.; Rogers, M. T. *Journal of the American Chemical Society* **1962**, *84*, 2249-&.

(27) Grant, D. M. *Journal of Chemical Physics* **1961**, *34*, 699-700.

(28) Closs, G. L.; Closs, L. E. *Journal of the American Chemical Society* **1960**, *82*, 5723-5728.

(29) Smidt, J.; Deboer, T. J. *Recueil des Travaux Chimiques des Pays-Bas-Journal of the Royal Netherlands Chemical Society* **1960**, *79*, 1235-1243.

(30) Williamson, K. L.; Lanford, C. A.; Nicholso, C. R. *Journal of the American Chemical Society* **1964**, *86*, 762-&.

(31) Hutton, H. M.; Schaefer, T. *Canadian Journal of Chemistry-Revue Canadienne de Chimie* **1963**, *41*, 2774-&.

(32) Schrumpf, G.; Luttke, W. *Tetrahedron Letters* **1969**, 2635-&.

(33) Sargeant, P. B. *Journal of Organic Chemistry* **1970**, *35*, 678-&.

(34) Williamson, K. L.; Braman, B. A. *Journal of the American Chemical Society* **1967**, *89*, 6183-&.

(35) Cavalli, L. *Organic Magnetic Resonance* **1970**, *2*, 233-244.

(36) Pena, F.; Ordaz, B.; Balleza-Tapia, H.; Bernal-Pedraza, R.; Marquez-Ramos, A.; Carmona-Aparicio, L.; Giordano, M. *Hippocampus* **2010**, *20*, 78-96.

(37) Kaminsky, Y. G.; Marlatt, M. W.; Smith, M. A.; Kosenko, E. A. *Experimental Neurology* **2010**, *221*, 26-37.

(38) Tomas, M.; Garcia, N.; Santafe, M. M.; Lanuza, M.; Tomas, J. *Journal of Alzheimers Disease* **2009**, *18*, 877-884.

(39) Kong, L. P.; Wu, L. Z.; Zhang, J.; Liao, Y. P.; Wang, H. Q. *Neural Regeneration Research* **2009**, *4*, 405-412.

(40) Fu, Z. M.; Luo, Y.; Derreumaux, P.; Wei, G. H. *Biophysical Journal* **2009**, *97*, 1795-1803.

(41) Arif, M.; Chikuma, T.; Ahmed, M. M.; Nakazato, M.; Smith, M. A.; Kato, T. *Neuroscience* **2009**, *164*, 1199-1209.

(42) Liu, R.; Gao, M.; Qiang, G. F.; Zhang, T. T.; Lan, X.; Ying, J.; Du, G. H. *Neuroscience* **2009**, *162*, 1232-1243.

(43) Hughes, E.; Burke, R. M.; Doig, A. J. *Journal of Biological Chemistry* **2000**, *275*, 25109-25115.

(44) Mikol, V.; Hirsch, E.; Giege, R. *Journal of Molecular Biology* **1990**, *213*, 187-195.

(45) Cho, C. H.; Urquidi, J.; Singh, S.; Robinson, G. W. *Journal of Physical Chemistry B* **1999**, *103*, 1991-1994.

(46) Longsworth, L. G. *Journal of Physical Chemistry* **1960**, *64*, 1914-1917.

(47) Ilyina, E.; Roongta, V.; Pan, H.; Woodward, C.; Mayo, K. H. *Biochemistry* **1997**, *36*, 3383-3388.

(48) Wattenbarger, M. R.; Bloomfield, V. A.; Bu, Z.; Russo, P. S. *Macromolecules* **1992**, *25*, 5263-5265.

(49) Momot, K. I.; Kuchel, P. W. *Concepts in Magnetic Resonance Part A* **2006**, *28A*, 249-269.

(50) Johnson, C. S. *Progress in Nuclear Magnetic Resonance Spectroscopy* **1999**, *34*, 203-256.

(51) Sorland, G. H.; Seland, J. G.; Krane, J.; Anthonsen, H. W. *Journal of Magnetic Resonance* **2000**, *142*, 323-325.

(52) Jerschow, A.; Muller, N. *Journal of Magnetic Resonance* **1997**, *125*, 372-375.

(53) Szilagyi, L. *Progress in Nuclear Magnetic Resonance Spectroscopy* **1995**, *27*, 325-443.

(54) Wishart, D. S.; Sykes, B. D. *Nuclear Magnetic Resonance, Pt C* **1994**, *239*, 363-392.

(55) Wishart, D. S.; Bigam, C. G.; Holm, A.; Hodges, R. S.; Sykes, B. D. *Journal of Biomolecular Nmr* **1995**, *5*, 67-81.

(56) Wishart, D. S.; Bigam, C. G.; Yao, J.; Abildgaard, F.; Dyson, H. J.; Oldfield, E.; Markley, J. L.; Sykes, B. D. *Journal of Biomolecular Nmr* **1995**, *6*, 135-140.

(57) Wuthrich, K. *NMR of Proteins and Nucleic Acids*; Wiley-Interscience: New York, 1986.

(58) Cavanagh, J.; Fairbrother, W. J.; Palmer III, A. R.; Skelton, N. J. *Protein NMR Spectroscopy Principles and Practice*; Academic Press, Inc.: New York, NY, 1996.

(59) Bothnerby, A. A.; Stephens, R. L.; Lee, J. M.; Warren, C. D.; Jeanloz, R. W. *Journal of the American Chemical Society* **1984**, *106*, 811-813.

(60) Dalgarno, D. C.; Levine, B. A.; Williams, R. J. P. *Bioscience Reports* **1983**, *3*, 443-452.

(61) Pastore, A.; Saudek, V. *Journal of Magnetic Resonance* **1990**, *90*, 165-176.

(62) Wishart, D. S.; Sykes, B. D.; Richards, F. M. *Febs Letters* **1991**, *293*, 72-80.

(63) Wishart, D. S.; Sykes, B. D.; Richards, F. M. *Biochemistry* **1992**, *31*, 1647-1651.

(64) Osapay, K.; Case, D. A. *Journal of Biomolecular Nmr* **1994**, *4*, 215-230.

(65) Szilagyi, L.; Jardetzky, O. *Journal of Magnetic Resonance* **1989**, *83*, 441-449.

(66) Williamson, M. P. *Biopolymers* **1990**, *29*, 1428-1431.

(67) Wishart, D. S.; Sykes, B. D.; Richards, F. M. *Journal of Molecular Biology* **1991**, *222*, 311-333.

(68) Clayden, N. J.; Williams, R. J. P. *Journal of Magnetic Resonance* **1982**, *49*, 383-396.

(69) Wishart, D. S.; Nip, A. M. *Biochemistry and Cell Biology* **1998**, *76*, 153-163.

(70) Merutka, G.; Dyson, H. J.; Wright, P. E. *Journal of Biomolecular Nmr* **1995**, *5*, 14-24.

(71) Urry, D. W.; Masotti, L.; Krivacic, J. R. *Biochimica et Biophysica Acta* **1971**, *241*, 600-612.

(72) Dyson, H. J.; Rance, M.; Houghten, R. A.; Wright, P. E.; Lerner, R. A. *Journal of Molecular Biology* **1988**, *201*, 201-217.

(73) Walsh, D. M.; Lomakin, A.; Benedek, G. B.; Condron, M. M.; Teplow, D. B. *Journal of Biological Chemistry* **1997**, *272*, 22364-22372.

(74) Walsh, D. M.; Hartley, D. M.; Kusumoto, Y.; Fezoui, Y.; Condron, M. M.; Lomakin, A.; Benedek, G. B.; Selkoe, D. J.; Teplow, D. B. *Journal of Biological Chemistry* **1999**, *274*, 25945-25952.

(75) Kirkitadze, M. D.; Condron, M. M.; Teplow, D. B. *Journal of Molecular Biology* **2001**, *312*, 1103-1119.

(76) Lee, S.; Kim, Y. *Bulletin of the Korean Chemical Society* **2004**, *25*, 838-842.

(77) Otvos, L.; Szendrei, G. I.; Lee, V. M. Y.; Mantsch, H. H. *European Journal of Biochemistry* **1993**, *211*, 249-257.

(78) Lee, S.; Suh, Y. H.; Kim, S.; Kim, Y. *Journal of Biomolecular Structure & Dynamics* **1999**, *17*, 381-391.

(79) Kohno, T.; Kobayashi, K.; Maeda, T.; Sato, K.; Takashima, A. *Biochemistry* **1996**, *35*, 16094-16104.

(80) Sticht, H.; Bayer, P.; Willbold, D.; Dames, S.; Hilbich, C.; Beyreuther, K.; Frank, R. W.; Rosch, P. *European Journal of Biochemistry* **1995**, *233*, 293-298.

(81) Bush, A. I. *Trends in Neurosciences* **2003**, *26*, 207-214.

(82) Adlard, P. A.; Bush, A. I. *Journal of Alzheimer's Disease* **2006**, *10*, 145-163.

(83) Gaggelli, E.; Kozlowski, H.; Valensin, D.; Valensin, G. *Chemical Reviews* **2006**, *106*, 1995-2044.

(84) Lau, T. L.; Gehman, J. D.; Wade, J. D.; Perez, K.; Masters, C. L.; Barnham, K. J.; Separovic, F. *Biochimica et Biophysica Acta-Biomembranes* **2007**, *1768*, 2400-2408.

(85) Faller, P.; Hureau, C. *Dalton Transactions* **2009**, 1080-1094.

(86) Talmard, C.; Yona, R. L.; Faller, P. *Journal of Biological Inorganic Chemistry* **2009**, *14*, 449-455.

(87) Gaggelli, E.; Janicka-Klos, A.; Jankowska, E.; Kozlowski, H.; Migliorini, C.; Molteni, E.; Valensin, D.; Valensin, G.; Wieczerzak, E. *Journal of Physical Chemistry B* **2008**, *112*, 100-109.

(88) Bush, A. I.; Pettingell, W. H.; Multhaup, G.; Paradis, M. D.; Vonsattel, J. P.; Gusella, J. F.; Beyreuther, K.; Masters, C. L.; Tanzi, R. E. *Science* **1994**, *265*, 1464-1467.

(89) Huang, X. D.; Atwood, C. S.; Moir, R. D.; Hartshorn, M. A.; Vonsattel, J. P.; Tanzi, R. E.; Bush, A. I. *Journal of Biological Chemistry* **1997**, *272*, 26464-26470.

(90) Raman, B.; Ban, T.; Yamaguchi, K.; Sakai, M.; Kawai, T.; Naiki, H.; Goto, Y. *Journal of Biological Chemistry* **2005**, *280*, 16157-16162.

(91) Gaggelli, E.; Grzonka, Z.; Kozlowski, H.; Migliorini, C.; Molteni, E.; Valensin, D.; Valensin, G. *Chemical Communications* **2008**, 341-343.

(92) Syme, C. D.; Viles, J. H. *Biochimica et Biophysica Acta-Proteins and Proteomics* **2006**, *1764*, 246-256.

(93) Zirah, S.; Kozin, S. A.; Mazur, A. K.; Blond, A.; Cheminant, M.; Segalas-Milazzo, I.; Debey, P.; Rebuffat, S. *Journal of Biological Chemistry* **2006**, *281*, 2151-2161.

(94) Danielsson, J.; Pierattelli, R.; Banci, L.; Graslund, A. *Febs Journal* **2007**, *274*, 46-59.

(95) Curtain, C. C.; Ali, F.; Volitakis, I.; Cherny, R. A.; Norton, R. S.; Beyreuther, K.; Barrow, C. J.; Masters, C. L.; Bush, A. I.; Barnham, K. J. *Journal of Biological Chemistry* **2001**, *276*, 20466-20473.

(96) Andersen, N. H.; Neidigh, J. W.; Harris, S. M.; Lee, G. M.; Liu, Z. H.; Tong, H. *Journal of the American Chemical Society* **1997**, *119*, 8547-8561.

(97) Jimenez, M. A.; Nieto, J. L.; Rico, M.; Santoro, J.; Herranz, J.; Bermejo, F. J. *Journal of Molecular Structure* **1986**, *143*, 435-438.

(98) Zimmermann, G. R.; Legault, P.; Selsted, M. E.; Pardi, A. *Biochemistry* **1995**, *34*, 13663-13671.

(99) Mills, R. *Journal of Physical Chemistry* **1973**, *77*, 685-688.

(100) Hazeki, N.; Tukamoto, T.; Goto, J.; Kanazawa, I. *Biochemical and Biophysical Research Communications* **2000**, *277*, 386-393.

(101) Filippov, A. V.; Suleimanova, A. V.; Grobner, G.; Antsutkin, O. N. *Colloid Journal* **2008**, *70*, 501-506.

(102) Narayanan, S.; Reif, B. *Biochemistry* **2005**, *44*, 1444-1452.

(103) Filippov, A.; Sulejmanova, A.; Antzutkin, O.; Grobner, G. *Applied Magnetic Resonance* **2005**, *29*, 439-449.

(104) Danielsson, J.; Jarvet, J.; Damberg, P.; Graslund, A. *Magnetic Resonance in Chemistry* **2002**, *40*, S89-S97.

(105) Cantor, C. R.; Schimmel, P. R. *Biophysical Chemistry, Techniques for the Study of Biological Structure and Function*; W.H. Freeman: San Francisco, CA, 1980.

(106) Tanford, C. *Physical Chemistry of Macromolecules*; Wiley: New York, NY, 1963.

(107) Krishnan, V. V. *Journal of Magnetic Resonance* **1997**, *124*, 468-473.

(108) Ryabov, Y. E.; Geraghty, C.; Varshney, A.; Fushman, D. *Journal of the American Chemical Society* **2006**, *128*, 15432-15444.

(109) Perrin, F. *Journal de Physique et Le Radium* **1934**, *5*, 497-511.

(110) Perrin, F. *Journal de Physique et Le Radium* **1936**, *7*, 1-11.

BIOGRAPHICAL SKETCH

David Warren Richardson was born in Orange Park, Florida, in 1980. His father, originally from the Boston area of Massachusetts, was stationed here while he was a Captain in the United States Navy. David grew up in this suburb of Jacksonville with his parents, older brother, and younger sister. He graduated from Middleburg High School in 1998.

In the fall of 1998, David began his academic career at the University of Florida, where he studied chemistry. During this time, he worked in the NMR lab under the advisement of Dr. Wallace Brey. In December of 2001, David graduated with a Bachelor of Science in Chemistry.

David continued to work in the NMR lab at UF for two years post baccalaureate. He returned to school by entering the graduate program at the University of Florida in August of 2003. Following the guidance of Dr. Brey and Dr. Ion Ghiviriga, he conducted his research and trained fellow researchers how to operate NMR instrumentation.